Hybrid Energy Storage Systems via Power Electronic Converters

PhD Student: ERIK GARAYALDE PEREZ

Supervisors: UNAI IRAOLA IRIONDO

IOSU AIZPURU LARRAÑAGA

Mondragon Goi Eskola Politeknikoa

Mondragon Unibertsitatea

Arrasate-Mondragon (Gipuzkoa), December 2019

ABSTRACT

In recent years, many research lines have focused their efforts on improving energy efficiency and developing renewable energy sources. In this context, the use of energy storage systems is on the rise, as they can contribute to the integration of renewables to the main electrical grid. However, energy storage systems are divided into high energy or high power devices. Due to the lack of a solution covering both aspects, researchers are forced to find alternatives. The hybridization of different energy storage technologies is presented as a suitable solution for this problem, since it combines high power and high energy within the same system.

The main goal of this thesis is the design and implementation of a hybrid energy storage system (HESS), capable of improving the performance provided by a single storage technology. As a first step in this direction, this document reviews and classifies the most relevant HESS topologies found in the literature. This allows a better understanding of the drawbacks and benefits of each configuration.

To ensure the optimal use of this HESS, it is essential to design a suitable energy management strategy and a proper power electronic converter control. To this end, the control structure has been analyzed from different approaches. On the one hand there would be the classic multilevel control structure, which usually consists of three levels among which are the operating constraints, the power sharing and at the lowest level the control of the converter. On the other hand there would be the single level control structure in which both, the power distribution and the control of the converter, are integrated within the same level by using modern MPC control algorithms.

Finally, three different case studies are presented to show the practical application of the developed control strategies together with the main conclusions of the thesis.

Keywords: *Hybridization, Energy storage systems, Batteries, BMS, Model predictive control, MPC, topology.*

LABURPENA

Azken urteetan, ikerketa-lerro askok eraginkortasun energetikoa hobetzeko eta energia berriztagarriak garatzeko ahaleginak egin dituzte. Testuinguru honetan, energia metatze sistemen erabilera geroz eta handiagoa da, berriztagarrien integrazioa sare elektrikoarekin erraztu dezaketelako. Hala ere, energia altuko edo potentzia altuko metatze sistemak bakarrik aukeratu daitezke. Horregatik, ikertzaileek alternatiba berriak bilatzera behartuta daude. Energia metatze sistema desberdinen hibridazioa, arazo horri irtenbidea ematen dio. Honekin, potentzia eta energia maila altuak sistema bakar batetan batu daitezke.

Tesi honen helburu nagusia, energia metatze sistema hibrido (HESS sigla, ingelesetik *Hybrid Energy Storage System*) bat diseinatzea eta inplementatzea da. Sistema honek, teknologia bakar batek eskaintzen duen errendimendua hobetzeko gai izan beharko luke. Lehen urratsa bezala, dokumentu honek literaturan aurkitutako topologia hibrido garrantzitsuenak laburbildu eta batzen ditu. Honi esker, konfigurazio bakoitzaren abantaila eta desabantailak hobeto ulertzea ahal da.

HESS honen erabilera optimoa bermatzeko, ezinbestekoa da energia kudeatzeko estrategia on bat diseinatzea bihurgailu elektronikoaren kontrol egokiarekin batera. Horretarako, kontrol egitura ikuspegi desberdinetatik aztertuko da. Alde batetik, maila anitzeko kontrol egitura klasikoa egongo litzateke, normalean hiru mailaz osatua dagoena. Goi mailan funtzionamendu eta segurtasun mugak egongo lirateke, erdiko mailan potentzia banaketa, eta azkenik bihurgailuaren maila baxuko kontrola.

Bestalde, maila bakarreko kontrol egitura egongo litzateke non mugak, potentzia banaketa eta bihurgailuaren kontrola maila berean integratzen dira kontrol iragarleko algoritmoen bidez (MPC).

Azkenik, hiru kasu desberdin aurkezten dira garatutako kontrolen aplikazio praktikoa erakusteko tesiaren ondorio nagusiekin batera.

Funtsezko hitzak: *Hibridazioa, Energia metatze sistemak, Bateriak, BMS, Ereduan oinarritutako kontrol iragarlea, MPC, topologia.*

RESUMEN

En los últimos años, numerosas líneas de investigación han centrado sus esfuerzos en mejorar la eficiencia energética junto con el desarrollo de fuentes de generación renovables. En este contexto, el uso de sistemas de almacenamiento de energía está al alza, ya que estos pueden contribuir a la integración de las renovables en la red eléctrica convencional. Sin embargo, la necesidad de elegir entre dispositivos de alta energía o alta potencia, obliga a los investigadores a buscar otras alternativas. La hibridación de diferentes sistemas de almacenamiento se presenta como una solución apropiada para este problema, ya que combina alta energía y alta potencia dentro de un mismo sistema.

El objetivo principal de esta tesis es el diseño e implementación de un sistema híbrido de almacenamiento de energía (sigla HESS, del inglés *Hybrid Energy Storage System*), capaz de mejorar las prestaciones que proporcionaría el uso de una única tecnología. Como primer paso en esta dirección, en este documento resume y clasifica las topologías de hibridación más relevantes encontradas en la literatura. Esto permite una mejor comprensión de los beneficios e inconvenientes de cada configuración.

Para garantizar el uso óptimo de dicho HESS, es esencial diseñar una estrategia adecuada de gestión de energía junto con un control óptimo del convertidor electrónico de potencia. Para lograr este fin, la estructura de control ha sido analizada desde diferentes enfoques. Por un lado se encontraría la estructura de control multinivel clásica, la cual generalmente consta de tres niveles. En el nivel más alto se encontrarían las restricciones operativas y de seguridad, en el intermedio se encontraría la división de potencia, y por último el control de nivel bajo del convertidor.

Por otro lado, se encontraría la estructura de control de un único nivel, en la que tanto las restricciones, el reparto de potencia y el control del convertidor se integran dentro del mismo nivel mediante algoritmos de control predictivo (MPC).

Finalmente, se presentan tres casos de estudio para mostrar la aplicación práctica de las estrategias de control desarrolladas junto con las principales conclusiones de la tesis.

Palabras clave: *Hibridación, Sistemas de almacenamiento, Baterías, BMS, Control predictivo en base a modelo, MPC, topología.*

AKNOWLEDGEMENTS

First of all, I would like to thank my director and co-director, Dr. Unai Iraola Iriondo and Dr. Iosu Aizpuru Larrañaga for their guidance and support during all these years. Their technical advices were of vital importance when there were problems to go ahead. I would also like to thank Aitor Idarreta and Jon Anzola for their help with the experimental platform.

Of course, I can´t forget many other people from Galarreta, Oier, Asier, Argiñe, Mazu, Ander, Asier, Antxon, Borja…other workmates from Arrasate, Eneko, Edu, Laura, Canales, Manex, Igor, Aritz, David, Gonzalo, Gaizka, Javi…thank you because it is a pleasure being with you when I go there.

I would also like to acknowledge colleagues from Universidad de Zaragoza, Iván, Carlos, Estanis, Antonio…and the rest of workmates from their department, for the opportunity to collaborate with them. We never stop learning with you, it has been a pleasure.

I would also like to express my gratitude to Paderborn University and especially to the people working in the department conducted by professor Daniel E. Quevedo, for giving me the opportunity to make a stay of 3 months there. I felt part of the team from the first day and I had very good experiences working there and learning from their researches.

Finally, I want to thank each member of the jury for coming to the thesis defense event and for giving me their point of view about the developed work.

Para acabar, me gustaría agradecer a todos mis amigos y familiares, pero sobre todo a mis padres por animarme a llegar hasta aquí y porque siempre han creído que lo podía hacer. Y gracias también por haberme enseñado a esforzarme para conseguir las cosas.

Eta azkenik zu Itxaso! Eskerrak eman behar dizkizut eskainitako maitasunagatik, pertsona bezala hazten lagundu nauzulako. Beti momentu on eta txarretan alboan eduki zaitudalako. Bion artean errazagoa izan da dena.

Eskerrik asko guztioi!

CONTENTS

GLOSSARY OF ABBREVIATIONS AND VARIABLES

Abbreviations

AC	Alternating current
BMS	Battery management system
CAES	Compressed air energy storage
CC	Constant current
CCS	Continuous Control Set
CV	Constant voltage
DC	Direct current
DFIG	Doubly-fed induction generator
DOD	Depth of discharge
DPC	Direct power control
DTC	Direct torque control
ESS	Energy storage system
EV	Electric vehicle
FC	Fuel cell
FCS	Finite Control Set
FES	Flywheel energy storage
FOC	Field-oriented control
GPC	Generalized predictive control
HESS	Hybrid energy storage system
HEV	Hybrid electric vehicle
LFP	Lithium iron phosphate
LPF	Low pass filter
MIMO	Multi-input multi-output
MOSFET	Metal-oxide-semiconductor field-effect-transistor
MPC	Model predictive control
MPPT	Maximum power point tracking
NPC	Neutral point clamped
OCV	Open circuit voltage
PbA	Lead-acid battery

PEC	Power electronic converter
PHES	Pumped hydroelectric energy storage
PI	Proportional integral
PID	Proportional integral derivative
PLL	Phase-locked loop
PSoC	Partial State of Charge
PV	Photovoltaic
PWM	Pulse width modulation
RMS	Root mean square
SMES	Superconducting magnetic energy storage
SOC	State of charge
SOH	State of health
UC	Ultracapacitor
UPS	Uninterruptible power supply
VOC	Voltage-oriented control
VRB	Vanadium redox battery (or Vanadium redox flow battery)

Symbols and variables

$\mathbf{A}$	State (or system) matrix (continuous time)
$\mathbf{B}$	Input matrix (continuous time)
C	Capacitance [F]
$\mathbf{C}$	Output matrix (continuous time)
d	Duty cycle
$\mathbf{D}$	Feedforward matrix (continuous time)
E	Stored energy [Wh]
f	Frequency [Hz]
i	Current [A]
$\boldsymbol{I}$	Identity matrix
J	Cost function
k	Discrete time step
L	Inductance [H]
$\mathbb{N}$	Natural number
P	Real power [W]
r, R	Resistance [Ω]
t	Time [s]
$u, \boldsymbol{u}$	Switch position, input (or manipulated) variable
Δu	Change in switch position
U	Sequence of switch positions (switching sequence)

v, V	Voltage [V]
$\boldsymbol{x}$	State variable
$\boldsymbol{y}$	Output variable
λ	Weighting factor
τ	Time constant [s]

Subscripts

$\mathbf{A}_d$	State (or system) matrix (discrete time)
$\mathbf{B}_d$	Input matrix (discrete time)
$\mathbf{C}_d$	Output matrix (discrete time)
$\mathbf{D}_d$	Feedforward matrix (discrete time)
f_{sw}	Switching frequency [Hz]
K_i	Integral gain factor
K_p	Proportional gain factor
N_p	Prediction horizon
n_p	Number of cells in parallel
N_{ph}	Number of parallel phases of the synchronous buck converter
n_s	Number of cells in series
P_{HF}	High frequency component of real power [W]
P_{LF}	Low frequency component of real power [W]
R_{DSon}	Drain-source on state resistance of the MOSFET [Ω]
T_s	Sample time [s]
u_{opt}	Optimal switch position
U_{opt}	Optimal sequence of switch positions (or input variables)
V_d	Dynamic part of the output voltage of the cell [V]
ε_i	Current tracking error
$\Delta\varepsilon_i$	Absolute current tracking error
λ_u	Weighting factor of the switching effort

Superscripts

i^*	Current reference
i^p	Predicted current

Operations

dx/dt	Time derivative of the variable x
e^x	Exponential of the variable x
$x \in S$	Variable x belongs to the set S

$\{a,\ b,\ ...\}$	Set consisting of the elements $a,\ b$ and so on
$[a,\ b]$	Closed interval between a and b
$\lvert x \rvert$	Absolute value of variable x

Chapter 1

INTRODUCTION

This chapter introduces the research work with a brief description of the actual energy system situation. In this context, it is important to highlight the intention of public administrations to promote renewable energy production and develop energy efficiency plans. To make this possible, energy storage systems will play a decisive role in the near future.

Apart from that, the contributions made during the thesis have been summarized and the outline of the document is presented.

1.1 Background and State of the Art

The energy efficiency is one of the main roadmaps for the European Union (EU) in the coming decades. Among the different programs promoted by public institutions, Horizon 2020 is the most important one at European level. Within this strategic program, the effort is focused on the fulfillment of climate and energy objectives until 2020, with the following targets in mind [1]:

- 20% cut in greenhouse gas emissions. (from 1990 levels)
- 20% of EU energy, generated by renewable energy sources.
- 20% of improvement in energy efficiency.

But the H2020 is not an isolated program, it will be succeeded by a framework program that is already being developed. In this sense, one of the main targets of this long term strategy, is the development of resource-efficient technology solutions to decarbonize the energy system in a sustainable way [2]. The decoupling of economic growth from the consumption of resources is one of the key issues to decrease the dependence on fossil fuels. In such a case, a better use of raw materials could be achieved.

The development of efficient energy management systems and the increase in renewable energy production is of great importance. New ways should be explored to save energy and considerably increase the share of renewable sources in the total energy supply. However, these actions have to be linked to a stable and safe electricity supply, which is not a trivial task when working with stochastic renewable energy sources.

The low predictability is the main problem of renewable energy sources, but not the only one. With the integration of renewable energy sources with the main electrical grid, stability problems are appearing. This is a direct consequence of the absence of inertia in the system, due to a reduction in the number of synchronous generators [3]–[5]. These two factors, together with the fact that these energy sources are not always available when needed, contribute to the development of grid connected Energy Storage Systems (ESSs) [6]. Several projects have been carried out in recent years to solve that issue [7], [8].

Nevertheless, the electricity market is not the only one promoting the use of energy storage to improve application performance. In grid connected traction applications such

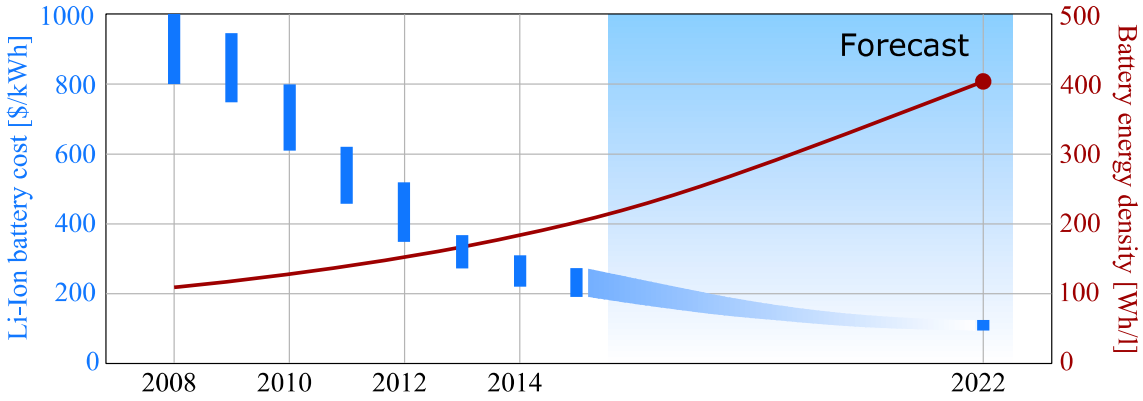

Fig. 1.1 Evolution of Li-Ion battery energy density and cost. [23]

as the elevator [9]–[15] and the railway industries [16]–[22], the use of batteries and ultra-capacitors has already become a reality. The same happens with electric vehicles, where the price of the batteries was the main obstacle for their commercialization in the past. However, this trend is set to change because Li-ion batteries are becoming increasingly price competitive (Fig. 1.1).

Traction applications have the particularity of combining constant consumption patterns together with transient high power levels, as occurs in accelerations and regenerative braking. This working mode can induce great stress in such storage devices, reducing their lifespan. To date, the solution to this problem has been to oversize ESSs entailing additional costs, volume and weight. Although the majority of current applications contain only one energy storage technology, the hybridization of different ESSs is gathering interest as it combines the advantages of different storage devices.

In this context, the implementation of Hybrid Energy Storage Systems (HESSs) has been studied for different applications with satisfactory results. Normally, hybridization is designed to handle independently the average consumption and power transients. These types of systems consist of at least two different storage devices: long-term and short-term devices. The former are characterized by having a relatively high energy density, whose job is to provide the average power required by the application. The short-term devices, however, have a high power density used for managing power transients. The classical operating mode consists of separating the current depending on its dynamics. The high power density device is responsible for absorbing the fast dynamics of the current, while the high energy density storage device absorbs the slow dynamics. There

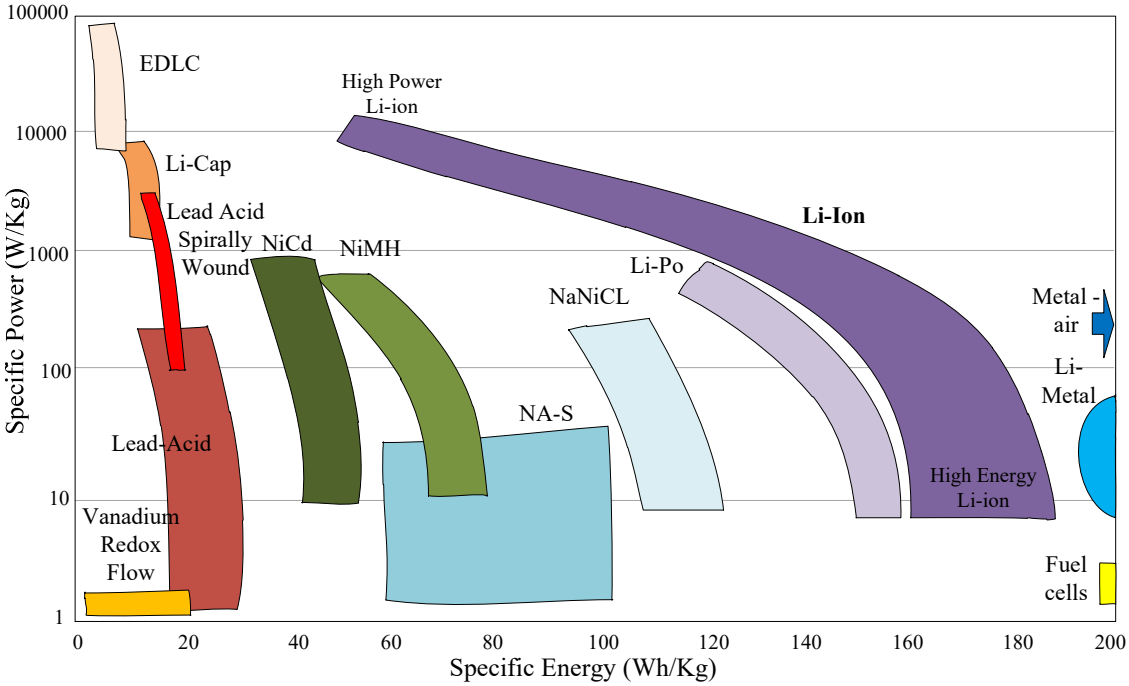

Fig. 1.2 Ragone plot of main battery energy storage technologies for gravimetric (Kg) characteristics. Analysis resume from [24]–[27].

exist other methods like state machines and virtual impedances, but the most suitable method to perform the power sharing will ultimately depend on the application requirements.

Apart from the benefits that the storage hybridization offers, providing a satisfactory solution is not an easy task in most cases. Depending on the HESS optimization level, it can be difficult to ensure its economic feasibility. Therefore, correct device selection and the proportion of each storage technology in the HESS are determining factors. For this work, the Ragone Plot (Fig. 1.2) is used as a first step since it offers a comparison of different ESSs depending on their values of specific energy (Wh/kg) and specific power (W/kg) [28].

1.2 Applications of Hybrid Energy Storage Systems

The hybridization of different ESSs is gaining interest because of the technical improvements it offers. The HESS concept provides several degrees of freedom, starting with the control and power sharing methods and following with the hardware and

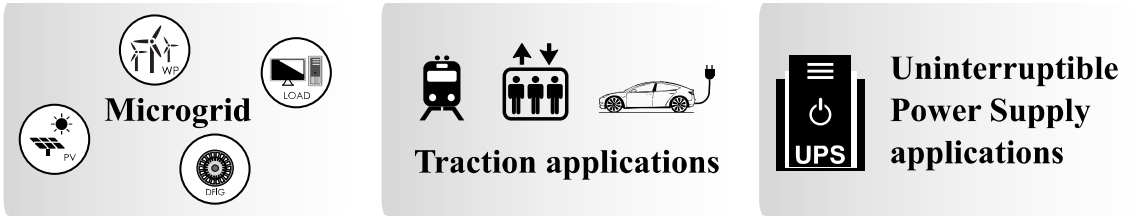

Fig. 1.3 Most common applications where HESSs are used.

connection topologies. For that reason it has been used for different applications, of which the most important ones are shown in Fig. 1.3.

The standard HESS configuration consists of at least two different ESS technologies working together. Nevertheless, despite using only two storage devices, there exist several ways to interconnect them to the common energy bus as it is shown in Chapter 2. Leaving aside the different connection modes, since these will be analyzed in depth in the following sections, the parallel connection of both storage devices will be considered as an example. In microgrid applications is very common to find this type of connection together with multiple energy sources and loads in the same energy bus. A comprehensive example of this is shown in Fig. 1.4, where the HESS, solar panels and loads are connected to a common DC bus. The HESS should maintain the bus voltage as constant as possible storing or providing energy to the system. The constant consumption would be fulfilled by the high energy density storage device (battery) while the high power density storage device (ultracapacitor) would do so with the power spikes. In this

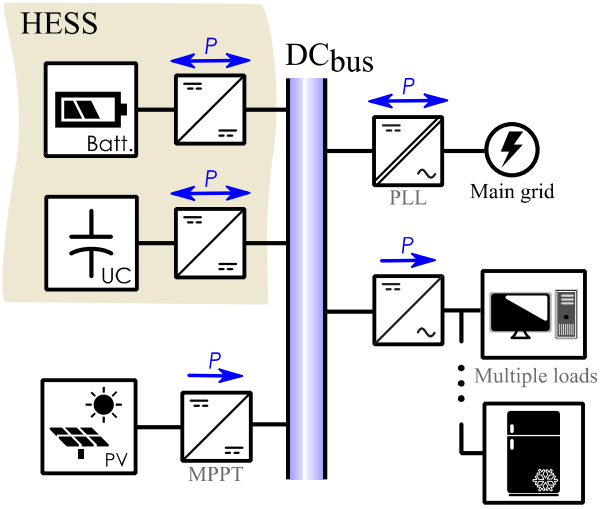

Fig. 1.4 DC bus connected HESS with multiple energy sources and loads.

case there also exists an interconnection between the DC bus of the microgrid and the main electrical grid, thus providing bidirectional power flow between both.

The power consumption profile in traction applications is slightly different, since the power required to accelerate is much higher than the average power. For these reason, the maximum power managed by the high energy density storage device, is limited to a safe value. On the other hand, the high power density storage device must be able to deliver the rest of the power required by the electric drive. An example of this working mode is presented in Fig. 1.5. Together with this, if the high energy density storage device is not able to react fast enough to an abrupt power increase, a change rate limit can be applied to its power reference.

Apart from the typical traction application where the hybridization is implemented to separate energy and power, there are others in which the HESS is performed with different purposes. In this sense, the hybridization is not only limited to the combination of different storage technologies. Within the same technology, there are batteries with differing features. In this sense there can be found batteries with high endurance against deep discharges, while others are only able to last for long if remain most of the time in floating mode. These two features can be used in a complementary fashion for some particular applications, such as stand-alone systems with constant consumption loads. The aim in these cases, is to make the most of the virtues of each battery so that the system does not run out of energy. In this context, the main battery is responsible for providing the daily consumption. While the secondary battery, works as an uninterruptible power supply (UPS) supporting the energy demand of the load when the principal battery is

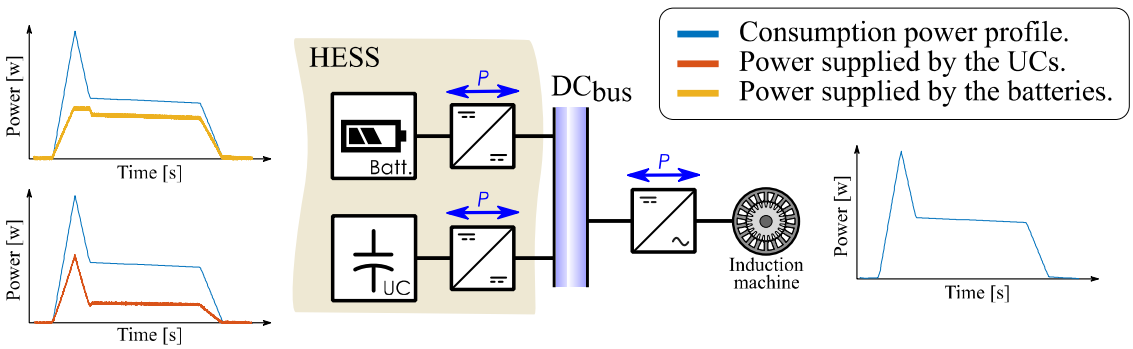

Fig. 1.5 HESS power sharing example in traction application.

depleted. This configuration has been proposed for similar applications [29], [30], where Lithium Ion batteries are combined with lead acid batteries.

For this kind of applications, the main battery is sized so that the secondary battery only has to be brought into operation a few times during the year. Following this criterion, the main ESS would be sized for the daily consumption requirements, for which the deep-cycle battery is selected. While the secondary ESS would consist of the battery specific for floating operation. In any case, the combination of batteries for cycling and floating operation does not necessarily require the use of Li-Ion technology. Within PbA technology low cost alternatives can be found for such application (Fig. 1.6).

In addition, there are other reasons why the hybridization of batteries with other storage technologies is of interest. The increment of the internal resistance due to aging effects, can make the batteries unable to reach the energy and power requirements of some applications such as electric vehicle (EV). However, there is the possibility of making the most of these batteries by operating at less demanding current rates, such as in residential applications [31], [32]. One possible way to achieve this is by the hybridization of these reduced performance batteries with UCs (Fig. 1.6). Nevertheless, not all batteries are good candidates for a potential second life use. Among the different battery types, LiFePO is one of the few technologies suitable to be given a second life, proving its feasibility in a laboratory environment [33], [34]. On the contrary, NMC technology has been tested for second-life use with less satisfactory results due to their fast degradation after reaching the 'ageing knee' [32]. The reuse of these so-called 'second life' batteries, can contribute to the reduction of the initial outlay in several applications. In the same vein, it serves as an efficient way to fully exploit the batteries before being disposed. But there are other technical considerations that should be taken into account, since the performance of second life batteries strongly depends on their first life usage. In the same way, the economic success is directly influenced by this factor as well.

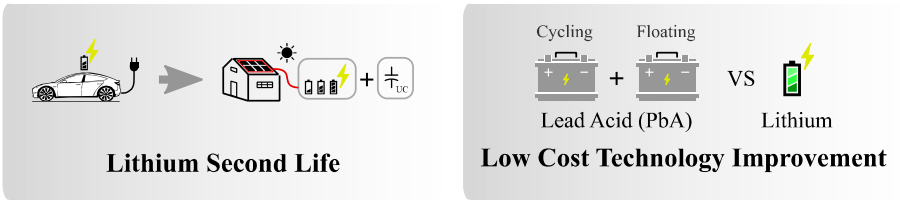

Fig. 1.6 Example of future potential HESS applications.

In any case, the hybridization concept offers multiple possibilities, as well as advantages and drawbacks as shown below.

The main advantages of HESSs are:

- *Performance improvement:* A case in which the hybridization could be useful, is when the instantaneous peak power is very high compared to the average power of the application. Additionally, in pulsed power applications, the hybridization of batteries and UCs achieves a reduction in the ripple content of the battery current, a fact which has been studied by many authors. As a result of this, it is possible to extend the battery life and provide better system performance. This will depend on the energy of each pulse, and the frequency of the pulsed consumption pattern.
- *Space saving:* For high instantaneous power applications, it is necessary to oversize the battery-pack in order to fulfil the peak power requirements. Some studies suggest that the use of HESSs makes it possible to obtain a smaller pack rather than using only one ESS technology.
- *Cost saving:* If the proportion of each storage technology that constitute the HESS is optimally selected, the final device will not only be more compact, but also cost effective. Together with this, if 'second life' batteries are used the initial outlay can be significantly reduced.
- *Reuse of batteries:* Hybridization concept makes it possible to take disposed batteries from demanding applications and reuse them for less demanding applications in complementary fashion with another storage technology.

Although the use of HESSs has advantages, there are some drawbacks as well:

- *Initial outlay:* The number of elements directly influences the final price, which may hamper the cost-effectiveness of the system. In some cases, the technical advantages offered by the HESS cannot justify the capital outlay. Thus, finding the best relationship between technical and economic aspects is of crucial importance.
- *Complexity:* Together with the points mentioned above, a greater amount of elements increases the overall system complexity.
- *Reliability:* A higher number of installed elements such as ESSs, control strategies and PECs, entails a greater failure probability of the system.
- *Control:* Another issue is the amount of different strategies that can be implemented in order to obtain a proper control of the HESS.

1.3 Degradation Mechanisms

In recent years, much is being said about the proper use of batteries and their lifespan extension. The way in which these batteries are used is a determining factor for that. In this context, there are several elements that negatively affect the battery life expectancy in power applications.

The principal factors that affect battery degradation are the temperature, high current rates, Depth of Discharge (DOD) and State of Charge (SoC). Indeed, not all factors affect each battery technology in the same way nor in the same proportion. In the case of high temperature and high current rates, it is widely known the negative impact of both factors for the great majority of battery chemistries [35]–[38]. However, taking PbA and Li-Ion batteries as an example, PbA technology results more affected under high temperature and current rates. In the case of DOD, although both technologies are affected when extremely depth discharges are performed, Li-Ion batteries are better able to handle this type of situations. With regard to the SoC, this affects both technologies almost inversely. While PbA experiments less degradation keeping it at high charge levels (floating mode), it is preferable to maintain the Li-Ion in a medium level SoC (between 20% and 80%) since out of this range its lifespan is reduced, particularly at high SoC [39]–[44].

Among the different degradation factors, temperature and current rate have the greater impact on the reduction of the battery life. Between both, we only can act upon the second one trying to reduce the stress suffered by the internal chemistry of the battery due to the high current rates. The main problems come from the heat generated due to high currents. As a result, this leads to an increase in Joule effect power losses which ends up causing excessive internal heat in the cells. This directly affects the behavior of the battery reducing its service life. In this context, the hybridization of these batteries with other storage devices (such as UCs) capable of providing high power peaks, may be the most suitable solution to consider. This will not only reduce the size of the storage system, but also its cooling system, if any.

Limiting the current rates in PbA batteries is not only a matter of trying to improve the instantaneous performance of the battery, but also a way of extending its service life.

This internal stress in PbA batteries, causes a temporary reduction in usable energy since the active material of the battery does not come into play in its entirety. But not only that, this intense use can reduce their service life due to different degradation mechanisms. Following on this subject, Li-Ion batteries present a higher robustness, indeed they are only affected if such current rates are much higher than for PbA.

As mentioned before, temperature is another key factor when working with batteries. It has direct influence in safety, performance and lifespan. Although the temperature does not affect all technologies in the same way, all are negatively affected by high temperatures. In PbA batteries for example, according to the Arrhenius law for every 10 degrees of increase in temperature, their life expectancy is reduced by half. Other battery technologies such as Li-Ion do not follow such degradation pattern, but they can present severe security problems. In this sense, if temperature is not maintained within safe limits, it is possible to trigger a chain reaction in which the battery can burn or even explode.

Nevertheless, high temperature operation is not the only factor that causes degradation in Li-Ion batteries. Low temperature conditions together with high charge rates may result in another way of degradation known as lithium plating [1]. Working under nominal conditions, there is no metallic lithium in the cell. However, under the charge conditions mentioned above, deposition of metallic lithium can occur. Depending on the anode material, the susceptibility of the cell to lithium plating varies [45]. On the one hand, graphitic anodes are more susceptible to lithium plating while on the other hand, lithium titanate anodes are less susceptible [45].

1.4 Objectives

The main goal of the thesis is the performance improvement of the existing energy storage systems, batteries in particular. To this end, the hybridization of different energy storage technologies has been considered as a promising option. The hybrid system should be able to provide high power and high energy at the same time. However, there is no single solution for all cases. In this sense, the design should be adapted in order to

obtain the best technical solution for each case study. The following objective is proposed to carry out this thesis.

Design and implementation of a Hybrid Energy Storage System, capable of improving the performance provided by a single storage technology.

To accomplish this main objective, the following points are fixed to divide the work to be carried out:

- **HESS topology selection:** Gathering and comparison of the most commonly used HESS topologies currently proposed in the literature.
- **Control strategies:** Revision of the currently used control strategies for these types of devices, as well as making an analysis of modern controls such as MPC.
- **Simulations:** Validate the topology and the control strategy via simulations.
- **Experimental validation:** Construction of an experimental platform to validate the simulations. This will require the design and building of bidirectional DC-DC converters.

1.5 Outline of the Thesis

Fig. 1.7 describes the structure of the thesis, gathering the different chapters according to the part of the work they represent.

As it can be seen in this figure, during Chapter 2 State of the Art references and publications about hybrid energy storage system topologies are reviewed. Therefore, a classification of the most relevant HESS topologies has been performed. To this end, a comprehensive analysis of the literature has been carried out. The benefits and drawbacks of each topology are presented and compared, so as to serve as an aid in future designs.

In Chapter 3, an overview of the most important energy storage systems is carried out. Together with this, the main requirements that have to be considered for battery and UC sizing are described. In this sense, some sizing examples are presented. Finally, battery and UC basic modeling techniques are explained.

In Chapter 4 our purpose is to develop the mathematical models of the hardware. The main purpose of this, is to develop a suitable controller design based on that models and serve as an aid for the control of the system.

Chapter 5 gathers the currently used control strategies for power converters together with modern control techniques. Multilevel and single-level control strategies are presented. Furthermore, different power sharing methods are analyzed in order to perform a suitable power distribution within the HESS.

Final Chapters (Chapter 6, Chapter 7, and Chapter 8) are focused on the experimental validation of the control techniques mentioned previously. Different scenarios are presented to finally validate the hybrid system in a real setting.

Finally, in Chapter 9 the most relevant conclusions and remarks are collected together with future research lines.

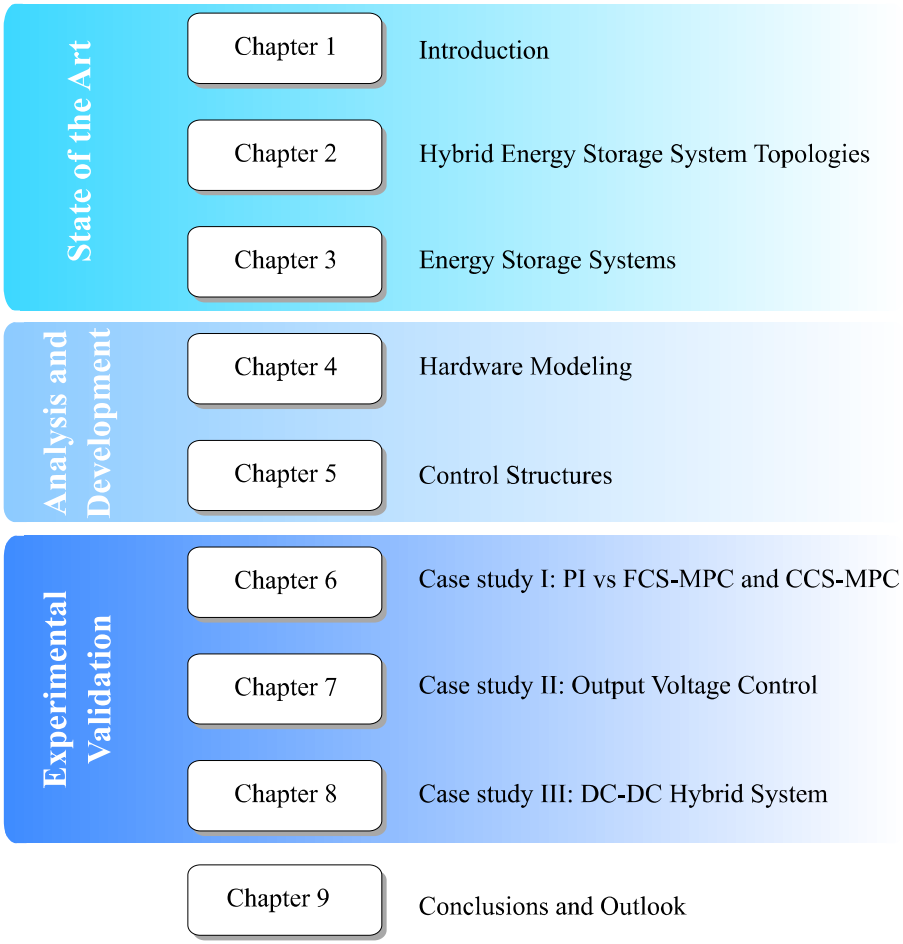

Fig. 1.7 Structure of the chapters of the thesis.

1.6 Scientific Contributions

- **Classification of Hybrid Energy Storage System topologies.**

  In this work, we propose a novel way of classifying Hybrid Energy Storage System (HESS) topologies. The classification is performed according to different parameters, such as the intermediate conversion stages or the layout. Following the abovementioned classification, benefits and drawbacks of each topology are analyzed and compared.

- **Single stage MPC for the HESS control**

  It is worth mentioning the novelty of using together the converter and storage device models for the control of a HESS using FCS-MPC. While other authors separate the MPC controller stage into different levels [46], [47], in this work all the necessary parameters to control the HESS were included in a single MPC cost function. This makes the algorithm more legible when programing while at the same time increases its execution speed.

1.7 Publications

Journal Papers

Sanz-Gorrachategui, I., Bernal, C., Oyarbide, E., Garayalde, E., Aizpuru, I., Canales, J. M., & Bono-Nuez, A. (2018). "New battery model considering thermal transport and partial charge stationary effects in photovoltaic off-grid applications." *Journal of Power Sources*, *378*, 311-321.

Sanz-Gorrachategui, I., Bernal Ruiz, C., Oyarbide Usabiaga, E., Bono Nuez, A., Artal Sevil, S. J., Garayalde Pérez, E., & Canales Segade, J. M. (2019). "Partial State-of-Charge Mitigation in Standalone Photovoltaic Hybrid Storage Systems". *Energies*, *12*(22), 4393.

Garayalde, E., Aizpuru, I., Iraola, U. Canales, J. M., Sanz-Gorrachategui, I., Bernal, C., Oyarbide, E., (2019) "Hybrid Energy Storage Systems: Review and Classification of Connection Topologies." *Journal of Power Sources*, → **Under revision**

Garayalde, E., Quevedo, D., Aizpuru, I. and Iraola, U. (2019) "Management of Hybrid Energy Storage Systems using Model Predictive Control." *IEEE Transactions on Energy Conversion* → **Under revision**

Conference Papers

Garayalde, E., Aizpuru, I., Canales, J. M., Sanz-Gorrachategui, I., Bernal, C., Oyarbide, E., (2017) "Análisis Experimental del Efecto de la Temperatura y la Tensión de Carga para la Optimización Energética de Sistemas de Almacenamiento de Instalaciones Fotovoltaicas Aisladas". In SAAEI 2017.

Garayalde, E., Aizpuru, I., Iraola, U., Sanz-Gorrachategui, I., Bernal, C., Oyarbide, E., (2019) "Finite Control Set MPC vs Continuous Control Set MPC Performance Comparison for Synchronous Buck Converter Control in Energy Storage Application." In ICCPE 2019.

Chapter 2

HYBRID ENERGY STORAGE SYSTEM TOPOLOGIES

During this Chapter State of the Art references and publications about hybrid energy storage system topologies are reviewed. Therefore, a classification of the most relevant HESS topologies has been performed. To this end, a comprehensive analysis of the literature has been carried out. The benefits and drawbacks of each topology are presented and compared, so as to serve as an aid in future designs.

Finally, main conclusions are resumed where the most interesting solution is presented. This will serve as a useful basis for the development of the research project.

2.1 Classification of HESS topologies

Several HESS topologies can be found in the literature, the majority of them focused on the hybridization of different ESSs operating in direct current (DC). However, the classification of different HESSs is not an easy task since certain authors refer to the same topologies using different nomenclatures. The present work therefore, sets out to classify HESS topologies in a unified way (Fig. 2.1). The first level in the chart refers to the connection mode between the storage devices and the energy bus. If the storage devices are connected to the bus by means of a PEC, the topology is considered *Decoupled*. On the other hand, if one or more storage devices are plugged directly into the energy bus in any of their operating modes, it is considered *Coupled*.

The following subdivision, depends on the interconnection between the different ESSs. For *Decoupled* topologies, in the case of having one single converter per storage device entirely dedicated to it, that topology is denominated as *Fully Decoupled*. Otherwise, it is classified as *Partially Decoupled*. Within the *Fully Decoupled* group, *Cascaded* and *Parallel* connection modes can be found. The difference between each, depends on the layout of the HESS.

In the case of *Coupled* topologies, as with *Decoupled*, those are divided into *Partially Coupled* and *Fully Coupled* configurations. The latter, frequently referred to as '*Passive Parallel*', has the particular feature of having all the energy storage devices plugged directly into the DC bus.

With regard to *Partially Coupled* topologies, these are divided into two subgroups: *Directly Connected* and *Switch Connected*. In the *Directly Connected* architecture, one of the energy storage devices is plugged directly into the DC bus without any type of

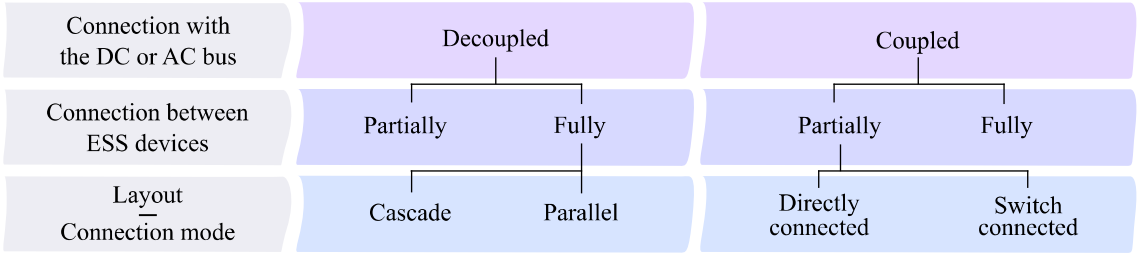

Fig. 2.1 HESS topology classification scheme.

interfacing system. While in the *Switch Connected* configuration, the storage devices remain isolated from the DC bus by means of a switch-diode set. In such cases, the connection moment and the energy transfer between the DC bus and the ESSs, can be partially controlled depending on the position of the diodes.

For some specific HESS configurations it is possible to install a diode in parallel to the PECs with the aim of bypassing them for some operating points [48]. The prime purpose of this, is to reduce the converter energy losses for high power handling applications such as electric vehicle (EV) [49], [50]. The disadvantage of this configuration is, however, its lack of discharge current control. Nevertheless, this bypassing technique has often been implemented in a number of the HESS topologies exposed in this review. These include the *Fully Decoupled*, DC bus connected *Partially Decoupled* and 2ESS *Directly Connected* topologies.

Many studies have been carried out to compare the performance of different HESSs [48], [49], [58]–[63], [50]–[57], but there is no single solution for every application. Besides, the behaviour of the installed storage technologies could influence the HESS topology selection. In the same vein, the unidirectional or bidirectional working mode of the bus-connected devices (Fig. 2.2) also has impact on the final decision. These types of systems composed of multiple devices connected to the same energy bus, together with ESS units constitute the basic structure of modern microgrids [64].

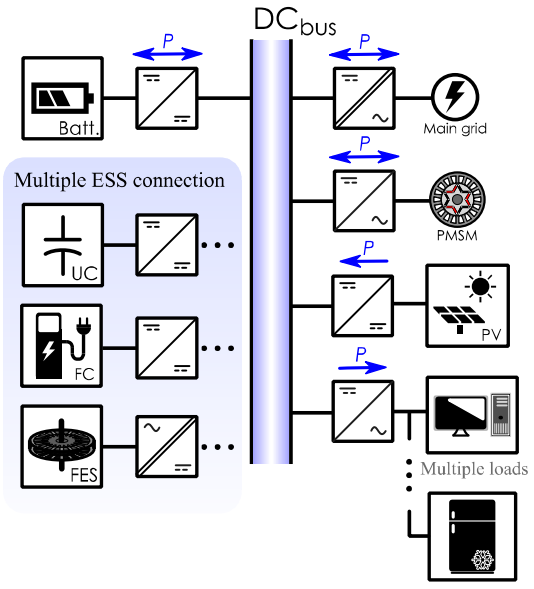

Fig. 2.2 Multiple DC bus connected devices.

2.2 Coupled topologies

2.2.1 Fully coupled

A greater number of power electronic converters increases the complexity and the power losses of the system. For this reason, simple and control-less topologies are also used. One clear example of this is the *Fully Coupled* topology (Fig. 2.3), also known as '*Passive Parallel*'. As in any type of hybridization, the main purpose of this configuration is to obtain a HESS pack with better characteristics than using only one storage technology. In this topology there is no control of the power sharing among the storage devices and it depends on the internal resistance of each ESS [65]. For this reason, the performance of both ESSs cannot be completely harnessed. In spite of this, the *Fully Coupled* topology has proved to offer an acceptable outcome for transient power events. It has been analysed in depth [66], [67] via simulations for constant and pulsed power loads with notable results. For constant consumption, the HESS has no noticeable enhancement compared to battery only ESSs. However, this topology shows a performance improvement in the case of pulsed power loads, due to the recharging of the UCs by the battery between each consumption pulse. In some other cases, this connection mode is used to prolong the battery life by using the UC as a peak power buffer [68]. In the same way, it was tested for vehicle start-stop applications [69]. In [70] a lead-acid battery only system, was compared to a UC-battery HESS for a nuclear plant uninterruptible power supply (UPS) application. In that particular case, despite PEC absence, this topology made it possible to reduce the installation space.

Apart from the typical configuration detailed above, there is a particular case where a switch-diode set is installed between both ESSs. This allows the disconnection of one storage device if necessary. Such a configuration was used in [71] for hybrid electric vehicle (HEV) application, where the regenerated energy was stored only in the UCs while preventing an uncontrolled battery recharge.

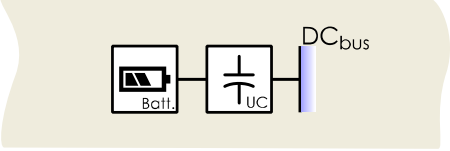

Fig. 2.3 Fully coupled HESS topology.

Benefits:

- Due to the lack of PECs, the cost and volume of the HESS are reduced.
- The implementation of a control strategy is unnecessary.

Drawbacks:

- The DC bus voltage, depends directly on the SOC of the storage elements.
- If a wide DC bus voltage variation is not allowed, the UC bank power capacity cannot be fully exploited.
- It is not possible to carry out an optimal power distribution between the different energy storage devices.
- If a higher bus voltage is required, an ESS serialization is completely necessary. A BMS is essential in that cases, which increases the complexity and the overall cost of the system.
- The considerable self-discharge of the UCs will also affect the battery SOC when the HESS is not used for a prolonged period of time.
- In the assembly and start-up moment of the HESS, it is necessary to carry out a UC pre-charging process before the battery-UC parallel connection, as mentioned in [72]. Otherwise, due to the voltage difference between the storage devices, high current levels could appear causing serious damage in both.
- Controlled energy transfer between both storage devices is not possible with this topology.

2.2.2 Partially coupled

The topologies under this denomination are characterized by having at least one of the storage devices connected to the energy bus. This connection can be performed directly without any type of interface elements, or by means of a diode-switch set.

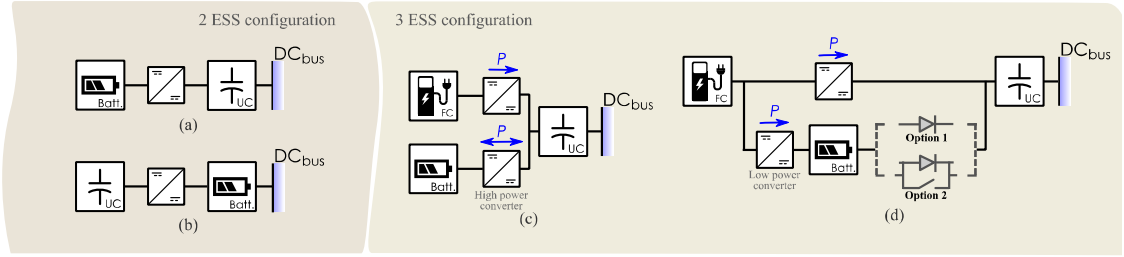

Fig. 2.4 Directly connected HESS topologies.

Therefore, the *Partially Coupled* topologies have been classified into *Directly Connected* and *Switch Connected*.

With regard to *Directly Connected* architectures, different configurations can be found in the literature in terms of ESS type, quantity and location of each device. Moreover, as can be seen in Fig. 2.4, there are two and three ESS configurations. *Directly Connected* 2 ESS configurations have gained interest for EV and photovoltaic (PV) applications, mainly thanks to their relative simplicity of control and reduced number of components. For this reason many authors have used them in their research [73]–[76]. There are two similar connection modes comprising this configuration. One has the UC bank directly connected to the bus, while the battery is decoupled by a DC-DC converter (Fig. 2.4a). Conversely, the second has the storage devices located in an inverted position (Fig. 2.4b). Both configurations have been widely used, but the one with the UC bank directly connected to the DC bus arouses greater interest. One of the reasons is its ability to absorb bus voltage variations without affecting the battery. The charge and discharge process of the battery can be accurately controlled, and thus extending its service life. Furthermore, as there are no interface elements between the DC bus and the UCs, the energy recovered from a regenerative braking can be more efficiently stored [76] [77].

The Fig. 2.4b connection mode is often implemented to improve the performance of systems formerly operated only by batteries. In this regard, in many lead acid powered applications, a UC - PEC set is added to the battery with the aim of extending the service life of the latter [72], [75], [78]–[83]. Due to the large amount of power managed by the UCs, a high power converter needs to be designed. An example of this, would be the 16 phase buck-boost interleaved converter built in [62] for traction applications.

In terms of interconnection with external equipment, these HESSs are normally connected to energy sources and loads by means of the DC bus. However, for some PV applications the converter responsible for implementing the maximum power point tracking (MPPT) algorithm is connected to the UC bank rather than the DC bus [75]. In such cases, the UC bank acts as a low pass filter supplying a smoother current to the battery.

Normally, the choice of using two ESSs for the HESS construction prevails over the multiple device options. However, combinations of standard topologies are sometimes used to create three ESS hybrid configurations (Fig. 2.4c and d). In this sense, different 3 ESS topologies composed of batteries, FC units and UCs have been studied in [84]–[86].

In Fig. 2.4c configuration, the regenerated energy can be stored in both the UCs and the battery. According to Bauman et al. [84], this topology is one of the most promising 3 ESS hybridization in the literature. Similarly, the same topology is used in EV applications with the particularity of exchanging the battery and UC positions [86]–[89]. This configuration has the disadvantage of using a high power converter to connect the battery with the DC bus.

The Fig. 2.4d topology was presented in [84], in order to improve the previous 3 ESS system performance. Compared to Fig. 2.4c topology, the mass, cost and power losses are minimized due to the converter size reduction. There are two different options in this architecture for interfacing the battery and the UCs. On the one hand, the first option consists of installing a diode allowing only the discharge of the battery, whilst, on the other hand, the incorporation of a switch-diode set allows the battery to charge from the DC bus. The latter option offers more operational flexibility, due to the battery charging capacity when a regenerative braking occurs.

Benefits:

- The direct connection of one storage device reduces power losses, as well as the overall cost of the system.
- It is possible to control the energy transfer between the storage devices. In Fig. 2.4 (d), this controllability is reduced due to the intermediate PEC suppression.

2ESS configuration:

- In Fig. 2.4 (a), the battery charge and discharge processes can be properly controlled, in this way lengthening its life.
- In Fig. 2.4 (b), the UC power capacity can be exploited in its entirety. The PEC located between both ESSs, allows the extraction of the energy stored in the UC bank without affecting the bus voltage.

- Due to the characteristics of each storage technology, the bus voltage will remain more constant in configuration (b) than in (a).

3ESS configuration:

- In both topologies, it is possible to store the regenerated energy not only in the UC but also in the battery.
- The (c) configuration, offers an accurate battery charge and discharge control due to the bidirectional converter.
- All the converters used in (d) are unidirectional, which means a decrease in cost and control complexity.
- The charge process efficiency is higher in (d) than in (c) due to the single conversion stage between the FC and the battery.

Drawbacks:

- In general, the directly connected storage device capacities are not completely harnessed.
- The DC bus voltage will depend on the SOC of the directly connected device.
- For high bus voltages, ESS serialization is unavoidable.

2ESS configuration:

- A wide DC bus voltage variation will occur in (a) if the UC bank is used in its entirety.
- In configuration (b), the battery energy is indirectly managed by controlling the UC currents, which is quite inaccurate.
- The PEC of (b) needs to be sized for managing the full power of the UCs, which increases the cost and size of the system.

3ESS configuration:

- The energy flow from the FC to the battery in (c) configuration needs to pass through two PECs, thus increasing the power losses.
- In contrast to the converters used in (d), those from (c) can manage more power, which increases the cost and size.
- In configuration (d), the switch and diodes used as interface elements between the main storage devices, makes it impossible to do a proper control of the current levels.

Switch Connected topologies (Fig. 2.5) have the singularity of using diodes and switches as interface elements between the ESSs and the DC bus. These topologies have been developed mainly for EV applications, due to the different operational modes they can offer. One of the most particular topologies is shown in Fig. 2.5a and was studied in [90] for the development of a EV prototype. This allows a series connection of the UCs and the PEC. Therefore, higher bus voltage levels can be obtained, while reducing the battery current demand. The energy stored in the UCs can be fully exploited in this configuration. When the energy of these is depleted, the control system automatically opens the switch and the diode bypasses the UCs leaving the load powered only by the battery. In the event of regenerative braking, the energy is stored only in the UCs by closing the switch, since the DC-DC converter leaves the battery disconnected.

The main characteristic of the topology shown in Fig. 2.5b is its simplicity and reduced number of components. As in the previous case, it has been studied for EV application [91]. In this case, PECs are not used and two switches are responsible for isolating the ESSs from the DC bus. When the switches are closed, there is no control over the power flow between the energy bus and the storage devices. In such an operating mode, it works like the *Fully Coupled* topology (Fig. 2.3).

With regard to Fig. 2.5c topology, there are two main layouts for interfacing the battery and the DC bus. On the one hand, D1 diode and S1 switch are used as interface elements; while on the other hand, D2, S2 and D4 are used. These two layouts have been more deeply studied in [57] and [92] respectively. Among the different operational modes, there are some common to both. In one of these, the UC bank is the only ESS directly connected to the DC bus by closing the S3 switch. In this mode, the energy transfer from the battery to the load is done via a DC-DC converter. If regenerative braking occurs and all the switches are opened, the bus voltage would rise above the UC bank voltage recharging it via the D3 diode. Moreover, in this configuration it is possible to transfer energy between the storage devices. This strategy is used to maintain the SOC of both ESSs at an appropriate level.

There are two possible modes to recharge the battery when the option 1 is used. One is the surplus power transferring through the PEC when the UC bank is fully charged, while the other consists of closing the S1 switch to allow a direct recharge from the DC bus. Furthermore, if the bus voltage drops below the battery voltage, the D1 diode will become forward biased, in this way discharging the battery. The charging via S1 and discharging via D1 takes place without a proper current control, which might not be the most appropriate working mode for the battery. In order to solve this problem, the option 2 incorporates an additional D4 power diode together with the reverse connection of D2. Therefore, an unexpected battery discharge is prevented and its charge process is always done in a controlled way via the DC-DC converter.

Benefits

- In configuration (a), the regenerated energy can be stored directly in the UC bank without the use of PECs, which increases efficiency.
- In (a), the converter can be sized for the battery voltage and current rates thus reducing the cost, weight and volume.
- Configuration (a) allows installing a low voltage UC bank, in this way reducing the number of serially connected devices. This eliminates the necessity of voltage balancing and reduces the equivalent serial resistance of the UCs.
- In the same way in (a), if a low voltage UC bank is used, it can be exploited in its entirety without significantly affecting the bus voltage stability.
- The configuration (b) is one of the simplest topologies due to the reduced number of components.
- The PEC absence in (b) provides a high charging and discharging efficiency.

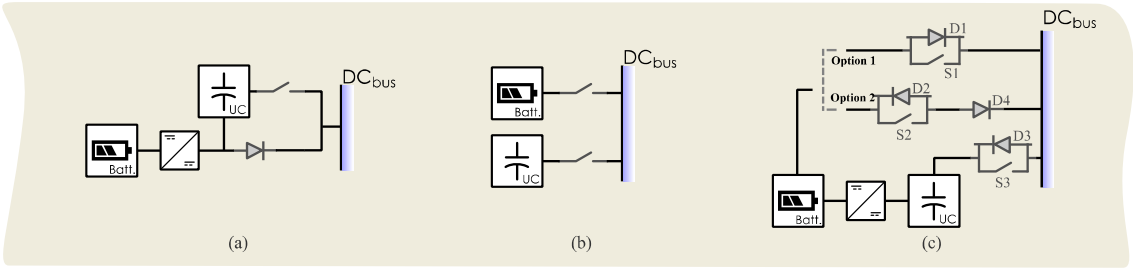

Fig. 2.5 Switch connected HESS topologies.

- For (c) configuration, the energy transfer between both storage devices can be done via the DC-DC converter and the battery charging process can be properly controlled.
- In configuration (c) option 2, an uncontrollable discharge of the ESSs cannot take place due to the diodes position.
- In (c) the PEC only needs to handle a portion of the total power.

Drawbacks

- When one of the storage devices is directly connected to the DC bus by means of a switch, the bus voltage will directly depend on its SOC.
- In configuration (a), the energy cannot be transferred from one ESS to the other, and the batteries cannot be charged from regenerative braking.
- In configuration (b), the power transfer between the energy bus and the storage devices cannot be controlled when the switches are closed.
- In case (c) option 1, if the DC bus voltage drops below the battery voltage level, the diode becomes forward biased and starts conducting regardless of the SOC of the battery. Depending on the battery technology this can cause serious damages.
- For configuration (c) option 2, despite being able to control the battery discharge moment with the S1 switch, when it closes there is no further control over the battery discharge current rates.

2.3 Decoupled topologies

2.3.1 Partially decoupled

In these topologies, both ESSs are decoupled from the energy bus by means of a bidirectional PEC. This allows an ESS terminal voltage variation without affecting the bus stability. In the configuration presented in Fig. 2.6a, the storage devices are connected in parallel without any type of interface element between them. In this case, the storage devices cannot be independently controlled, thus the power distribution will directly depend on the internal resistance of each device as in the *Fully Coupled* topology (Fig. 2.3). In [65], a mechanical switch is located in series with each storage device, to isolate them from the converter. This offers the option of disconnecting one or both ESSs, depending on the application requirements. In another vein, the storage devices are

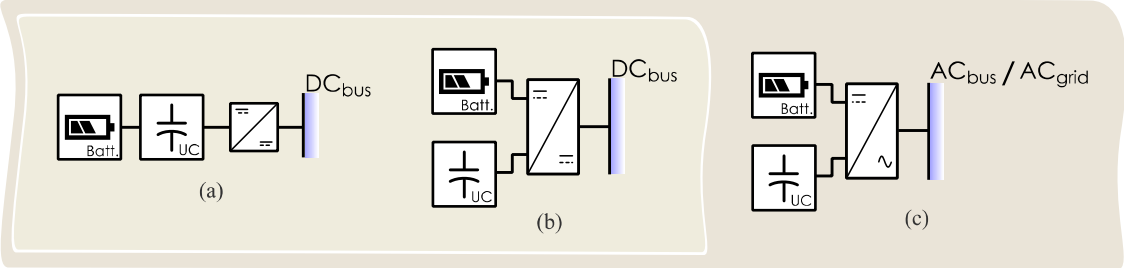

Fig. 2.6 Partially decoupled HESS topologies.

normally recharged from the DC bus via PEC, but an external charger is sometimes used for this work to recharge the batteries directly from the main electrical grid [49].

With regard to *Partially Decoupled* (b) and (c) topologies from Fig. 2.6, these are characterized by using multiple input PECs. Normally, HESS configurations are designed to work with DC energy buses, but in some cases, AC system configurations are also used. Regardless of being the same HESS configuration, the operation mode can be different depending on the converter used. In the case of DC bus connected configurations (Fig. 2.6b) [93], opted for a three half-bridge isolated multi-input PEC for combining storage devices with different voltage levels. This bidirectional multi-input converter topology was studied further in [94]. Another isolated multi-input PEC topology is presented in [95], for the hybridization of batteries and UCs. This particular configuration is not as common as that studied in [94], but proper simulation results have been reported with it. There is no single opinion about the economic feasibility of this multi-input DC bus connected topology. On the one hand, as mentioned in [50], this configuration is cheaper than those using one converter for each ESS. On the other hand, the authors of [57] say that the cost of the PEC is not suitable for the commercial market. What is clear, however, is that the complexity of the converters used for this particular topology, is higher than the rest. In any event, different multiple-input converter topologies have been analyzed in the literature [49], [96]–[99].

Continuing with multiple input converter topologies, AC bus connected configurations (Fig. 2.6c) have gained interest mainly for microgrid applications. An example of this, is studied in [100], where a 3 level neutral point clamped (NPC) converter is used for the hybridization of UC and vanadium redox battery. The main disadvantage of the 3L NPC converter is the lack of flexibility compared to other topologies studied

[101]. Apart from this, other different converter types can be found in the literature for similar purposes. In [102], [103] a typical Z-source converter was modified with the aim of building a HESS composed of a battery and a UC bank. This study showed it was possible to obtain a volume and cost saving due to the single conversion stage configuration. A variant of this, is the ΓZ-source converter used in [104] for the hybridization of batteries and FCs. Conventional PEC topologies, such as the boost converter, are also used for the same aim [105], [106]. These topologies, allow a converter power loss reduction due to a fewer number of conversion stages between the storage elements and the AC side. On the other hand, for the interconnection with an AC bus or microgrid, the implementation of a phase-locked loop (PLL) algorithm is necessary [107] which increases the system complexity.

Benefits

- The energy bus voltage is completely independent from the storage SOC.
- For configurations (a), (b) and (c), having only one converter increases the efficiency of the system. In the same way, the reduced number of PECs increases its cost effectiveness.
- Compared with other AC bus connected configurations, the use of the 3L NPC converter in (c) provides a significant reduction of power losses. This reduction is due to a smaller number of conversion stages.
- Furthermore, in (b) and (c) topologies, the energy management control can be done independently for each ESS.
- In (c), the use of one single conversion stage for the connection with an AC bus provides efficient energy management.

Drawbacks

- The use of multi-input PECs in (b) and (c), imply an increase of the control complexity compared to (a) topology.
- As in *Fully Coupled* topology (Fig. 2.3), it is not possible to do a proper energy sharing between both ESS in (a).
- It is not possible to transfer energy between the different storage devices due to the lack of control.

- Furthermore, the considerable self-discharge of the UCs will also affect the battery SOC when the HESS is not used for a prolonged period of time.
- In (c) the implementation of a PLL algorithm increases control complexity even further.

2.3.2 Fully decoupled

The main characteristic that describes *Fully Decoupled* topologies is the control flexibility they offer, which is achieved by the use of one PEC per storage device. However, there are two different connection modes, the cascaded and the parallel, each one with its features and specifications.

The *Cascaded* connection mode is quite similar to the *Directly Connected* topology shown in Fig. 2.4a and b, with the difference of incorporating an additional DC bus side PEC [60]. This extra converter provides voltage level decoupling, so that the DC bus voltage no longer depends on the storage SOC. However, this connection mode is not only used for DC systems, but also for AC microgrid applications [108].

As can be seen in Fig. 2.7a and b, there are two different HESS configurations under the *Cascaded* denomination. The response speed and performance of the system differs depending on the location of each storage device. In this sense, the transient power response of the HESS will be faster if the high power capacity device is closest to the energy bus. This needs to be taken into account especially for EV applications, where large amounts of power are managed in both accelerations and regenerative braking. Furthermore, it is quite normal to store the regenerated energy only in the UCs, which contributes to reducing the battery stress. This makes it possible to install a unidirectional converter in the middle of both storage devices [58].

The *Parallel* connection mode (Fig. 2.7c) is one of the most commonly used HESS topologies, primarily because it allows a direct control of each storage device. The flexibility that this topology offers makes it easily scalable in terms of power level and the amount of storage devices that can be installed. In this configuration, each converter is designed to manage the power levels of a single storage device, thus optimally sizing it. In addition, the efficiency of energy transfer between both ESSs is another factor to

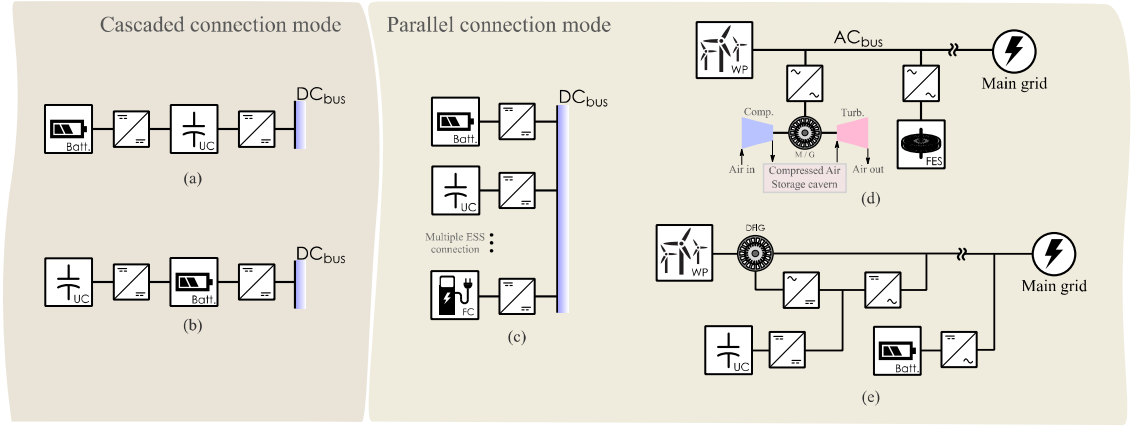

Fig. 2.7 Fully decoupled HESS topologies.

take into consideration. The flow of energy through two PECs, is less efficient than other cases where a single converter is used. To deal with this problem, some authors such as [109] propose the use of actively controlled switches to allow an optional PEC bypass.

The *Parallel* connection mode is not just limited to combinations of only two storage devices. In this regard, combinations of three ESS technologies have been made by different authors [52], [110]–[114]. In this regard, it supports the combination of nearly any type of storage technology, from the most common FCs, UCs and batteries [60], [65], [121], to the most unusual CAES and FES [52], [117]–[119]. In the *Parallel* connection mode, AC energy bus configurations are also used [108], [120]. This can be seen in [117], where a wind power generation plant is assisted by an FES and CAES hybridization (Fig. 2.7d). In an additional wind power application, a particular connection mode was presented in [121]–[123] for a doubly-fed induction generator (DFIG). In this case, UCs and batteries are used to achieve a performance improvement of a wind power generation plant (Fig. 2.7e). The battery pack is connected directly to the grid by means of a DC-AC converter; whereas the UCs are connected via a DC-DC converter to the DC bus of the back-to-back converter. Leaving aside wind power generation, but making use of the same connection mode, a FES - battery HESS was presented in [118]. In this case, the flywheel is located in the position formerly occupied by the DFIG, and the batteries are connected to the DC bus of the back-to-back converter replacing the UCs of the previous case.

Benefits:

- Each ESS can be sized to work with a different voltage level, which allows an optimal series-parallel design of the packs.
- The energy bus voltage is completely independent from the storage SOC.
- It is possible to carry out an optimal power distribution between the different energy storage devices.
- Due to the decoupling between the DC bus and the storage devices, the capacities of the latter can be fully exploited.

Cascaded

- The energy transfer between both ESSs is carried out by a single PEC, which reduces power losses.

Parallel

- This topology ensures the most accurate control for the charge and discharge of both ESSs at any time.
- The converters can be sized for the specific current and voltage requirements of each storage device.
- This topology is easily scalable as can be seen in Fig. 2.7c.
- In the case of failure of one PEC, the system could continue operating with a single ESS-PEC set.

Drawbacks:

- Despite obtaining a more optimized converter design, the use of one converter for each ESS tends to increase the cost of the HESS in comparison with other more simple topologies.
- In this context, a greater number of converters also means an increase in weight and volume.

Cascaded

- In the event of bus connected PEC critical failure, the whole system would go out of service.
- The bus connected converter needs to be sized for managing the full power provided by both ESSs, in this way increasing the cost of the HESS.

- The charge/discharge energy efficiency of the furthest storage device is lower due to the two power conversion stages.
- If the control of the PECs is not accurately designed, the charge/discharge currents of the furthest device can affect the behavior of the device closest to the DC bus.
- Cycling of the ESS in the intermediate stage.

Parallel

- The energy transferred from one storage device to the other needs to pass through two PECs, which makes this procedure less efficient than the cascaded one.

2.4 Discussion

A comparative analysis has been developed in Table 1 in order to highlight the features that determine the performance of the HESSs.

- *Volume:* The volume of the system directly depends on the interface devices (power converters and electro-mechanical switches) interconnecting the ESSs and the energy bus. A greater number of converters increases the total volume.
- *Cost:* Considering that the same types of storage technologies are selected for all topologies, the capital cost of the HESS will increase with a greater number of interface elements. The cost of the overall system increases due to a greater number of components. Furthermore, converter-based systems are more expensive than others using electro-mechanical switches.
- *Reliability:* The number and arrangement of the different components affect the reliability of the HESS. This feature jointly evaluates two aspects of the system. On the one hand, the capacity of the system to remain functional, at least in part, in the event of a failure. While on the other hand, evaluates its life expectancy.
- *Scalability:* This property indicates the ability of a HESS to increase its power capacity without losing performance. Depending on the application scale, not every topology is a proper option. Power converter based HESSs will always be more scalable, due to the flexibility that converters offer.
- *Modularity:* This feature compares the capacity of the HESSs to increase their rated power and energy in a modular way. These modules are composed of at least one storage device and its corresponding control module (power converter or switch).
- *Controllability:* The control capabilities depend directly on the interface stages. In this regard, power converters provide higher accuracy than electro-mechanical switches in the power and energy distribution.

Table 1:
Comparative evaluation of HESS topologies.

Feature	Partially Decoupled	Fully Decoupled		Partially Coupled		Fully Coupled
		Cascade	Parallel	Directly connected	Switch connected	
Volume	Medium	High	High	Medium	Mid-Low	Low
Cost	Medium	High	High	Medium	Mid-Low	Low
Reliability	Mid-Low	Mid-Low	High	Medium	Medium	Medium
Scalability	Mid-High	Mid-High	High	Mid-High	Low	Low
Modularity	Medium	High	High	Mid-Low	Low	Low
Controllability	Mid-Low	Mid-High	High	Mid-High	Low	None
Energy	Medium	Low	Medium	High	Mid-High	High

- *Energy efficiency:* This feature depends directly on the number of conversion stages or interface elements. The greater the amount of conversion stages, the lower the efficiency of the system. The type of interface element also affects, since converters generate more power losses than electro-mechanical switches.

As stated above, one of the main factors affecting the performance of the HESSs, are the interface elements. It is unavoidable the necessity to reach a compromise among the different features that determine the performance of the HESS. In any case, the most appropriate topology will depend on the specific characteristics of each application.

Fig. 2.8 shows the utilization rate of each topology in the articles under study. As it can be seen, *Fully Decoupled Parallel* and *Partially Coupled Directly Connected* are the most used topologies. With regard to the latter, it is noteworthy to mention that its main field of application is the electric and hybrid vehicle with the 87% dedicated to that. This is because it offers high energy efficiency together with a good controllability in the middle price range.

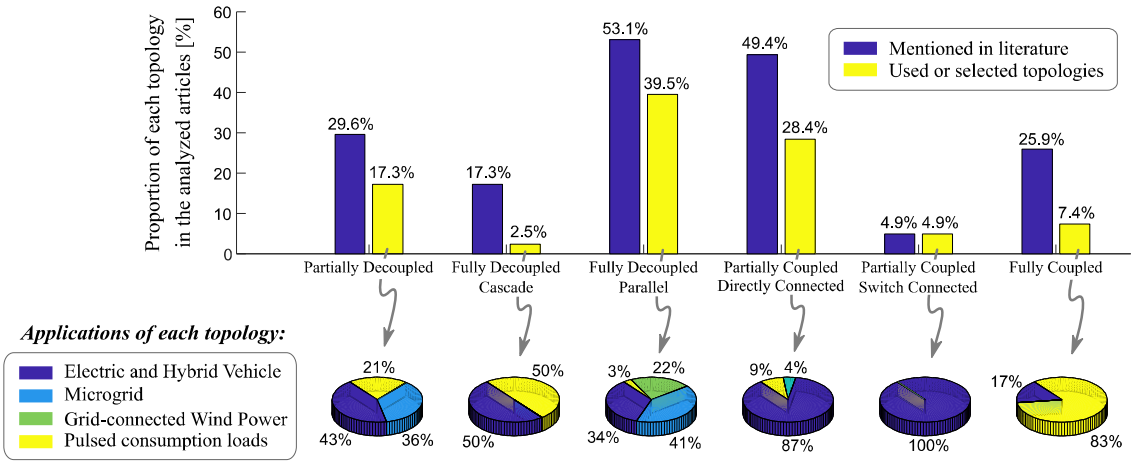

Fig. 2.8 Utilization rate of each topology and their applications.

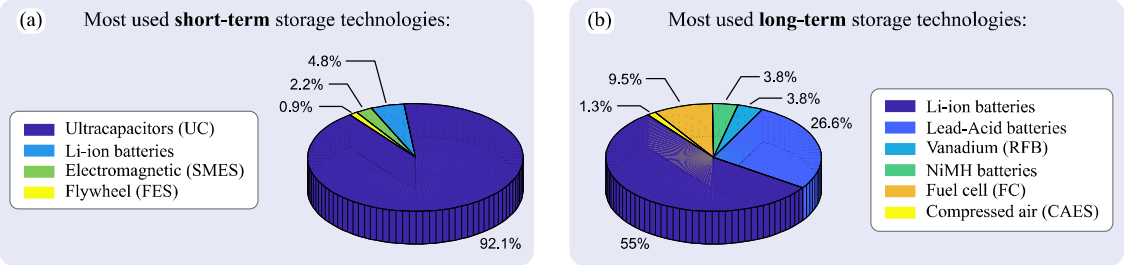

Fig. 2.9 Most used short-term (a) and long-term (b) storage technologies to develop a HESS.

In the case of *Fully Decoupled Parallel* topology, it is the most widely used one as it can be seen in Fig. 2.8. In contrast to other topologies, its use is not so concentrated in a single application. It also offers high scalability, controllability and reliability, which are very important aspects for microgrid and grid-connected wind power applications. Furthermore, due to the overall performance offered by this topology it is also suitable for EV and HEV applications, which represent a third of the total.

Fig. 2.9 shows the most used energy storage technologies for the development of HESSs. Among the short-term energy storage devices (a), UCs stand out as the most important ones since are used in the 92,1% of the analyzed hybridizations. The use of other high power density technologies such as SMES or FES is very limited and normally oriented to large scale applications.

With respect to long-term storage devices (b), the utilization rate of the different technologies is more distributed. In this high energy density group, various electrochemical storage devices prevail over the rest. However, Li-ion batteries are the first choice in the 55% of cases, followed by lead-acid batteries with the 26,6%.

Considering all the above, it can be said that the *Fully Decoupled Parallel* topology is the preferred option for many researchers. In addition to this, UCs are selected as the first option among short-term storage technologies. Regarding long-term storage devices, Li-ion batteries are the most popular ones followed by lead-acid batteries.

2.5 Conclusions

The difference between peak power and average consumption limits the performance of multiple applications. The hybridization of different storage technologies is emerging as a suitable solution to solve this problem. In this regard, several studies have been carried out with the purpose of identifying topologies and control strategies capable of meeting these needs.

Regarding the different energy storage devices, there are multiple options in terms of technology, power versus energy ratio and scale of the application. An analysis of the literature was made to observe the trends with regard to the number of studies or real installations using each storage technology. Taking this into account it can be said that the most common technologies used for developing the storage hybridization concept are electrostatic (Ultracapacitors) and electrochemical. Among the latter, Li-ion batteries stand out as the most used ones, followed by Lead-Acid batteries and Fuel cells.

After reviewing the most relevant benefits and drawbacks of HESSs, a classification scheme of the most widely used topologies has been presented. The different connection architectures have been divided into *Coupled* and *Decoupled*. In general, *Coupled* topologies are cheaper and easier to operate due to the reduced number of components such as PECs and control units. Among *Coupled* topologies, the *Fully Coupled* is the simplest configuration, as it has no PECs installed. In addition, *Partially Coupled* topologies present limited control flexibility, since one of the storage devices is plugged directly into the energy bus. Nevertheless, the latter have demonstrated their suitability for applications as demanding as EV.

Among *Decoupled* topologies, both *Partially Decoupled* and *Fully Decoupled* provide voltage level decoupling between the DC bus and the energy storage devices. *Fully Decoupled* configurations offer enhanced performance and better technical features than *Partially Decoupled*. They also allow a more accurate energy management, due to a greater number of PECs. In this sense, a greater number of converters makes it possible to apply different control strategies, but reduces the energy efficiency of the system. In general, the energy efficiency and control capacity are inherent to the topology used.

Finally, it is concluded that the *Fully Decoupled Parallel* connection mode is the most flexible HESS topology for the analysis. It also provides modularity and high scalability, which are important attributes to develop different configurations in terms of power scale.

Chapter 3

ENERGY STORAGE SYSTEMS

In this Chapter an overview of the most important energy storage technologies is carried out. Together with this, the main concepts and terminology related to batteries are described.

The main parameters to be considered in the battery and UC sizing process have been analyzed. In this case, different examples from the literature and from manufacturer data have been presented. Together with this, the main methods for battery and UC modeling have been presented.

3.1 Overview

There are many types of energy storage technologies, as it can be seen in Fig. 3.1, classified according to their physical characteristics. Each technology has weaknesses and strong points. For this reason, the choice of one or other will depend on the requirements of each particular use case. As a first stage, the application scale should be taken into account to select the most suitable energy storage technology. In this regard, mechanical and thermal technologies are more commonly used for large scale ESSs [117], as well as electromagnetic devices [124]. On the other hand, electrochemical and electrostatic storage devices are normally used for small scale ESSs. Nevertheless, there are exceptions among electrochemical storage systems as is the case of the redox flow battery (RFB), which is highly scalable and currently used for large scale storage applications [125].

Regarding mechanical storage systems, these can be divided into two groups. On the one hand, there would be the group of long-term storage devices composed of compressed air energy storage (CAES) [130] and pumped hydroelectric energy storage (PHES) [131]. Both are used for delivering a relatively constant power supply. On the other hand, flywheel energy storage (FES) [133], classified as a short-term device due to its fast response. The high power capability and the possibility of using it as a large scale ESS, makes it ideal to support the integration of renewable energy sources to the electrical grid [134], [135].

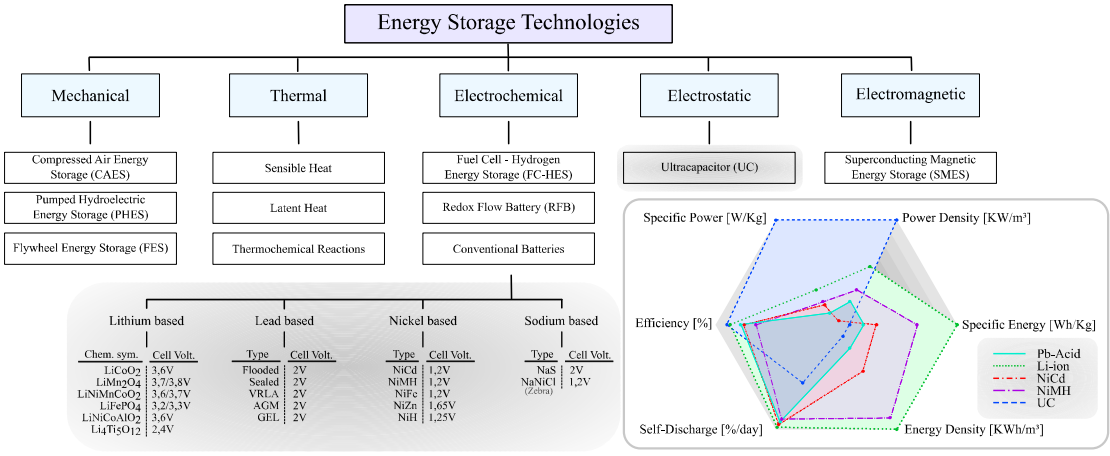

Fig. 3.1 Energy storage technology classification and brief comparison. [87], [126]–[132]

There are multiple thermal energy storage types, the most important of which are sensible heat, latent heat and thermochemical energy storage [136]. These systems are widely used as an effective way to store energy for some industrial processes, but uncommon for thermoelectric conversion apart from energy harvesting techniques.

Within the electric energy storage group, electrostatic and electromagnetic technologies can be found. Both of them are used as short-term storage devices due to their low energy density. Superconducting magnetic energy storage (SMES) is normally used for large scale applications, because of the high capital cost and the required cooling system. Recently, electrostatic devices have become more popular in countless applications. The high performance of ultracapacitors (UCs) as short-term devices has made them a suitable device for high power low energy applications. Developments in traction applications have launched this technology to the forefront of research. An example of this is the use of UCs for the braking energy recovery system in railway applications [137], [138]. UCs have been also used for special applications such as the start-stop system in automotive applications [139] or wind turbine pitch control system [140]–[142].

Among the different ESS technologies, electrochemical is the most predominantly used in commercial products. Fuel cells (FCs) and conventional batteries in particular, have experienced an increase in their use. On a separate issue, it should be noted that FCs are more appropriately classified as generation devices, but have been categorized as storage to adhere to common convention [128].

In this context, the most commonly used HESS configuration is comprised of electrochemical and electrostatic energy storage technologies. The electrostatic device supplies the power spikes, while the electrochemical one does so with the average power. A brief comparison of these devices has been done in the spider chart of Fig. 3.1. Among the benefits of the hybridization, battery life extension is one of the most important. In the case of lead acid batteries, their combination with ultracapacitors can ensure a reduction in the operating current rates. This improves the available capacity while reduces the early degradation. Lithium ion batteries support higher current rates than lead acid ones. However, they also undergo self-heating when dealing with high power spikes.

3.2 Classification and Comparison

3.2.1 Mechanical Energy Storage

Among the different mechanical energy storage systems, compressed air, pumped hydroelectric and flywheel are the most important ones. Compressed air energy storage (CAES) uses the surplus electrical energy to drive a compressor and then to store the compressed air into an underground cavern or a high pressure tank (Fig. 3.2). To recover the stored energy, the compressed air is released to drive a turbine and thus produce electricity. In this process, a small amount of fuel is burned in this air and after the combustion products are expanded through the turbine. This combustion process consumes significantly less fuel than a conventional gas turbine per unit of energy delivered, which reduces the greenhouse gas emissions [143]. One of the central applications for CAES is to balance the fluctuations in wind power plants. These types of applications require both large-scale and long duration energy storage. However, the use of this storage technology is directly conditioned by the geological features and wind resources of each particular location.

Pumped hydroelectric energy storage (PHES) is one of the most mature storage technologies for large-scale applications such as electrical grid applications. It is considered by different studies as one of the most feasible storage technology for the integration of renewable energy sources like photovoltaic or wind power [144]. In this case, the surplus electrical energy is used to pump water to an upper reservoir (Fig. 3.3).

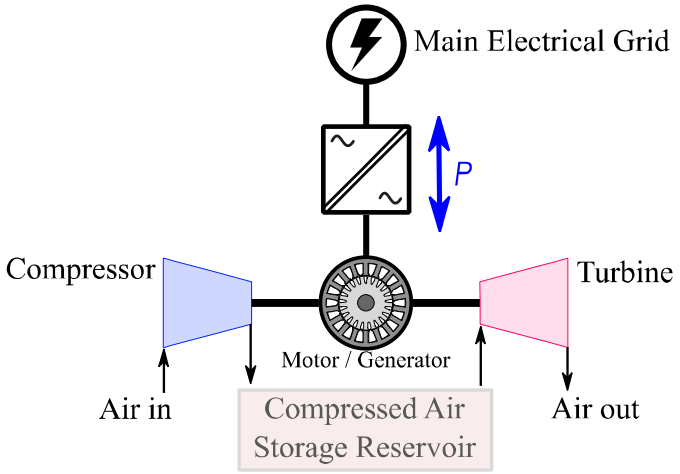

Fig. 3.2 Compressed Air Energy Storage (CAES).

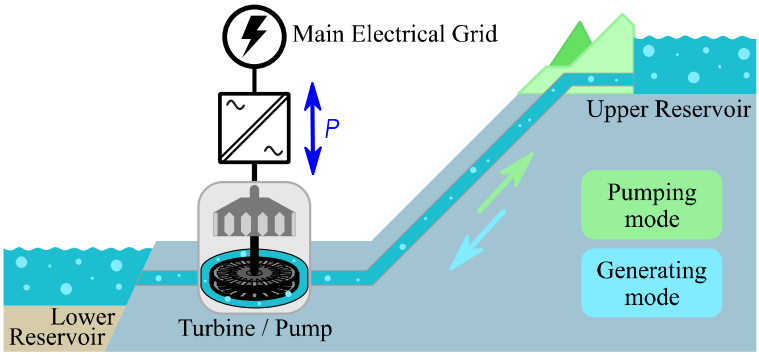

Fig. 3.3 Pumped Hydroelectric Energy Storage (PHES).

In this way, the off-peak electricity is transformed into potential energy for later use. To recover the stored energy, the water is used to drive a turbine to produce electricity. In some particular studies, a distinction is made between two types of PHES [145]. On the one hand there would be what is called pure PHES, whose operation principle is based exclusively on the water that is pumped from a lower reservoir to an upper reservoir. On the other hand there would be pump-back PHES, which consists of a combination of pumped water to the upper reservoir together with natural inflow. The latter is mainly installed in the course of some rivers. The selection of a commercially and technically feasible location is another important aspect to consider. The selected location should, among other things, provide an adequate difference in height between the two reservoirs and sufficient access to water.

The flywheel energy storage (FES) transforms electrical energy into rotational kinetic energy (Fig. 3.4). When storing energy, the rotor of the flywheel is accelerated thanks to an electrical machine coupled to it. In the opposite case, the electrical machine works as a generator discharging the energy stored in the flywheel in this way decreasing its rotational speed. Several years ago, the use of heavy materials like steel was very common for the flywheel construction. However, nowadays more modern materials such as carbon fiber or composites are used with the aim of reaching higher rotational speeds. The reason for this is that the energy stored in a flywheel present a linear relationship with respect to the moment of inertia, which is mass dependent, and quadratic with respect to the rotational speed. The possible applications of these devices can vary in terms of scale, since these can be manufactured in different sizes and energy densities. In this sense, it has been used in lots of applications such as electric vehicle, railway industry, renewables, power network, maritime industry and aerospace industry [133].

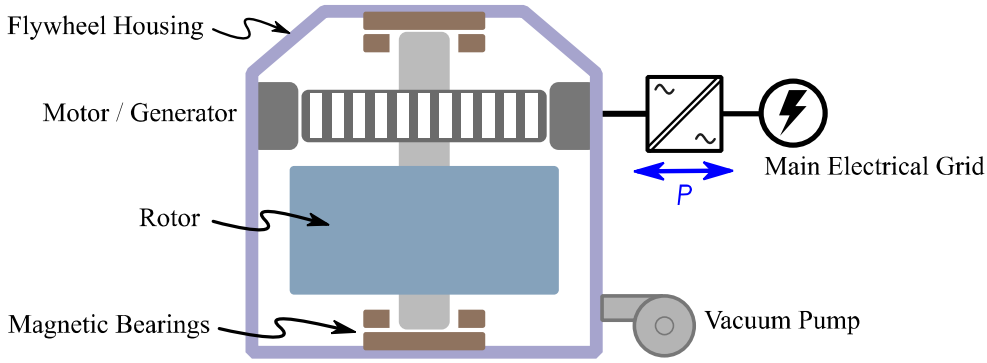

Fig. 3.4 Flywheel Energy Storage (FES).

With regard to the use of mechanical energy storage to develop a hybrid system, these technologies can be divided into two groups. On the one hand, the group of long-term storage devices composed of compressed air energy storage (CAES) and pumped hydroelectric energy storage (PHES). Both are used for delivering a relatively constant power supply for a long period of time. This period of time may vary depending on the particularities of each storage plant but it can range from several hours to some days. On the other hand, flywheel energy storage (FES), is classified as a short-term device due to its fast response. Its high power capability and the scalability that it offers, makes it ideal to support the integration of renewable energy sources to the electrical grid[134], [135]. The reaction time of the flywheel is very fast, being able to deliver high power levels for some seconds of even several minutes depending on the device.

3.2.2 Thermal Energy Storage

There are multiple thermal energy storage types, the most important of which are sensible heat, latent heat and thermochemical energy storage.

In the case of sensible heat, the material used to store thermal energy is not subject to phase changes during the process as it can be seen in Fig. 3.5(a). In this case, the temperature of the material increases linearly with the stored energy. Just the opposite happens in the case of latent heat energy storage, where the phase change of the materials is used to store energy (Fig. 3.5(b)). The abovementioned phase change normally consists of the transformation of the material from solid to liquid when energy is stored, and from liquid to solid when the stored energy is returned. For that purpose, there are some criteria to select the most appropriate phase change material for each case.

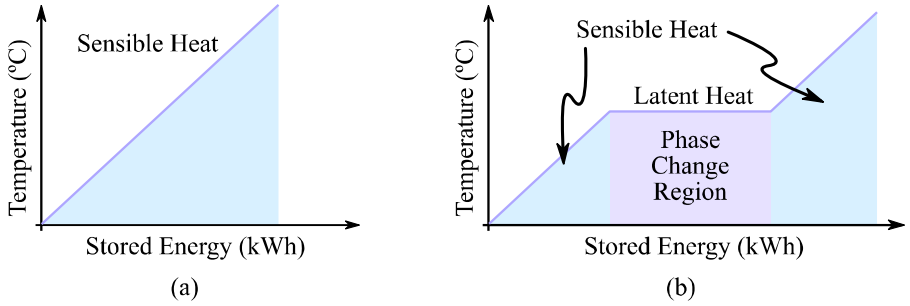

Fig. 3.5 Sensible Heat (a) and Latent Heat (b) Energy Storage Temperature vs. Stored Energy.[146]

- To have a melting point in the desired temperature range. (Phase Change Region)
- Small volume changes during phase transition.

Studies conducted to compare sensible heat and latent heat energy storage, have shown that the latter can provide a significant reduction in the device volume [147].

As far as the thermochemical storage system is concerned, it stores the energy making use of the heat to foster a chemical reaction that dissociates the reactants into two different byproducts which are stored separately (Fig. 3.6). The chemical reaction that takes place in the energy storage process is endothermic, while the reaction responsible for returning the stored energy is exothermic. These thermal storage systems are widely used as an effective way to store energy for some industrial processes, but uncommon for thermoelectric conversion apart from energy harvesting techniques. To date most of the studies have focused on sensible and latent heat energy storage.

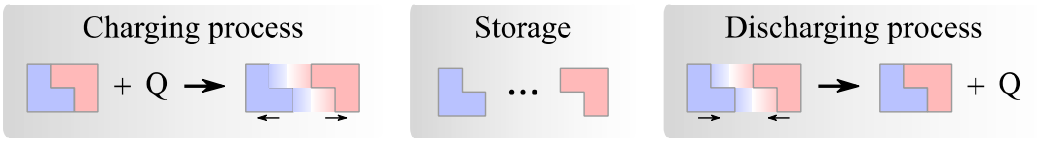

Fig. 3.6 Thermochemical Energy Storage.

3.2.3 Electrochemical Energy Storage

Within the electrochemical energy storage group, batteries are the most commonly used devices. They produce electricity with a certain voltage level thanks to electrochemical reactions. The voltage level of a single cell will depend on the specific chemistry used (Fig. 3.1). Thus, for higher voltages, multiple cells must be connected in series.

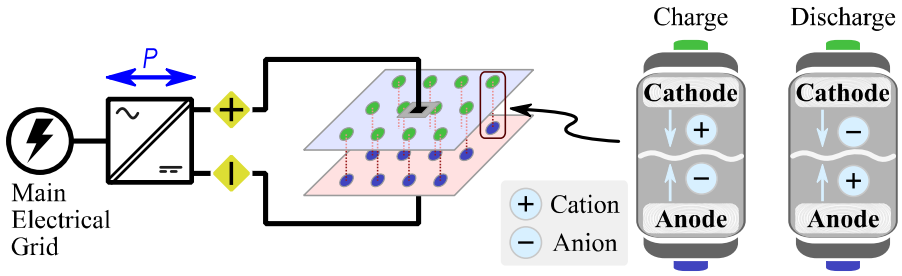

Fig. 3.7 Battery inner workings and ion motion.

Fig. 3.7 shows the simplified working principles of a battery. Each cell contains two electrodes, anode and cathode, submerged in electrolyte. The arrows represent the movement of the ions (anions and cations) through the salt bridge during both charge and discharge processes [129]. This salt bridge allows the ions to pass while blocking the passage of electrons.

In a two electrode battery configuration, the electrolyte provides both the cation and the anion which are intercalated into the anode and cathode [148]. From an external point of view, during discharge process the freed electrons flow as an electric current from the anode to the cathode [129]. On the other hand, during the charging process the reverse reaction occurs and the electrons flow from the cathode to the anode.

Leaving aside the general working principles of the batteries, each chemistry presents different and particular features. Batteries have become very popular due to the use in consumer electronics. Nevertheless, the choice of one battery technology or another will depend on each application requirements.

In this regard, lithium based batteries have gained greater popularity due to their use in electronic gadgets and electric mobility. They have a high energy density which allows to create relatively light products and with long autonomy. However, they also have weak points that must be solved using electronics and control. As it has been mentioned before, it is mandatory to maintain the lithium cell voltage always within safe operating range.

Another widely used technology is PbA, mainly due to its low price and safety in use. This technology has been used for very specific applications, among which Uninterruptible Power Supplies (UPS) and photovoltaic installations stand out. Both

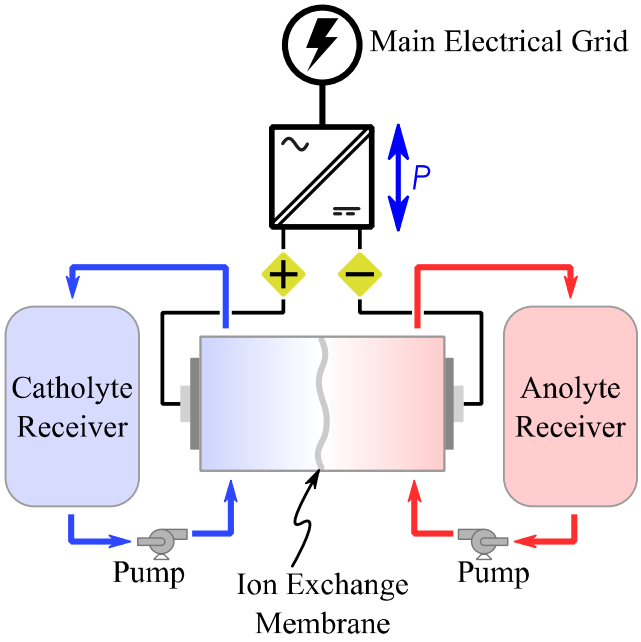

Fig. 3.8 Redox Flow Battery (RFB).

applications are characterized by providing long floating periods to the battery with SOC levels close to 100%, which is an ideal feature when working with PbA.

Apart from conventional batteries, there also exist the so called Redox Flow Batteries (RFB) (Fig. 3.8). In these kinds of batteries, all the electro-active materials are dissolved in a liquid electrolyte. This is the main difference compared to conventional batteries, in which the electrochemical reactions create solid compounds that are stored directly on the electrodes. These batteries have some advantages over conventional batteries in terms of power and energy sizing. In this sense, a high power RFB can be designed without the need to increase the energy density, which avoids the oversizing of the battery. This is possible due to the fact that power and energy sizing mechanisms are independent. In the same way, a longer durability can be achieved since the electrodes do not undergo physical and chemical changes during operation.

Lastly, with regard to electrochemical storage technologies, Fuel Cells are increasingly used for traction and grid applications. The Fuel Cell – Hydrogen Energy Storage (FC-HES) is composed of three main stages. The first stage is the water electrolysis unit, where the electrical energy surplus is used to generate hydrogen. Secondly, the generated hydrogen is stored. This can be done as compressed gas, liquefied

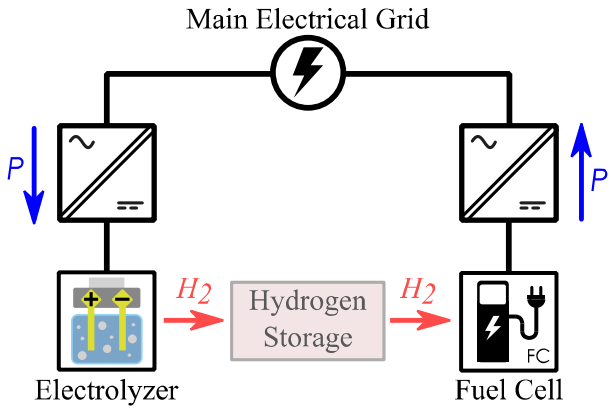

Fig. 3.9 Fuel Cell – Hydrogen Energy Storage (FC-HES).

gas, metal hydrides or carbon nanostructures. Finally, a fuel cell is used to convert the stored hydrogen back into electrical energy.

3.2.4 Electrostatic Energy Storage

Normal capacitors consist of two electrodes separated by a dielectric. The dielectric separator is commonly made of solid non-conductive materials like glass, paper, plastic or ceramic. In this case, the energy is stored in form of electrostatic potential by oppositely charging the two electrodes (Fig. 3.10). These oppositely charged electrodes generate an electric field across the dielectric in this way generating a voltage difference.

The amount of energy (E) that can be stored in a capacitor will directly depend on construction parameters like capacitance value, and the voltage (V) level (eq.(3.1)). Thus, its capacitance (C) is directly proportional to the surface area (A) of the electrodes and the dielectric constant (ε) while it is inversely proportional to the distance (d) between the electrodes (eq.(3.1)) [149].

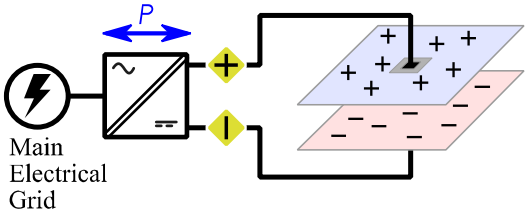

Fig. 3.10 Electrostatic Energy Storage.

$$E = \frac{1}{2} C V^2 \quad \rightarrow \quad C = \frac{A \cdot \varepsilon}{d} \tag{3.1}$$

Ultracapacitors are slightly different than ordinary capacitors, since they have an ion-permeable membrane together with an electrolyte solution between the electrodes instead of solid dielectric [150]. In this sense, it can be said that UCs employ two forms of energy storage: electrostatic storage and electrochemical storage [149].

3.2.5 Superconducting Magnetic Energy Storage

SMES system stores energy in a magnetic field created by the flow of direct current through a superconducting coil [150], [151] (Fig. 3.11). In order to obtain a nearly zero electrical resistance, the superconducting coil needs to be cryogenically cooled below the critical temperature of its superconducting material.

A power electronic converter is required to operate this storage device. It is responsible for the charge and discharge of the coil maintain the current within safety limits. The electrical current introduced in the coil is limited by the critical current density of the coil material. If this value is exceeded the material will move out of its

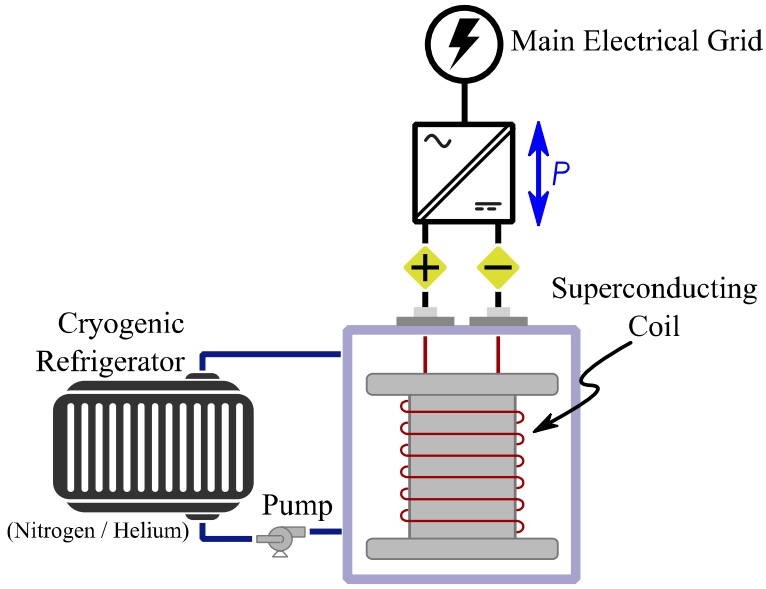

Fig. 3.11 Superconducting Magnetic Energy Storage (SMES).

superconducting state in this way increasing its electrical resistance. Modern SMES devices use ceramic superconducting coils in order to manage higher current densities.

The short reaction time of SMES compared to other energy storage systems, is one of its main advantages. Due to its internal operating mode, there is almost no time delay in dealing with abrupt power changes, thus causing the control electronics to limit its dynamics. In the same way, since this technology is motionless and it does not present any chemical reaction, it is suitable for applications involving a large amount of charge/discharge cycles.

3.3 Battery and UC Hybridization

Batteries are the most widely used ESS technology when working with small-scale electric power. In the same vein, the use of UCs is on the raise due to their ability to support high charge-discharge power levels, which is very useful in some applications.

As it has been mentioned before, these two storage technologies present opposed characteristics in terms of power and energy. This is clearly reflected in the Ragone Plot (Fig. 1.2) where the different battery technologies and UCs are graphically classified according to their power and energy densities. In this context, the hybridization of batteries and UCs is expected to have direct benefits for applications were both characteristics are required.

In order to determine numerically the potential benefits of the hybridization, it is of vital importance to first analyze the sizing process of each technology individually. By doing this, the points that cause oversizing in the design of battery packs can be observed.

If the storage system is uniquely composed of batteries, it may be necessary to increase the installed capacity in order to deal with consumption power spikes. On the other hand, if the storage system is only composed of UCs, a hypothetical application with a medium to high average energy consumption will make it necessary to oversize the UCs considering their relatively low energy storage capacity. Taking into account both scenarios, the final task is to perform a more optimized sizing that ensures a better

use of each storage device comprising the HESS. This will be further analyzed in subchapter 3.4.

Normally the sizing is done based on predefined operating parameters of an application. However, in order to know how these parameters affect dynamically in the normal operation, it is necessary to obtain a reliable model of the storage system. This model will serve to verify that the system is properly sized without physically building it. The basic steps to develop battery and UC mathematical models are presented in the subchapter 3.5.

Before proceeding, in order to familiarize the reader with the most used terms in the field of batteries, it is referred to Annex A.

3.4 Sizing

When performing the sizing for an application that uses one single storage technology, it must be ensured that the selected storage device fulfills both the power and energy requirements of the application. In this sense, an iterative calculation is usually done until both requirements are met.

The need to meet both requirements often generates an excessive oversizing of the storage system, which results in higher initial costs and suboptimal use of the storage system capabilities. This is where the development of a hybrid system could come into play. The hybrid system would be sized decoupling the two variables and sizing them considering the consumption profile of the application.

Although the main objective is always the optimal calculation of the storage system, all the designers apply a safety coefficient in their final calculations in case of working under unfavorable conditions.

The first step is always the selection of the storage technology to be used. For this purpose, it must be taken into account both the consumption profile of the application and the environment in which it will work. Although in this case the study is focused on batteries and UCs, environmental factors are an important aspect when selecting the right electrochemistry. Once the storage technologies to be hybridized are selected, the sizing process starts. This process requires the series-parallel association of multiple cells, as explained in the following point.

3.4.1 Series-parallel association

The chemistry of a battery fixes its cell voltage range. In this sense, depending on voltage and capacity requirements of each application, cell association is unavoidable to obtain bigger packs. The battery-pack is a combination of cells mechanically and electrically connected. The voltage of the pack is the sum of all the individual cell voltages. Assuming that all are equal, then we have:

$$v_{pack} = n_s \cdot v_{cell} \tag{3.2}$$

In these cases, the cell voltage needs to be controlled in order to maintain the charge level as equal as possible in all cells. When an unbalance occurs, the battery management system (BMS) together with different cell balancing techniques, are responsible for compensating the charge level of each cell [152]–[154].

For high current battery-packs, it is necessary to connect cells in parallel. The resulting current will be the sum of all the parallel cell currents as it can be seen in equation (3.3). The same happens with the total capacity (equation (3.4)). The parallel connection of several cells increases the total capacity of the pack while reducing the current rate for a given power consumption level.

$$i_{pack} = n_p \cdot i_{cell} \tag{3.3}$$

$$C_{pack} = n_P \cdot C_{cell} \tag{3.4}$$

The battery-pack construction is often done using modules. Each module comprises a small group of series and parallel connected cells. The modules are connected in series and/or parallel to fulfil the overall battery-pack objective. This simplifies the design and reuse of the same modules for multiple applications.

The nomenclature used for the battery-pack identification is based on the amount of serial (S) and parallel (P) connected cells. An example of this is shown in Fig. 3.12.

$$n_S\mathrm{S}\,n_P\mathrm{P} \rightarrow \begin{cases} n_S : \text{Number of cells in series.} \\ n_P : \text{Number of cells in parallel.} \end{cases}$$

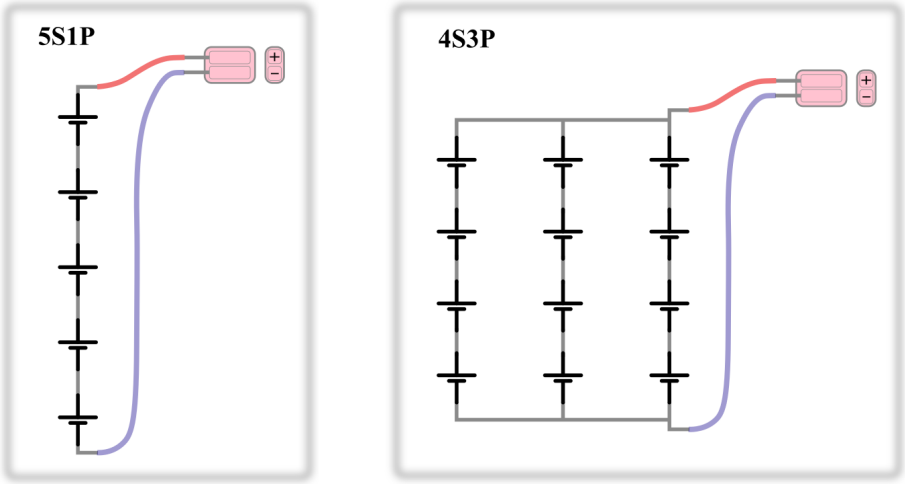

Fig. 3.12 Example of battery-pack construction nomenclature.

In the same way as with the batteries, the series-parallel association of multiple UC cells is unavoidable to fulfill the voltage and energy requirements. In the case of UC cell association, the resulting capacitance and equivalent series resistance (ESR) is calculated in the same way as for normal capacitors. In a series connection, the capacitance (equation (3.5)) and ESR (equation(3.6)) is calculated as follows:

$$\frac{1}{C_{pack}} = \sum_{i=1}^{n_s} \frac{1}{C_i} \tag{3.5}$$

$$ESR_{pack} = \sum_{i=1}^{n_s} ESR_i \tag{3.6}$$

Where C_{pack} is the total capacitance of the series connected UC cell array, and ESR_{pack} is the resulting equivalent series resistance. For the case of parallel association of multiple cells, the resulting capacitance (equation(3.7)) and ESR (equation(3.8)) is calculated as follows:

$$C_{pack} = \sum_{i=1}^{n_p} C_i \tag{3.7}$$

$$\frac{1}{ESR_{pack}} = \sum_{i=1}^{n_p} \frac{1}{ESR_i} \tag{3.8}$$

3.4.2 Battery sizing

Battery sizing is not a trivial task since many parameters that affect its performance are beyond our control. The particularities of each application can also affect the amount of variables to be considered for the correct ESS sizing. The sizing of regular batteries has been studied by different authors for standalone photovoltaic applications [155], [156] where solar panel production capabilities and the storage capacity are determining factors. In general terms, variables such as the level of autonomy or the probability of not being able to supply the load under low photovoltaic generation, are important design parameters specific for this kind of applications.

In the same way, past experience and manufacturer guidelines are often used to define the required battery capacity. Continuing with standalone photovoltaic systems, it is common to find manufacturers that give some tips for lead acid battery sizing. Among these guidelines and recommendations, one or more correction factors are usually applied to compensate the effect of temperature, aging, and other causes that affect the performance of lead acid (PbA) batteries. The following is an example of lead acid battery sizing calculation for standalone photovoltaic application [157].

C_{pack}: Capacity of the total battery pack [Ah]

C_{day}: Amp-hour Consumption per day [Ah]

Tc: Temperature Correction Factor
- ► Correction factors for PbA batteries are shown in (Table 2)

DA: Days of Autonomy
- ► Aprox. Range: 2-10, Recommended for standalone solar: 5

DM: Design Margin
- ► Range: 1-1.25, Recommended: 1.10

DoD: Depth of Discharge
- ► Max. recommended 20%, and occasionally 80% during cloudy days.

$$C_{pack} = \frac{C_{day} \cdot Tc \cdot DA \cdot DM}{DoD} \tag{3.9}$$

Table 2:
Temperature correction factor for Lead Acid batteries [157].

Temperature [°C]	Lead Acid Battery Technologies		
	Flooded	AGM	GEL
25	1.00	1.00	1.00
10	1.19	1.08	1.11
0	1.39	1.20	1.25
-10	1.70	1.35	1.42

Other manufacturers such as Saft [158], perform a similar calculation for Nickel-Cadmium (NiCd) batteries in photovoltaic application. In this case, instead of using tables they use predefined curves to select the proper correction factors. In general terms they perform the sizing in a similar way to the previous case, with the only difference of using an aging compensation factor instead of the design margin factor.

C_{pack}: Capacity of the total battery pack [Ah]
A: Required Autonomy [h]
L: Daily Load Consumption [A]
Ac: Ageing Compensation Factor (Fig. 3.13(a))
Tc: Temperature Correction Factor (Fig. 3.13(b))
Dc: DoD Correction Factor (Fig. 3.13(c))

$$C_{pack} = A \cdot L \cdot Ac \cdot Tc \cdot Dc \qquad (3.10)$$

Historically, PbA batteries and large format NiCd cells have been used in autonomous photovoltaic installations. Nevertheless, the environmental problems derived from the recycling process of NiCd batteries have caused their use to decrease. Since the power requirement of this kind of applications is quite constant and normally below 5kW, the capacity of the battery needs to be oversized to ensure at least 5 years of service life.

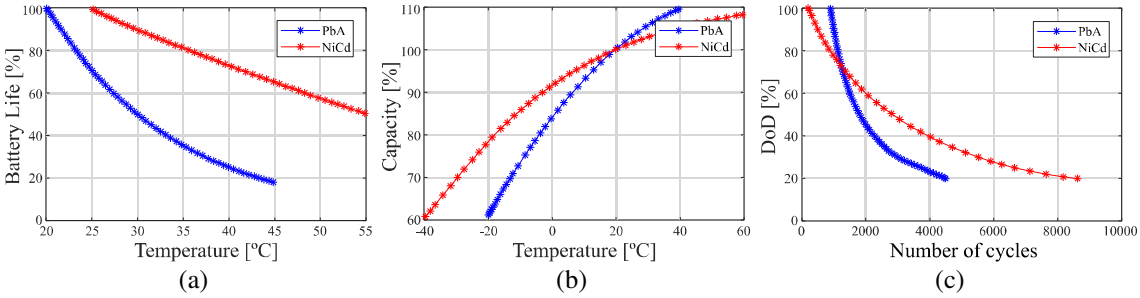

Fig. 3.13 Data provided by PbA [159] **and NiCd** [158] **battery manufacturers. (a) Battery life reduction depending on temperature. (b) Instantaneous available capacity depending on temperature. (c) Number of cycles the battery can perform depending on the DoD.**

3.4.3 UC sizing

As it happens in the case of batteries, the required number of UC cells is directly determined by the application. However, in this case there are certain design parameters that differ with respect to the battery sizing. One of the most significant is the voltage range in which the application should operate. This point is not only important to determine the number of cells connected in series, but also to calculate the total capacity that the entire storage device must have. This can be seen in the equation (3.1), which defines the energy stored in a capacitor. This shows a quadratic relationship between the stored energy and the voltage

That is why normally the minimum voltage level for the UC is set at 50% of the rated voltage, since at this point the 75% of the energy will be already depleted [160].

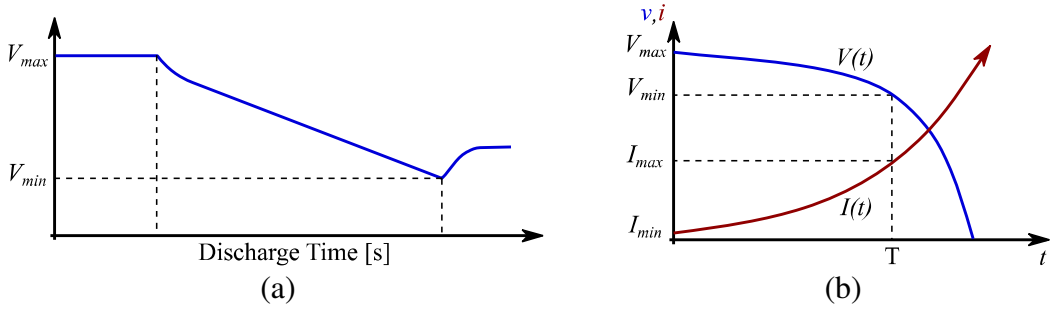

Fig. 3.14 (a) Voltage evolution of UC discharge under constant current profile. (b) Voltage and current evolution of UC discharge under constant power profile.

In order to determine the capacitance value for the UCs, apart from the operating voltage range, the average current and the time constant of the capacitor should be considered [161].

$$C_{UC} = \frac{i}{V_{\max} - V_{\min}}(\tau) \tag{3.11}$$

This sizing procedure is valid for constant current discharge profile (Fig. 3.14 (a)) but not for constant power discharge (Fig. 3.14 (b)) where we have:

$$V_{\min} = \sqrt{V_{\max}^2 - \frac{2 \cdot P \cdot T}{C}} \tag{3.12}$$

3.4.4 HESS Sizing

In order to perform a correct sizing, it is necessary to take into account the effect of variables such as temperature or charge/discharge current, over the rest. In this sense, it is convenient to perform several iterations to achieve a more optimized value. After all, the previous sizing examples only provide an approximate capacity value. Another key aspect is the Energy Management Strategy (EMS) followed by the application control algorithm. This EMS may include some operating constraints that must be considered in the design process to ensure that the HESS can deliver the performance demanded [162].

On the technical level, the first step is to define the consumption profile of the application, and also the production capabilities in the case of stand-alone photovoltaic systems. Once this is known, it is necessary to know how the EMS will work and the power constraints it will apply to each storage device. Finally, after knowing the maximum allowed power for the HESS, the autonomy is defined for the worst case scenario and the sizing process is developed accordingly.

In renewable energy source applications like isolated wind energy, the sizing is performed in a similar way. Authors like [163] define the sizing criteria on the basis of the peak load power and average energy demand. The same sizing criteria is often considered for isolated photovoltaic systems [160]. Nevertheless, recent studies bring a new approach that goes beyond the classic HESS sizing criteria. In [164], a HESS composed by lead acid (PbA) batteries and Li-ion batteries was installed in a stand-alone PV system to mitigate the Partial State of Charge (PSoC) problem caused by daily shallow charge-discharge cycles. Its main contribution is the development of the HESS sizing so

that the PSoC effect of PbA batteries is reduced making use of a small amount of Li-ion batteries.

Some other studies focused on electric vehicle (EV) application perform the sizing by means of an optimization where the driving performance requirements are introduced as the optimization constraints [162]. In this kind of applications, maximum speed, acceleration time or driving autonomy are determinant parameters to be considered in order to define the capacity of each energy storage device as well as the hybridization ratio.

Apart from technical criteria, several authors working on the abovementioned applications focus more on economic aspects, thereby considering the ESS degradation cost as the principal parameter to perform the HESS sizing. This can be clearly seen in

Table 3, which contains a summary of different articles found on the literature about HESS sizing topic. It is true that technical parameters are always taken into consideration for the sizing. However, in most of the studies the HESS sizing criteria is based on cost optimization. The evaluation of these costs is not always done in the same way, but the main aspects to consider are the initial outlay, maintenance cost and cycle life of the storage devices. As stated above, the latter is not a fixed value and will always depend on the specific working conditions suffered by the ESS.

Table 3:
Summary of literature on sizing Hybrid Energy Storage Systems.

Application	Storage Technologies	Sizing Optimization Criteria	Year	Ref.
PV in Household app.	Batt / UC and FC-HES	Better use of generated energy.	2007	[165]
Stand-alone PV	PbA batt. and FC-HES	Cost optimization while satisfying application performance.	2009	[166]
Stand-alone Wind Pow	PbA batt. and UC	Decoupling of peak power and average consumption.	2010	[163]
Stand-alone PV	PbA batt. and UC	Decoupling of peak power and average consumption.	2012	[160]
Stand-alone PV	PbA batt. and FC-HES	Better use of generated energy while being cost effective.	2012	[167]
EV (Traction app)	Batt. and UC	Cost optimization while satisfying application performance.	2012	[168]
Microgrid	UC and FC-HES	Decoupling of peak power and average consumption.	2013	[169]
HEV (Traction app)	Li-Ion batt. and UC	Minimum ESS cycle life cost with ESS power constraints.	2013	[170]
EV (Traction app)	Li-Ion batt. and UC	Cost optimization while satisfying application performance.	2014	[171]
PV and Wind Pow	Batt. and UC	Cost optimization while satisfying application performance.	2014	[172]
Wind Power	PbA batt. and UC	Minimum ESS cycle life cost with ESS power constraints.	2015	[28]
Microgrid	Batt. and UC	Cost optimization while satisfying application performance.	2015	[173]
EV (Traction app)	Li-Ion batt. and UC	Minimum ESS cycle life cost with ESS power constraints.	2015	[82]
Stand-alone Wind Pow	Batt. and UC	Power balance and system stability at the lowest cost.	2015	[174]
EV (Traction app)	Li-Ion batt. and UC	Cost optimization while satisfying application performance.	2016	[175]
Household	PbA batt and SMES	Decoupling of peak power and average consumption.	2016	[176]
PV (Trigeneration sys)	PbA batt and PHES	Cost optimization while satisfying application performance.	2016	[177]
PV, Wind and biomass	PbA batt. and FC-HES	Optimal long-term energy management.	2016	[178]
Microgrid	Batt. and FC-HES	Cost optimization while satisfying application performance.	2017	[179]
Stand-alone PV	PbA batt. and UC	Minimum ESS cycle life cost with ESS power constraints.	2018	[180]

3.5 Modeling

The principal aim of the battery and UC models is to replicate the real behavior of the storage devices by means of mathematical equations. This notably assists the design process allowing the simulation of the system before physically testing it.

In this particular case, the model will be developed to estimate SoC and voltage values of the battery. This information will be used to make high level control decisions such as power sharing. The obtained battery and UC models do not consider the State of Health (SoH) evolution since it is not necessary for the control that we implement. In this sense, the development of such accurate models is out of the scope of this work.

The degree of coincidence between the actual behavior of the physical device and the mathematical model will depend on the level of detail of the latter. At the same time, greater precision also implies an increase in the complexity of the model. For this reason, it is vital to seek a compromise between the complexity of the model and its ability to provide a behavior sufficiently close to the reality.

There exist different ways to model batteries and UCs. However, electrical models are the most used methods in the field of engineering thanks to the advantages they offer in terms of accuracy and low complexity.

3.5.1 Batteries

The main objective is to replicate the battery charge over time and provide the resulting battery voltage. The most basic battery model is composed of two components (Fig. 3.16). One of those is a voltage source representing the Open Circuit Voltage (OCV) of the cell, while the other one is a series connected impedance representing the internal resistance of the cell. Within the cell model, the series resistance represents the frequency independent part of the electrochemical impedance. In more complex battery models, the series impedance consists in a combination of a series resistance followed by one or more RC tanks as will be described hereafter. These capacitive elements emulate the electrical dynamics of the cell. If the battery under study presents a notable self-discharge, as is the

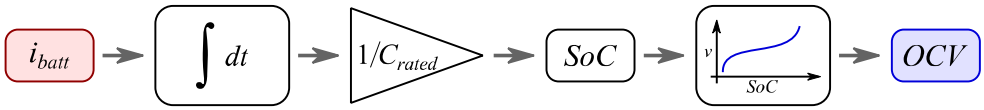

Fig. 3.15 Open Circuit Voltage (OCV) estimation.

case for VRLA batteries, it can be modeled as a high value resistor connected in parallel with the OCV voltage source.

In the basic model, the SoC is the only state variable used since it directly relates the stored charge and the OCV. The SoC is directly estimated by using the Coulomb Counting (CC) method. This method calculates the remaining capacity by integrating the current in and out of the battery. Due to this, the accuracy of this calculation will depend on a precise measurement of the current and a proper estimation of the initial SoC.

Once the SoC is known, the next step is to define the corresponding OCV. This OCV value is taken from a look-up table that contains all the data from laboratory tests relating SoC with OCV (Fig. 3.15). In short, the OCV curve is displayed as a function of SoC. The effect of the temperature is not considered for this basic model, but it should be included in the more advanced models in this way leaving the OCV as a function of the two parameters mentioned OCV=$f(SoC,T)$.

There exist two ways to obtain the OCV data of a cell. The first one is to perform a complete charge-discharge process at very small current rate in order to mitigate the effect of the series resistance. In this test, the voltage is measured together with the accumulated ampere-hours in order to obtain the relationship between both. The second option consists in charge and discharge the cell gradually in a pulsed way. In the charging process, for example, each of the applied pulses charges the battery a 10% applying long standby times between each of the pulses. This allows the voltage in the cell to stabilize, so that the OCV measurement can be made at the end of the standby period. Since there is always a hysteresis due to the difference between the charge and discharge voltages, an average of both curves is performed in order to enter a single curve in the look-up table. In more advanced models, this hysteresis can be emulated including both OCV curves in such a way that one is used for charging and the other one for discharging.

The model is finally completed integrating the OCV value in the electrical model shown in Fig. 3.16. Once the model is finished, if the internal resistance of the battery is fixed and the OCV is known for a given operating point, it is possible to determine the output battery voltage (v_{batt}) by knowing the current.

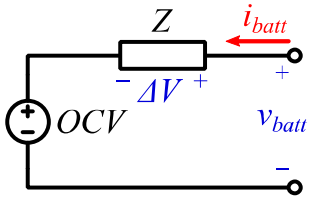

Fig. 3.16 Basic battery electric model.

This model is simple to implement but it does not represent any of the battery dynamics. To solve that, one or more RC tanks are introduced so that the model can more accurately represent the actual dynamic behavior of the battery. This equivalent electrical circuit that consists in a combination of resistive and capacitive elements is called Randles model. The number of RC tanks connected in series corresponds to the number of time constants of the model. Normally, One Time Constant (OTC) models (Fig. 3.17(a)) or Two Time Constant (TTC) models (Fig. 3.17(b)) are used, but multiple RC tanks could be added depending on the accuracy required. Considering the OTC model from Fig. 3.17 (a), the differential equation that defines the voltage across the RC tank can be described as follows (eq(3.13)):

$$\frac{dV_P}{dt} = \frac{1}{C_P} \cdot i_{C_P} = \frac{1}{C_P}\left(i_{batt} - \frac{V_P}{R_P}\right) \tag{3.13}$$

Once that the differential equation describing the system is known, the inputs and outputs should be defined. Since the charging process of a battery contains Constant Current (CC) and Constant Voltage (CV) charging phases, the battery voltage and current can be either system inputs or outputs. When the battery is getting charged in CC mode, the charger sets i_{batt} current in this way turning v_{batt} into an output of the system (eq(3.14)).

$$v_{batt} = OCV + i_{batt} \cdot R_S + V_P \tag{3.14}$$

Once the battery is close to be fully charged and v_{batt} reaches the float voltage level, the charger changes to CV mode and sets v_{batt}. In this case, the v_{batt} voltage will become an input and hence i_{batt} will be an output of the system (eq(3.15)).

$$i_{batt} = \frac{V_S}{R_S} = \frac{v_{batt} - V_P - OCV}{R_S} \tag{3.15}$$

The next step is to obtain the impedance values necessary to build the equivalent electrical circuit model. There are two ways to identify the impedance parameters, making measurements in the frequency domain or in the time domain.

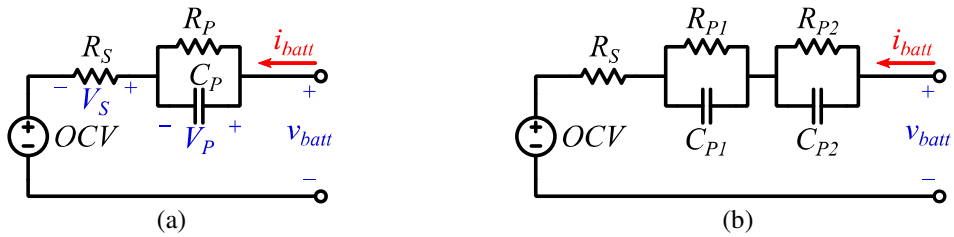

Fig. 3.17 (a) OTC impedance model, (b) TTC impedance model.

In the first method, an Electrochemical Impedance Spectroscopy (EIS) measurement provides the necessary information to build the Randles model. To perform this measurement an impedance spectrum analyzer is required, what makes it a simple and accurate method but at the same time expensive. The analyzer excites the cell with a sinusoidal alternating current and measures the voltage response at the cell terminals. These measurements should be done for the whole SoC range in steps of 10%. To avoid measurement disturbances, this test should be performed using four leads grouped into two pairs. One pair conducts the power while the other pair measures the voltage across the cell. Finally, an approximation of the obtained data provides the required resistance and capacitance values to build the model. The non-linear least squares method is widely used for this fitting process.

In the second method, the parameter identification is performed by measuring simultaneously voltage and current in the time domain. This method is widely used for impedance parameter identification because it does not require specific equipment to perform the tests. The battery is tested under a pulsed current pattern to later analyze the evolution of the voltage with each pulse (Fig. 3.18). The pulse pattern applied in this test has two particular characteristics. On the one hand, the pulse width must vary in order to

observe the frequency response. While on the other hand, it is also necessary to vary the amplitude of the pulses to observe the response of the cell under different current levels [181].

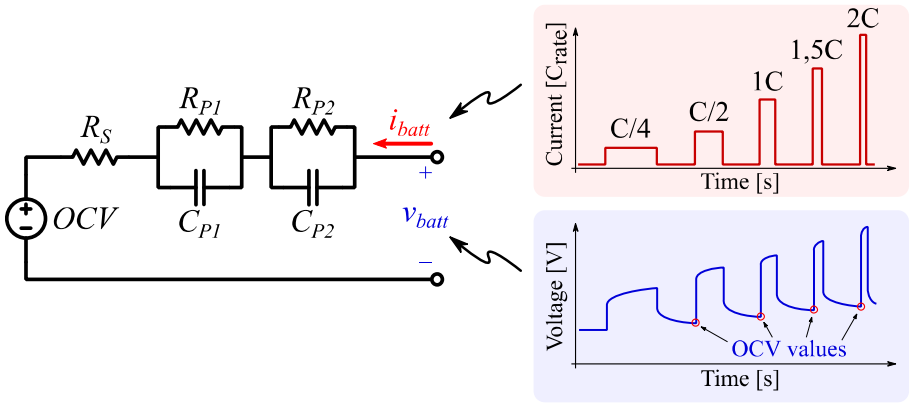

Fig. 3.18 Battery test under pulsed current pattern and its voltage response.

The instantaneous response of the voltage to a change in the input current presents an exponential decay. When the pulse finishes, the voltage converges to steady state (OCV value). These dynamic characteristics can be mathematically described as a sum of exponential functions with real positive time constants τ_i and amplitude coefficients A_i [181]. This particular behavior is described mathematically in equation (3.16).

$$V_d(t) = \sum_{i=1}^{M} A_i e^{-\frac{t}{\tau_i}} \qquad \begin{cases} A_i, \tau_i > 0 \\ 0 < t < \infty \end{cases} \tag{3.16}$$

3.5.2 UC

There exist different kinds of ultracapacitor models in the literature. Nevertheless electric circuit models are the most commonly used ones to perform simulations and electrical system designs [182]. As it happens in the case of batteries, UC equivalent circuit models combine different electrical components with the aim of emulating the behavior of a real device.

The simplified UC circuit model is composed of a capacitor with a resistor connected in series in this way creating a single RC branch (Fig. 3.19 (a)). In slow discharge applications this simplified model provides a good enough approximation to the actual UC behavior [183]. The model can also include a resistor connected in parallel

to the capacitor, in order to model the current leakage effect due to the self-discharge impact over a long period of time.

The suitability of the model will always depend on the required accuracy. If a single time constant model is not enough to model the transient response of the UC, it would be necessary to add more time constants. Ideally, a large number of RC branches would provide a high level of accuracy but it would not be very practical. Normally, two or three RC branches are used to emulate the UC dynamics (Fig. 3.19 (b)). This kind of multiple RC branch models can also include non-linear capacitance effects in one of the branches in order to increase the model accuracy. Each of the branches is modeled with a different time constant, in this way differing from the others in more than an order of magnitude [184].

Other authors have developed other kind of models, similar to those used in batteries where one or more RC tanks are connected in series (Fig. 3.19 (c)) [185]. In this case, the equivalent circuit also includes a series connected resistor and a capacitor as it can be seen in Fig. 3.19 (c) [182]. As it happens in other equivalent circuit models, the resistance and capacitance values can be temperature or voltage dependent in order to improve the model accuracy. Among its benefits, the authors in [185] highlight the reduced amount of experimental parameters to develop the model compared to parallel RC branch models.

Finally, there also exists another UC model referred to as transmission line model (Fig. 3.19 (d)) [182], [186], [187]. Normally, the transmission line model is used to emulate the internal physical dynamics of the UCs [182]. It can also include voltage and

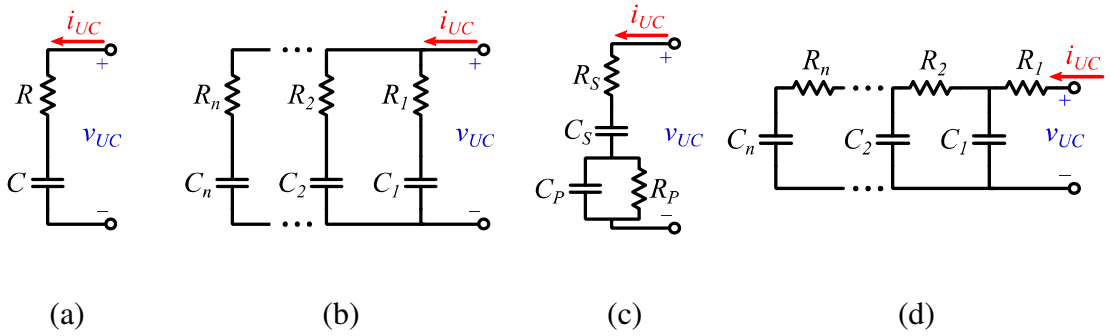

(a) (b) (c) (d)

Fig. 3.19 Different ultracapacitor equivalent circuit models.

temperature dependent non-linear capacitances to provide higher accuracy. Nevertheless, its use is not very extended in the sense that the details about such inner workings are not required for common application.

In this work, a two time constant UC model (Fig. 3.19(b)) will be used since it offers a good relationship between output voltage estimation accuracy and model complexity. As mentioned above, each of the parallel branches will provide a different dynamic in order to approximate the model to the real UC behavior.

Unlike batteries that consist of different charging phases (CC and CV), the control variable that is generally set for the UC charge and discharge control is the UC current. With this in mind, the UC voltage becomes an output variable of the system. The general equation describing the UC output voltage is developed in (eq(3.17)):

$$v_{UC}(t) = i_{C_1}(t) \cdot R_1 + v_{C_1}(t) = i_{C_2}(t) \cdot R_2 + v_{C_2}(t) \tag{3.17}$$

With respect to the total i_{UC} current, it will be the sum of the currents flowing through the parallel branches. In this sense, the individual currents shown in equation (3.18) are derived from the general capacitor differential equation:

$$i_{C_1}(t) = C_1 \frac{dv_{C_1}}{dt}, \qquad i_{C_2}(t) = C_2 \frac{dv_{C_2}}{dt} \tag{3.18}$$

Chapter 4

HARDWARE MODELING

In this Chapter the selected converter topology is presented. In this sense, the reasons for this choice are explained always taking into account the design parameters of our application.

Together with this, the converter modeling process is explained starting from the non-linear switched model, to end up with the Linear Time Invariant model.

4.1 Converter topology

The selection of an appropriate power electronic converter (PEC) is not a trivial matter. Different types of PECs are used for energy storage applications, from non-isolated topologies [188] to isolated ones [56], [189]–[192]. Non-isolated topologies are more often used if the voltage difference between the energy bus and the storage devices is not too large. If not, the transformer used in isolated topologies solves the issue. In any case, the bidirectional power flow capacity must be common to isolated and non-isolated converters in energy storage applications.

In this particular case, due to the use of batteries and UCs the system will work with low voltage levels. To be more precise, the converter will have to be designed for voltage ranges around 12 to 48 volts. Taking this into account, the best option in terms of design simplicity and capital cost is to use a non-isolated converter.

Among the different non-isolated DC-DC converters, the Synchronous Buck converter is the most commonly used one. It is a variant of the classical Buck converter with the difference of using a second power switch instead of a diode. The purpose of using two switches is to provide bidirectional power flow capacity and to increase the energy efficiency. The power losses generated by the diode forward voltage drop are greater than those generated by the $R_{DS(on)}$ of the mosfet at full load.

One of the main drawbacks of this configuration is the additional driver circuit for the low side switch. The implementation of a dead time needs to be considered in this context in order to avoid a short circuit across the switches.

In order to increase the power capacity of the converter, the Multiphase Synchronous Buck configuration is a proper option (Fig. 4.1). This configuration offers

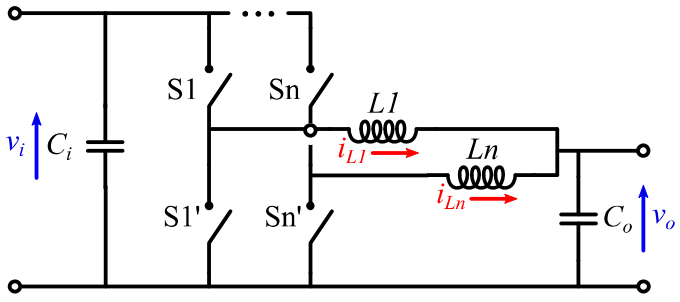

Fig. 4.1 Multiphase synchronous buck converter.

significant benefits, but also involves a greater number of components and control complexity. Multiphase or interleaved buck converter consists of the parallel connection of several buck converter circuits. The activation of each phase is sequential and uniformly shifted depending on the number of phases installed. This allows the current splitting among all the parallel branches reducing conduction losses.

The total current ripple is also reduced (Fig. 4.2), obtaining a ripple cancellation in both input (a) and output (b) filter stages at specific operating points [193]. These points depend on the number of phases N_{ph} and the duty cycle. Therefore, the size of the components can be reduced, in particular the magnetics and capacitors. With smaller magnetic components, there is a smaller amount of energy stored in each inductor which allows faster response to load transients [194]. This makes it a very attractive converter for high power density storage devices such as ultra-capacitors.

Normally, the storage devices are connected to the low voltage side of the converter. This has the advantage of providing a smoother current and stable voltage to the energy storage device due to the LC filter location. Besides that, the low voltage side of the converter avoids large cell serializations in the case of installing batteries or UCs.

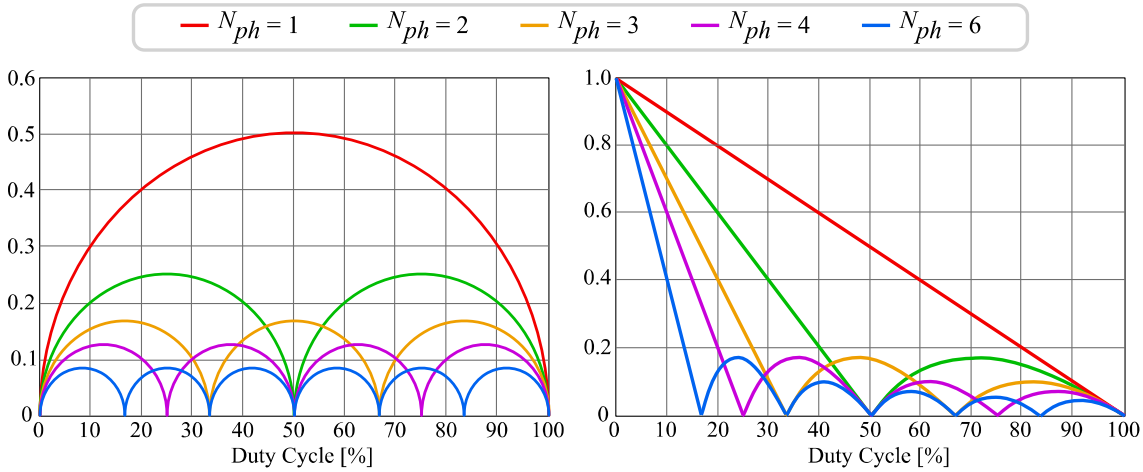

Fig. 4.2 Normalized input (a) and output (b) RMS current ripple as a function of duty cycle. [195]

4.2 Mathematical Modeling

There exist different ways to represent and model a system. In this sense, a linear system can be represented in the frequency domain as a transfer function or in the time domain as a linear differential equation. It will always depend on our knowledge about the system to use one method or another. If the internal working mode of the system is unknown and the only information available is its transient step response, a system identification process can be performed to obtain its transfer function. To determine the transfer function, first of all the settling time and overshoot should be measured followed by the natural frequency and the damping ratio. With that information the standard form of the second order system can be built.

On the other hand, if the physical characteristics of the system under study are known, it can be modeled in a more accurate way taking into consideration all the existing system states. In the case of highly nonlinear systems like power electronic converters, at any moment in time the system has a state. Indeed, the behavior of the system is linear within each state but is the transition from one state to the other what makes it non-linear. This set of all possible states where the converter can be in, is known as the switched model. It can be represented in state-space form, where every single condition the system can experience is included. One of its strengths is the remarkable number of control techniques that are built on state space models like Kalman Filters, Robust control, LQR control and MPC, to name a few.

Making use of the switched model of the converter, the averaged model can be developed. Nevertheless, due to the abovementioned characteristics of power converters, the averaged model is still non-linear (Fig. 4.3). After obtaining the averaged state-space model, it should be linearized if classical system control techniques need to be applied. The idea is to take the set of non-linear equations that describe the system and linearize them over a point of operation to develop a Linear Time Invariant (LTI) model. Once the LTI model is obtained, Laplace transform can be used to derive the transfer functions that describe the system. Making use of the transfer functions, a suitable compensator can be designed for the converter control using linear control techniques. All these steps presented in Fig. 4.3 have been further developed in the following subchapters.

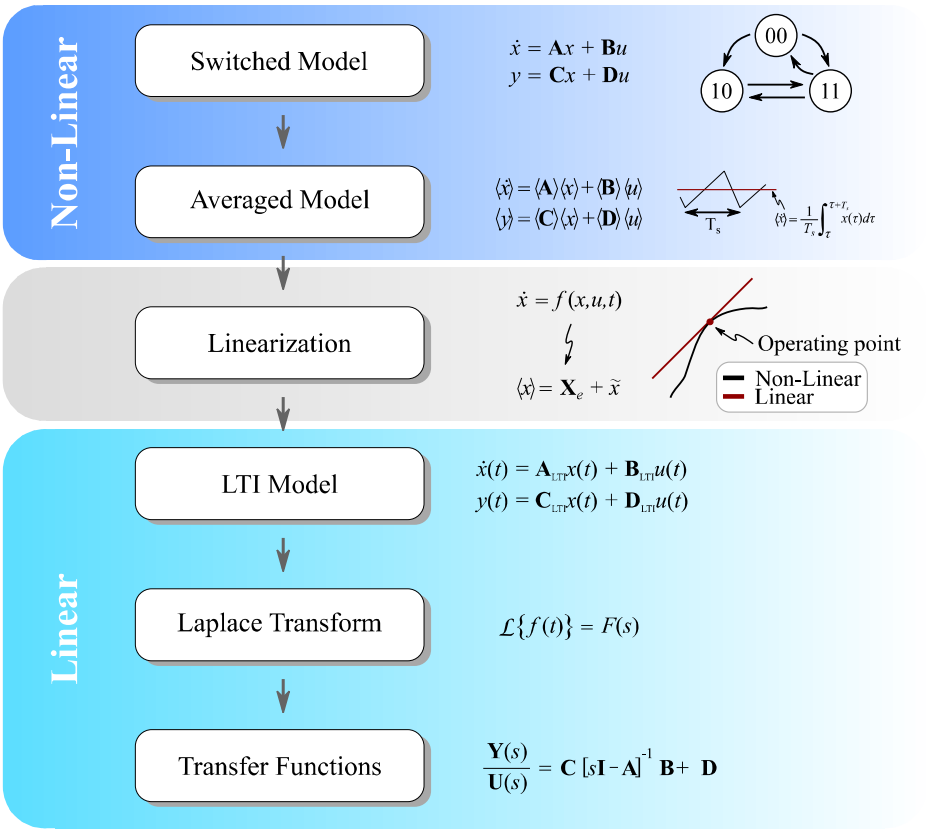

Fig. 4.3 Steps followed for obtaining a linear model, on the basis of a non-linear system.

In this case, the mathematical model of the Synchronous Buck converter (Fig. 4.4) is developed. The physical state variables of a system are usually associated with the storage of energy. In the particular case of power electronic converters, the physical state variables are the inductor current and the capacitor voltages. The independent inputs of the system, such as the battery voltage (v_{batt}) and DC bus voltage (v_{bus}), are included in the input (or control) vector. The output vector contains the variables that are of interest for the designer. These variables might be a combination of state variables and input variables. In this particular case, there is interest in computing the battery current i_{batt} and the DC bus current i_{bus}. As it can be observed, having a voltage source on each side of the converter increases the complexity of the model, since the bidirectional behavior of the converter can cause the voltages to be considered as inputs or outputs of the system.

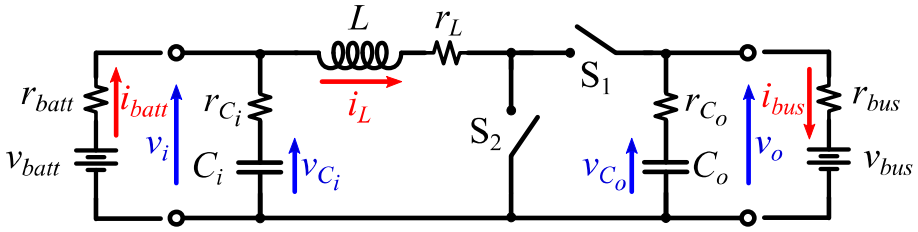

Fig. 4.4 Synchronous Buck converter schematic.

4.2.1 Switched model

For the Synchronous Buck converter there are two possible switching states shown in Fig. 4.5 and Fig. 4.6. Note that power MOSFETs are modelled as a resistance when are closed. This resistance is equivalent to their R_{DSon}. In this sense, r_1 and r_2 resistances correspond to S_1 and S_2 MOSFETs respectively.

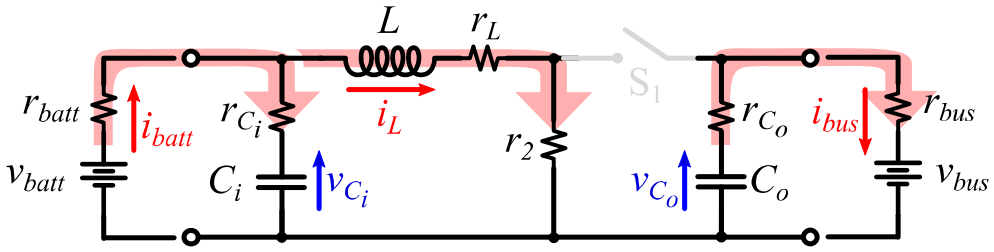

Fig. 4.5 Switching state 1 of the Synchronous Buck converter.

Applying Kirchoff's current and voltage laws to the switching state 1 (Fig. 4.5), the following system of differential equations is obtained.

$$\frac{dv_{C_i}}{dt} = -\frac{1}{C_i(r_{C_i}+r_{batt})}\cdot v_{C_i} - \frac{r_{batt}}{C_i(r_{C_i}+r_{batt})}\cdot i_L + \frac{1}{C_i(r_{C_i}+r_{batt})}\cdot v_{batt} \tag{4.1}$$

$$\frac{dv_{C_o}}{dt} = -\frac{1}{C_o(r_{C_o}+r_{bus})}\cdot v_{C_o} + \frac{1}{C_o(r_{C_o}+r_{bus})}\cdot v_{bus} \tag{4.2}$$

$$\frac{di_L}{dt} = \frac{r_{batt}}{L(r_{C_i}+r_{batt})}\cdot v_{C_i} - \left(\frac{r_{C_i}\cdot r_{batt}}{L(r_{C_i}+r_{batt})} + \frac{r_L + r_{DS_{on}}}{L}\right)\cdot i_L + \frac{r_{C_i}}{L(r_{C_i}+r_{batt})}\cdot v_{batt} \tag{4.3}$$

Equations (4.4) and (4.5) define the output variables in the switching state 1.

$$i_{batt} = -\frac{1}{r_{C_i}+r_{batt}}\cdot v_{C_i} + \frac{r_{C_i}}{r_{C_i}+r_{batt}}\cdot i_L + \frac{1}{r_{C_i}+r_{batt}}\cdot v_{batt} \tag{4.4}$$

$$i_{bus} = \frac{1}{r_{C_o}+r_{bus}}\cdot v_{C_o} - \frac{1}{r_{C_o}+r_{bus}}\cdot v_{bus} \tag{4.5}$$

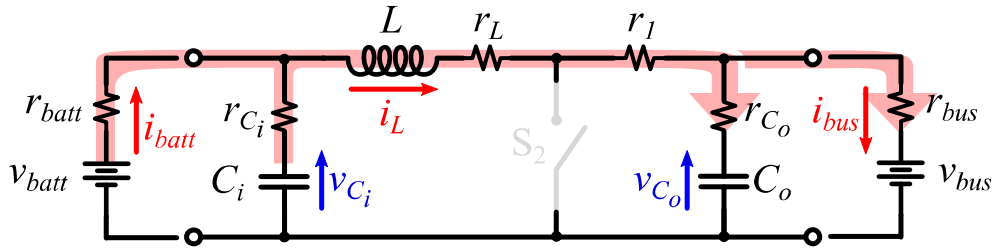

Fig. 4.6 Switching state 2 of the Synchronous Buck converter.

As in the previous case, the following set of differential equations are obtained from the resulting circuit of switching state 2.

$$\frac{dv_{C_i}}{dt} = -\frac{1}{C_i(r_{C_i}+r_{batt})}\cdot v_{C_i} - \frac{r_{batt}}{C_i(r_{C_i}+r_{batt})}\cdot i_L + \frac{1}{C_i(r_{C_i}+r_{batt})}\cdot v_{batt} \tag{4.6}$$

$$\frac{dv_{C_o}}{dt} = -\frac{1}{C_o(r_{C_o}+r_{bus})}\cdot v_{C_o} + \frac{r_{bus}}{C_o(r_{C_o}+r_{bus})}\cdot i_L + \frac{1}{C_o(r_{C_o}+r_{bus})}\cdot v_{bus} \tag{4.7}$$

$$\begin{aligned}\frac{di_L}{dt} = {} & \frac{r_{batt}}{L(r_{C_i}+r_{batt})}\cdot v_{C_i} - \frac{r_{bus}}{L(r_{C_o}+r_{bus})}\cdot v_{C_o} - \left(\frac{r_{C_i}\cdot r_{batt}}{L(r_{C_i}+r_{batt})} + \frac{r_L + r_{DS_{on}}}{L} + \frac{r_{C_o}\cdot r_{bus}}{L(r_{C_o}+r_{bus})}\right)\cdot i_L + \\ & + \frac{r_{C_i}}{L(r_{C_i}+r_{batt})}\cdot v_{batt} - \frac{r_{C_o}}{L(r_{C_o}+r_{bus})}\cdot v_{bus}\end{aligned} \tag{4.8}$$

Equations (4.9) and (4.10) define the output variables in the switching state 1.

$$i_{batt} = -\frac{1}{r_{C_i}+r_{batt}}\cdot v_{C_i} + \frac{r_{C_i}}{r_{C_i}+r_{batt}}\cdot i_L + \frac{1}{r_{C_i}+r_{batt}}\cdot v_{batt} \tag{4.9}$$

$$i_{bus} = \frac{1}{r_{C_o}+r_{bus}}\cdot v_{C_o} + \frac{r_{C_o}}{r_{C_o}+r_{bus}}\cdot i_L - \frac{1}{r_{C_o}+r_{bus}}\cdot v_{bus} \tag{4.10}$$

4.2.2 Averaged Large Signal Model

Equations (4.1) to (4.10) are now written in the matrix form. From which the state equation (4.13) and output equation (4.15) are obtained.

$$\underbrace{U=1 \;\rightarrow\; \begin{cases} S1:0 \\ S2:1 \end{cases}}_{\text{State 1}} \qquad \underbrace{U=0 \;\rightarrow\; \begin{cases} S1:1 \\ S2:0 \end{cases}}_{\text{State 2}} \tag{4.11}$$

The variable U represents the position of the switches at each instant (Equation (4.11)). Assuming that State 1 corresponds to $U=1$ and State 2 to $U=0$, the averaged state equation can be written as follows:

$$\langle \dot{x} \rangle = (\mathbf{A}_1 U + \mathbf{A}_2(1-U)) \cdot \langle x \rangle + (\mathbf{B}_1 U + \mathbf{B}_2(1-U)) \cdot \langle u \rangle \tag{4.12}$$

$$\begin{bmatrix} \left\langle \frac{dv_{C_i}}{dt} \right\rangle \\ \left\langle \frac{dv_{C_o}}{dt} \right\rangle \\ \left\langle \frac{di_L}{dt} \right\rangle \end{bmatrix} = \langle \mathbf{A} \rangle \cdot \begin{bmatrix} \langle v_{C_i} \rangle \\ \langle v_{C_o} \rangle \\ \langle i_L \rangle \end{bmatrix} + \langle \mathbf{B} \rangle \cdot \begin{bmatrix} \langle v_{batt} \rangle \\ \langle v_{bus} \rangle \end{bmatrix} \tag{4.13}$$

$$\langle \mathbf{A} \rangle = \begin{bmatrix} -\frac{1}{C_i(r_{C_i}+r_{batt})} & 0 & -\frac{r_{batt}}{C_i(r_{C_i}+r_{batt})} \\ 0 & -\frac{1}{C_o(r_{C_o}+r_{bus})} & \frac{(1-U)\cdot r_{bus}}{C_o(r_{C_o}+r_{bus})} \\ \frac{r_{batt}}{L(r_{C_i}+r_{batt})} & -\frac{(1-U)\cdot r_{bus}}{L(r_{C_o}+r_{bus})} & -\left(\frac{r_{C_i}\cdot r_{batt}}{L(r_{C_i}+r_{batt})} + \frac{r_L + r_{DS_{on}}}{L} + \frac{(1-U)\cdot r_{C_o}\cdot r_{bus}}{L(r_{C_o}+r_{bus})} \right) \end{bmatrix}$$

$$\langle \mathbf{B} \rangle = \begin{bmatrix} \frac{1}{C_i(r_{C_i}+r_{batt})} & 0 \\ 0 & \frac{1}{C_o(r_{C_o}+r_{bus})} \\ \frac{r_{C_i}}{L(r_{C_i}+r_{batt})} & -\frac{(1-U)\cdot r_{C_o}}{L(r_{C_o}+r_{bus})} \end{bmatrix}$$

The matrices C and D can be achieved if the output vector y is a combination of the state variables and inputs, as it happens in this case. In this way, the output equation is written as follows:

$$\langle y \rangle = (\mathbf{C}_1 U + \mathbf{C}_2 (1-U)) \cdot \langle x \rangle + (\mathbf{D}_1 U + \mathbf{D}_2 (1-U)) \cdot \langle u \rangle \tag{4.14}$$

$$\begin{bmatrix} \langle i_{batt} \rangle \\ \langle i_{bus} \rangle \end{bmatrix} = \langle \mathbf{C} \rangle \cdot \begin{bmatrix} \langle v_{C_i} \rangle \\ \langle v_{C_o} \rangle \\ \langle i_L \rangle \end{bmatrix} + \langle \mathbf{D} \rangle \cdot \begin{bmatrix} \langle v_{batt} \rangle \\ \langle v_{bus} \rangle \end{bmatrix} \tag{4.15}$$

$$\langle \mathbf{C} \rangle = \begin{bmatrix} -\dfrac{1}{r_{C_i} + r_{batt}} & 0 & \dfrac{r_{C_i}}{r_{C_i} + r_{batt}} \\ 0 & \dfrac{1}{r_{C_o} + r_{bus}} & \dfrac{(1-U) \cdot r_{C_o}}{r_{C_o} + r_{bus}} \end{bmatrix}$$

$$\langle \mathbf{D} \rangle = \begin{bmatrix} \dfrac{1}{r_{C_i} + r_{batt}} & 0 \\ 0 & -\dfrac{1}{r_{C_o} + r_{bus}} \end{bmatrix}$$

4.2.3 Linearized model

In order to design a suitable compensator for the feedback control of the plant, it is necessary to obtain a linear model of the system. In this case, given the non-linear nature of power electronic converters, it is necessary to perform a linearization. As it is not possible to get a linear model that works well over the entire state-space, the non-linear system is linearized at specific operating points where the lowest error is desired.

Let us consider the set of continuous-time non-linear differential equations that describe the system in the following form and assuming the duty cycle d as the input variable:

$$\dot{x} = f(x,u,t) \tag{4.16}$$

$$y = g(x,u,t) \tag{4.17}$$

The main goal is to find a suitable Linear Time Invariant (LTI) combination of system states and inputs that produce similar results as the non-linear system. To this end it is necessary to fit the model, which is a non-linear function of state variables and inputs, to the linear form shown in (4.18) and (4.19).

$$\dot{x} = f(x,u,t) \quad \longrightarrow \quad \dot{\mathbf{x}}(t) = \mathbf{A}_{\mathrm{LTI}}\mathbf{x}(t) + \mathbf{B}_{\mathrm{LTI}}\mathbf{u}(t) \tag{4.18}$$

$$y = g(x,u,t) \quad \longrightarrow \quad \mathbf{y}(t) = \mathbf{C}_{\mathrm{LTI}}\mathbf{x}(t) + \mathbf{D}_{\mathrm{LTI}}\mathbf{u}(t) \tag{4.19}$$

The LTI state-space model emulates an approximation of the local behavior of the non-linear model, assuming small deviations from a set of equilibrium points. In most cases, the equilibrium point is selected so that the system therefore stays at steady state. This implies that when the system is initialized at this state, then the states would not change over time.

$$\dot{\mathbf{x}}(t)=0 \quad \longrightarrow \quad 0=f(\mathbf{X}_e,\mathbf{U}_e)=\mathbf{A}\mathbf{X}_e(t)+\mathbf{B}\mathbf{U}_e(t) \tag{4.20}$$

$$\mathbf{Y}_e(t)=\mathbf{C}\mathbf{X}_e(t)+\mathbf{D}\mathbf{U}_e(t) \tag{4.21}$$

The next step is to use the Taylor series expansion assuming small deviations around the equilibrium points. In this sense, the duty cycle together with averaged values of state, input and output vectors can be separated into steady state (equilibrium) value and small signal value which is denoted by tilde symbol:

$$\langle x \rangle = \mathbf{X}_e + \tilde{x} \tag{4.22}$$

$$\langle u \rangle = \mathbf{U}_e + \tilde{u} \tag{4.23}$$

$$\langle y \rangle = \mathbf{Y}_e + \tilde{y} \tag{4.24}$$

$$d = \mathrm{D}_e + \tilde{d} \tag{4.25}$$

$$\langle \dot{x} \rangle = 0 + \tilde{\dot{x}} \tag{4.26}$$

In this case, instead of keeping all of the Taylor series expansion terms out to infinity, higher order terms are ignored since they do not affect the system that much. In this way only the 0^{th} and the 1^{st} order terms (first derivatives) are considered. At the most basic level, we are looking at the first order partial derivatives of a function at a steady state (equilibrium) operating point, making the assumption that the slope is a good enough approximation of the non-linear function as long as we stay close to the operating point.

$$\dot{x} = f(x,u,t) \quad \longrightarrow \quad \tilde{\dot{x}} = \frac{\partial f}{\partial x}\left(\tilde{x}\right) + \frac{\partial f}{\partial u}\left(\tilde{u}\right) \tag{4.27}$$

$$y = g(x,u,t) \quad \longrightarrow \quad \tilde{y} = \frac{\partial g}{\partial x}\left(\tilde{x}\right) + \frac{\partial g}{\partial u}\left(\tilde{u}\right) \tag{4.28}$$

All the partial derivatives are evaluated at the predefined equilibrium points and then stored into matrixes. The resulting matrixes containing the partial derivatives are called Jacobian matrixes. At this point we have reached the LTI state-space form of the system model.

$$\mathbf{A_{LTI}} = \begin{pmatrix} \left.\frac{\partial f_1}{\partial x_1}\right|_{(\tilde{x},\tilde{u})} & \cdots & \left.\frac{\partial f_1}{\partial x_n}\right|_{(\tilde{x},\tilde{u})} \\ \vdots & \ddots & \vdots \\ \left.\frac{\partial f_n}{\partial x_1}\right|_{(\tilde{x},\tilde{u})} & \cdots & \left.\frac{\partial f_n}{\partial x_n}\right|_{(\tilde{x},\tilde{u})} \end{pmatrix}_{\mathbf{Xe,Ue}\ \ n\times n} \qquad \mathbf{B_{LTI}} = \begin{pmatrix} \left.\frac{\partial f_1}{\partial u_1}\right|_{(\tilde{x},\tilde{u})} & \cdots & \left.\frac{\partial f_1}{\partial u_m}\right|_{(\tilde{x},\tilde{u})} \\ \vdots & \ddots & \vdots \\ \left.\frac{\partial f_n}{\partial u_1}\right|_{(\tilde{x},\tilde{u})} & \cdots & \left.\frac{\partial f_n}{\partial u_m}\right|_{(\tilde{x},\tilde{u})} \end{pmatrix}_{\mathbf{Xe,Ue}\ \ n\times m}$$

$$\mathbf{C_{LTI}} = \begin{pmatrix} \left.\frac{\partial g_1}{\partial x_1}\right|_{(\tilde{x},\tilde{u})} & \cdots & \left.\frac{\partial g_1}{\partial x_n}\right|_{(\tilde{x},\tilde{u})} \\ \vdots & \ddots & \vdots \\ \left.\frac{\partial g_p}{\partial x_1}\right|_{(\tilde{x},\tilde{u})} & \cdots & \left.\frac{\partial g_p}{\partial x_n}\right|_{(\tilde{x},\tilde{u})} \end{pmatrix}_{\mathbf{Xe,Ue}\ \ p\times n} \qquad \mathbf{D_{LTI}} = \begin{pmatrix} \left.\frac{\partial g_1}{\partial u_1}\right|_{(\tilde{x},\tilde{u})} & \cdots & \left.\frac{\partial g_1}{\partial u_m}\right|_{(\tilde{x},\tilde{u})} \\ \vdots & \ddots & \vdots \\ \left.\frac{\partial g_p}{\partial u_1}\right|_{(\tilde{x},\tilde{u})} & \cdots & \left.\frac{\partial g_p}{\partial u_m}\right|_{(\tilde{x},\tilde{u})} \end{pmatrix}_{\mathbf{Xe,Ue}\ \ p\times m}$$

Once we have obtained the LTI matrixes of the system, Laplace transformation can be used to pass from state space representation (MIMO) to transfer functions (SISO).

4.2.4 Transfer function of the system for linear controller design

A transfer function can be defined as the Laplace transform of the impulse response of a LTI system when the initial conditions are set to zero. In our case, since a TF only relates one input with one output and what we have is a MIMO system, there will be multiple transfer functions describing the system.

Every TF is composed of two polynomials, one in the numerator and the other one in the denominator. The polynomial in the denominator is called the characteristic equation. In order to apply classical control theory to design a suitable compensator for the system, first it is necessary to put the characteristic equation into the correct form. To do this, the system should be described by a second order transfer function. This allows us to see how varying any parameter in the system affects the location of the poles. Together with this, it should be noted that design concepts like Damping ratio ζ and Natural frequency ω_n are only defined for a second order system (4.29), and lose their sense for higher order systems.

$$\frac{\mathbf{Y}(s)}{\mathbf{U}(s)} = \frac{\omega_n^2}{s^2 + 2\zeta\omega_n s + \omega_n^2} \tag{4.29}$$

Based on the previously shown LTI state-space model, this can be Laplace transformed to obtain the transfer functions of the system. After performing the Laplace transform and rearranging terms, we obtain:

$$\mathbf{X}(s) = [s\mathbf{I} - \mathbf{A}]^{-1}\mathbf{B}\,\mathbf{U}(s) \tag{4.30}$$

$$\mathbf{Y}(s) = \mathbf{C}[s\mathbf{I} - \mathbf{A}]^{-1}\mathbf{B}\,\mathbf{U}(s) + \mathbf{D}\,\mathbf{U}(s) \tag{4.31}$$

Combining equations (4.30) and (4.31) we obtain the generic transfer function of the system (4.32):

$$\frac{\mathbf{Y}(s)}{\mathbf{U}(s)} = \mathbf{C}[s\mathbf{I} - \mathbf{A}]^{-1}\mathbf{B} + \mathbf{D} \tag{4.32}$$

In this case, as it happens very often when the inverse of a matrix needs to be computed, due to the characteristics of **A** matrix it is non-invertible. As it has been mentioned before, in our case Matlab was used to obtain the solution for this problem.

Internally, Matlab performs an optimization to solve the system of nonlinear equations. The method used by Matlab to find the solution for this optimization problem is based on trust-region dogleg algorithm. Nevertheless, the working principles of this optimization algorithm are out of the scope of this work. For more information about it, the reader is referred to [196] and [197].

As a result of multiple iterations inside the Matlab algorithm, the resulting transfer functions are described by high order polynomials both in the numerator and the denominator. As mentioned before, if we want to apply the classical system control theory to our problem, we need to have a second order system or at least our system needs to have a pair of dominant poles that made it behave like a second order system.

In this case, the system behaves like a second order system so the transfer functions can be easily adapted using '*balred*' Matlab function. This function computes a reduced-order approximation of the LTI model. Fig. 4.7 shows the step response comparison of the former high order system and the new second order system. As it can be seen, a small error is assumed when performing the system order reduction but it is small enough to ignore.

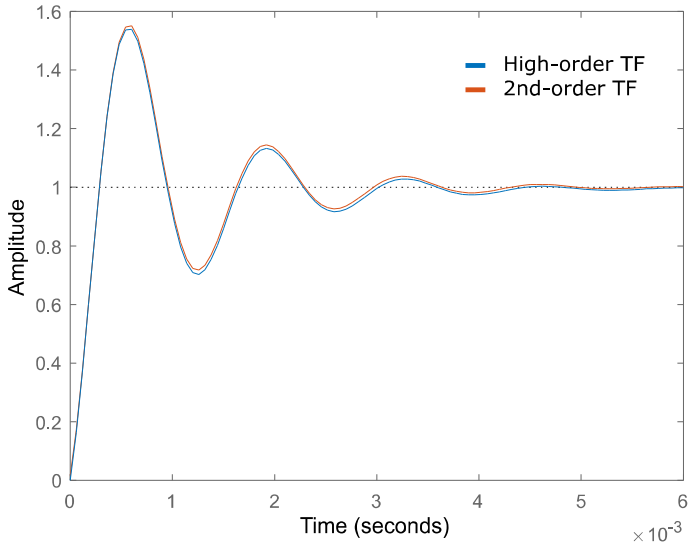

Fig. 4.7 Step response comparison of high order TF and approximated second order TF.

Now that we have a second order equation describing our system, we can find the proper gain values for the compensator to fulfil the damping ratio, overshoot and settling time.

Chapter 5

CONTROL STRUCTURES

The control of HESSs has often been divided into different levels. Each level corresponds to different priorities in the control actuations. Furthermore, this multilevel control structure is widely used for electrical grid and microgrid applications. In this sense, most of the used control methods are based on PI controllers.

In order to simplify the multilevel control structure, different alternatives have been sought. The idea is to reduce the system to a single level structure. In order to achieve that, the Model Predictive Control is presented as a suitable solution.

This Chapter also gathers the currently used control strategies for power sharing in Hybrid Energy Storage Systems.

5.1 Multilevel control structures

Multilevel control structures have been widely used in classical control schemes for electrical grid and microgrid applications. This hierarchical control structure normally consists of three different levels; primary, secondary and tertiary levels to be precise. This kind of control structures are composed of multiple PI control loops, tuned to meet different operating dynamics based on priority criteria.

Based on this, multilevel control structures have been widely used for the HESS energy management. Fig. 5.1 shows the general scheme of this control structure and the role of each control level within the system. As it can be seen, the control has been divided into three different levels. Note that the inertial response is included even though we cannot control it since depends on physical parameters.

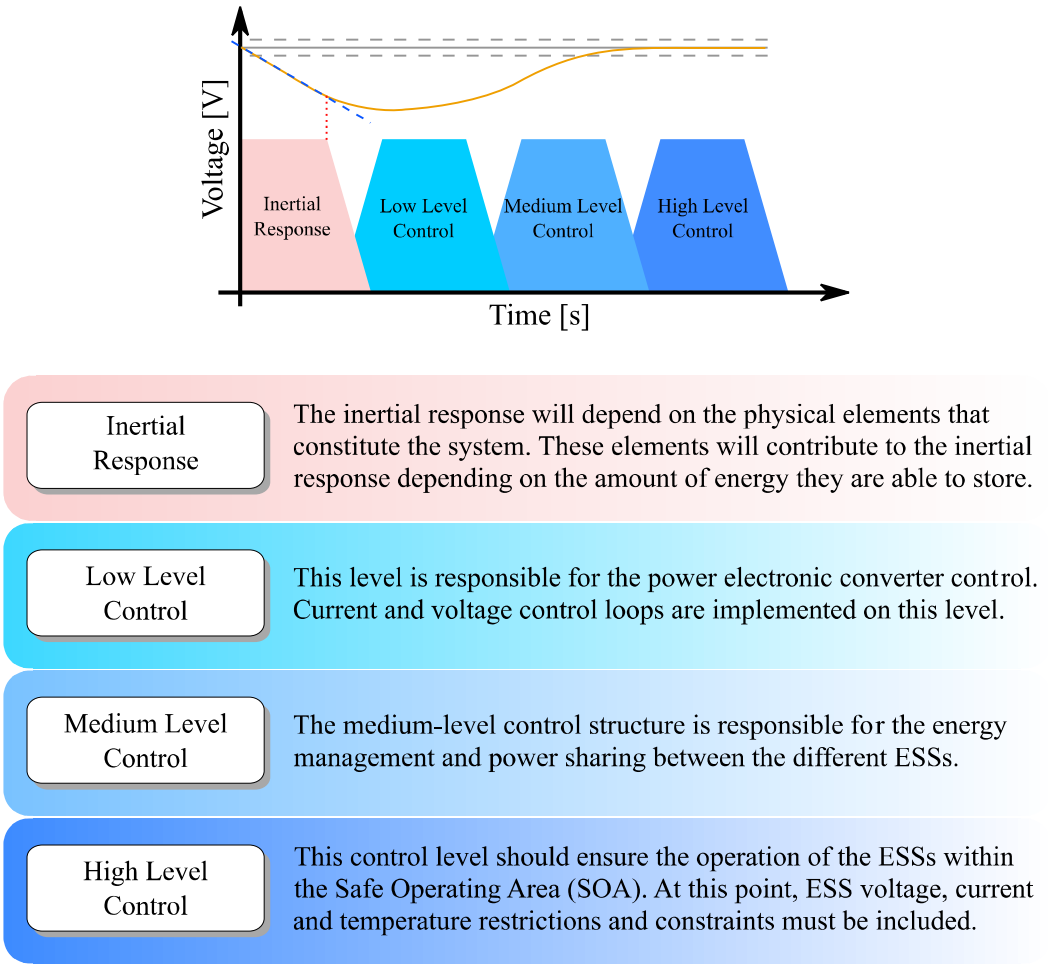

Fig. 5.1 Hierarchical control based multilevel control structure for voltage regulation in DC systems with energy storage devices.

5.1.1 High Level Control

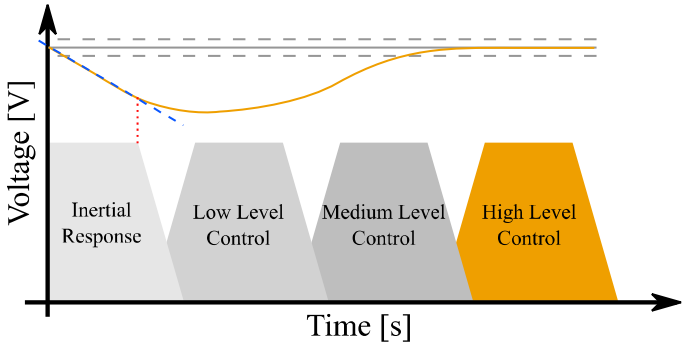

Fig. 5.2 High Level Control operating range within a multilevel control structure.

This control level should ensure the operation of the ESSs within the Safe Operating Area (SOA), regarding voltage, current and temperature restrictions (Fig. 5.2). At this point, all the ESS restrictions and constraints must be included. Especially when working with batteries, due to the hazardous nature of some chemistries. Protecting the battery from working out of the SoA is fundamental. Operating out of its specified working limits can result in an irreversible failure of the battery. Fig. 5.3 presents the SoA for Lithium-

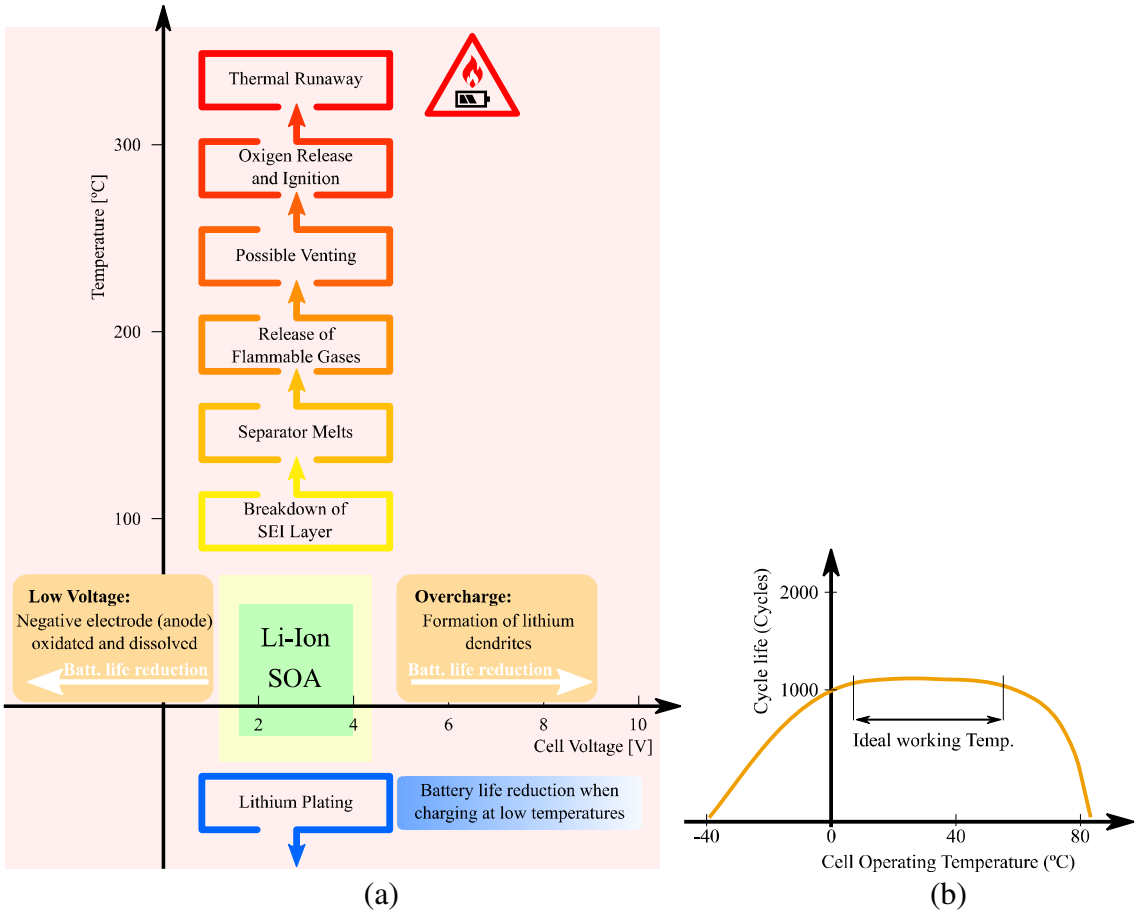

Fig. 5.3 BMS safety and energy requirement issues. a) SOA of Li-ion technology for a voltage vs. temperature chart [198]. b) Cycle life improvement vs. operating temperature [199].

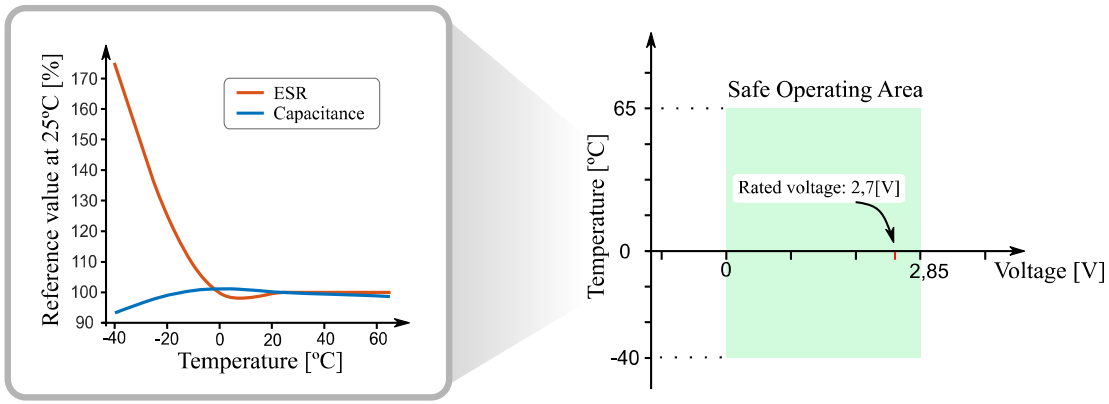

Fig. 5.4 Ultracapacitor safe operating area [200]**.**

Ion batteries, together with some information about the problems caused by operating out of it.

In addition to the above, this level should include the charging procedure for the batteries. This comprises the typical constant current constant voltage (CC/CV) charging mode. The charging mode may have slight differences depending on the battery technology used. This is an essential feature since the batteries can be damaged if an inappropriate charging procedure is applied.

All this must contribute to the normal and safe operation of the system, together with providing a battery life extension.

Ultracapacitors are affected by the temperature and overvoltage as well (Fig. 5.4). Operating at high temperatures will reduce the life of the UC cells, while low temperatures will increase their internal resistance. Moreover, in the event of exceeding the maximum voltage, the cell can be damaged or even destroyed.

5.1.2 Medium Level Control

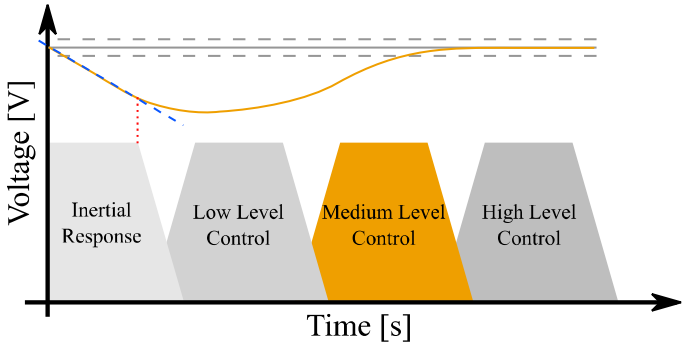

Fig. 5.5 Medium Level Control operating range within a multilevel control structure.

The medium-level control structure is responsible for the energy management and power sharing between the different ESSs (Fig. 5.5). This can be done in different ways. Firstly, the power demand is calculated, and after, the total power is divided among the different energy storage devices [201]. Different methods can be found on the literature to perform this division.

One of the simplest methods consists of applying a power level threshold to divide the power between the ESSs. In this sense, the high power density ESS would supply all the power demand exceeding the predefined threshold. Some other methods are based on reference tables to perform the power distribution [202]. Depending on the power level managed at each time, some predefined patterns are used to distribute it between the storage devices. These patterns stored into the reference tables can be modified and adjusted based on the requirements of each application. Another option is to combine together multiple reference tables and use one or the other depending on the operating mode required at each moment.

Other methods perform the power sharing by means of a high pass filter to separate the high frequency and low frequency components of the power signal [203]. The high pass filter consists of a low pass filter, whose output is subtracted from the original signal. In this way, as the high energy density ESS (typically a battery) manages the low frequency component of the required power, lower and more constant discharge rates are applied to it. Other authors make use of weighting factors to determine the power proportion supplied by each storage device. Due to the difference in power to energy ratios of some storage technologies, a dynamically varying weighting factor is applied in [204].

5.1.3 Low Level Control

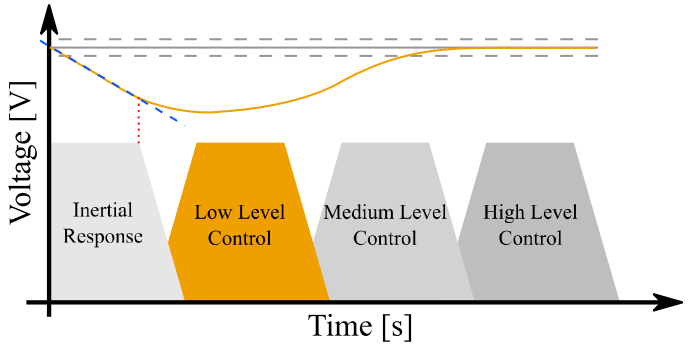

Fig. 5.6 Low Level Control operating range within a multilevel control structure.

This level is responsible for the control of the power electronic converter. Current and voltage control loops are implemented on this level (Fig. 5.6). There are several methods for the control of power converters and drives, from the classical PID controllers to the modern predictive controls. Some of them are very simple like the hysteresis control, while other more modern controls are more complex and have a higher computational burden.

When the converter uses a modulator, a linear controller can be used to control it. In this sense, the most common choice is the use of proportional-integral (PI) controllers. Normally, in DC-DC converters this type of control is composed of two loops, voltage and current loops to be precise.

With the aim of improving the dynamic response of these types of systems, the option of studying modern control strategies has been considered. After analysing some recent publications, it has been established that the Model Predictive Control (MPC) can be a strong candidate [205]–[208]. Not only for the low-level control, but also for the control of the whole HESS [209]. Unlike PI controllers, MPC is a multivariable control method that is ideally suited for multi-input multi-output (MIMO) systems. In addition, anti-windup mechanisms are not required in MPC since it does not accumulate the tracking error while trying to reach the reference value. This simplifies the design, analysis, and tuning process.

5.2 Single level control structures

In order to simplify the multilevel control structure, different alternatives have been sought. Currently, new applications require more demanding technical specifications including low level hard constraints that must be met by the control algorithm. On the one hand, it is intended to avoid the multilevel hierarchical scheme while at the same time the control includes all the required constraints and low level control within the same structure.

Regarding the low level control of the converter, obtaining a good performance over a wide operating range is particularly important. Nevertheless, this becomes a difficult objective due to the adjustment of the controllers for a single operating point of the linearized converter model.

For these reasons, the Model Predictive Control (MPC) has been considered as a suitable alternative to classical control techniques for this kind of applications.

5.2.1 Model Predictive Control

The Model Predictive Control for industrial applications appeared in the late 1970s. At that time, various prediction algorithms were developed relying on dynamic models of the process involved. Those algorithms were able to predict future output actions, by means of the predicted error minimization subject to some operating constraints.

In the beginning, MPC was successfully applied in the chemical industry where time constants are long enough to perform all the required calculations [210]. However, its application in power electronics and drives is more recent due to the fast sampling times that are required in these systems.

The Predictive Control is not a specific control strategy, but is a broad field of control methods developed around certain common ideas. Despite the different MPC variations, five key attributes can be identified that are common to the family of model based predictive controllers:

- The use of a dynamic model to predict future outputs of the system.
- Constraints can be included, such as admissible switching transitions.

- A cost function that represents the desired behavior of the system.
- An optimization stage responsible for minimizing the cost function.
- The implementation of a receding horizon strategy.

5.2.1.1 Model predictive control strategy

MPC is an optimization problem that consists of minimizing the cost function *J*, subject to the model of the system and its constraints. At each *t* instant, future outputs are predicted for a given horizon N_p, also referred to as prediction horizon. The optimization problem is solved at each sampling instant, considering the new measured data and obtaining a new sequence of optimal actuations each time. This is called a *receding horizon* strategy [210].

Unfortunately, the computational burden of the MPC associated with solving the optimization problem, is dependent on the length of the prediction horizon. The number of possible solutions increases exponentially when extending the length of the prediction horizon, in the same way as the computational burden.

When the MPC is implemented in a real system, the time interval for calculations is very small. In that case, one of the possible solutions is the offline optimization using the system model, in what is termed explicit MPC. The result is a look-up table containing the optimal solution as a function of each state of the system.

Considering the discrete nature of power electronic converters, it is possible to simplify the optimization problem considering the finite number of switching states. This reduces the number of calculations and allows its online implementation in the algorithm.

The general MPC scheme for power converter control is shown in Fig. 5.7. The main considerations for the MPC design and application are described below.

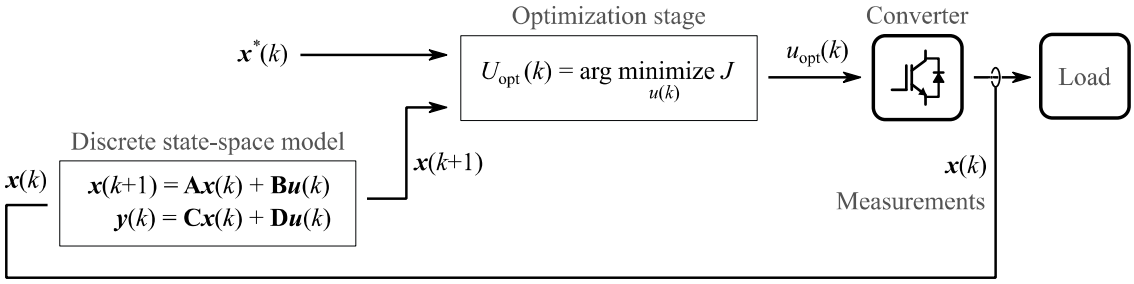

Fig. 5.7 General control scheme for MPC applied to power converters.

5.2.1.2 Dynamic Model

The internal dynamic model enables MPC to predict the sequence of future system states and outputs for a given sequence of manipulated variables. In power electronics, when choosing voltages or currents as state and output, the continuous-time state-space representation can be written in the following matrix form:

$$\frac{d\mathbf{x}(t)}{dt} = \mathbf{A}\mathbf{x}(t) + \mathbf{B}\mathbf{u}(t) \tag{5.1}$$

$$\mathbf{y}(t) = \mathbf{C}\mathbf{x}(t) + \mathbf{D}\mathbf{u}(t) \tag{5.2}$$

Most linear MPC strategies are formulated in the discrete-time domain using a constant sampling period T_s. The manipulated variable changes only at $t = kT_s$ discrete sampling instants, where $k \in \mathbb{N} = \{0,1,2,...\}$ denotes the time steps. Integrating from $t = kT_s$ to $t = (k+1)T_s$ and knowing that $\mathbf{u}(t) = \mathbf{u}(k)$, the discretization with zero order hold method can be applied. The resulting discrete-time state-space representation can be written in the following form:

$$\mathbf{x}(k+1) = \mathbf{A}_d\mathbf{x}(k) + \mathbf{B}_d\mathbf{u}(k) \tag{5.3}$$

$$\mathbf{y}(k) = \mathbf{C}_d\mathbf{x}(k) + \mathbf{D}_d\mathbf{u}(k) \tag{5.4}$$

Where discrete matrixes can be computed as:

$$\mathbf{A}_d = e^{\mathbf{A}T_s} \tag{5.5}$$

$$\mathbf{B}_d = \int_0^{T_s} e^{\mathbf{A}\tau} d\tau \mathbf{B} = \frac{(\mathbf{A}_d - \mathbf{I})\mathbf{B}}{\mathbf{A}} \tag{5.6}$$

$$\mathbf{C}_d = \mathbf{C} \tag{5.7}$$

$$\mathbf{D}_d = \mathbf{D} \tag{5.8}$$

A simpler way for the model discretization is the forward Euler method. Where the discrete state equation is written as follows:

$$\boldsymbol{x}(k+1) = \underbrace{(\mathbf{I} + T_s\mathbf{A})}_{\mathbf{A}_d}\boldsymbol{x}(k) + \underbrace{(T_s\mathbf{B})}_{\mathbf{B}_d}\boldsymbol{u}(k) \tag{5.9}$$

One of the weaknesses of MPC is the need of an accurate model of the system. Generally, the quality of the controller depends on the quality of the model.

5.2.1.3 Constraints

Constraints are added to prevent the system from operating outside of its safe operating limits. However, there are two main different types of constraints depending on the physical nature of the manipulated variable.

When the manipulated variable is indirectly controlled as in the case of voltage or current, the upper and lower constraints can be slightly violated even though at a high cost. In that case, the constraints are defined as *soft constraints*.

Conversely, the switch position u of the converter is an integer value. There are only two states for ideal power switches: on and off. Due to its physical nature, these constraints are defined as *hard constraints*. In the case of the synchronous buck converter for example, the input constraint are:

$$u(k) \in \{0,1\} \tag{5.10}$$

For each step, only one switch transition is allowed. In other words, at time step k the admissible $u(k)$ differ by at most one step from the previous $u(k-1)$ switch position.

$$\Delta u(k) = u(k) - u(k-1), \left|\Delta u(k)\right| \leq 1 \tag{5.11}$$

If the converter uses a modulator, then $u(k)$ will be constrained to a bounded continuous set. In that case, the components of the output vector will correspond to duty cycles $d(k)$, or PWM signals [211].

$$u(k) = d(k) \in [-1,1] \tag{5.12}$$

5.2.1.4 Cost Function

In a traditional control scheme, the limitation of internal variables is achieved by including saturations for the reference of these variables. In a predictive control scheme, these limitations can be included in the cost function. Therefore, a cost function that represents the desired behavior of the system needs to be designed.

The cost function penalizes the deviation of controlled variables from their references. However, that penalization have different impact depending on the norm used. In this sense, predictive current control with reference tracking was originally proposed with the 1-norm, where the tracking error cost depends linearly on the current error. On the other hand, if a 2-norm is used, the tracking error cost will depend quadratically on the current error.

The following cost function example (eq.(5.13)) consists of two terms. The first term penalizes the predicted current tracking error quadratically. The second term penalizes the switching effort and λ is a weighting factor that can be adjusted in order to modify the importance of its corresponding term.

$$J = \left(i^{*}\left(k+1\right) - i^{p}\left(k+1\right)\right)^{2} + \lambda_{u}\left|\Delta u\left(k\right)\right| \tag{5.13}$$

5.2.1.5 Optimization stage

The discrete time domain model is used to predict the controlled variable, current for example, at time-step $k+1$ for all admissible $u(k)$ switch positions. The argument of the result is the optimal sequence of manipulated variables $U_{opt}\left(k\right)$. The optimization problem is stated as

$$U_{\text{opt}}\left(k\right) = \arg\underset{u(k)}{\text{minimize}}\, J \tag{5.14}$$

The optimal switch position is obtained by minimizing the cost function J. That switching state is applied during the next sampling period.

5.2.1.6 Receding Horizon

Solving the optimization problem future outputs of the system are predicted from $k+1$ to $k+N_p$, though only the first element is used. At the next sampling step $\left(k+1\right)$ the system state $\boldsymbol{x}\left(k+1\right)$ is estimated and the horizon is shifted by one step in what is called *receding horizon*.

In general, the use of a one step prediction horizon is more intuitive and easier to implement in power electronics. For direct MPC with reference tracking, the computational cost of solving the optimization problem normally limits the prediction horizon to one. In some cases, long prediction horizons can improve the converter performance at steady-state operation, nevertheless in most cases a prediction horizon of one suffices.

5.2.2 MPC working example

All the concepts about MPC mentioned above, are shown graphically in Fig. 5.8. As illustrated here, the dynamic model of the system is evaluated at instant *t*(*k*) and future

system states are calculated for $t(k+1)$. In this specific example, only two possible switching states are considered for the converter. After evaluating the cost function for these two options, the switch position that provides the smallest cost function value is selected and applied. Note that the cost function not only considers the current tracking error, but also penalizes the switching effort (eq.(5.13)). After applying the new switching state, all the process is repeated at the next sampling instant in what is called receding horizon.

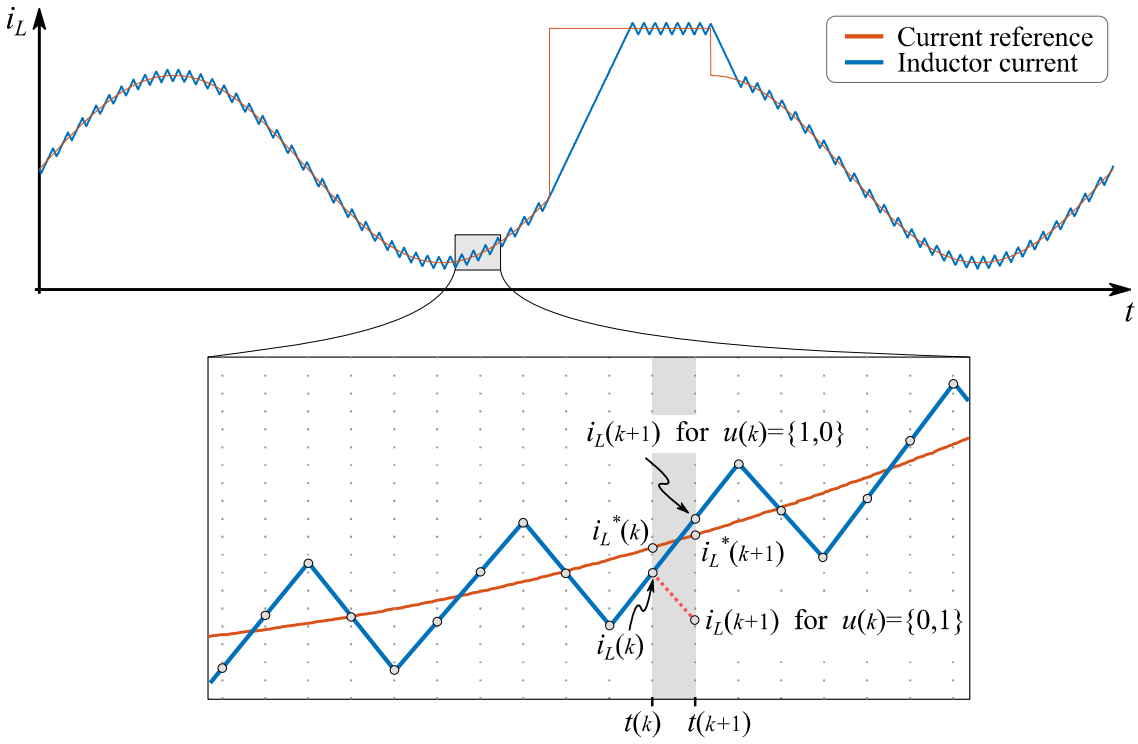

Fig. 5.8 MPC working principle simulation example for inductor current control.

5.3 Power Sharing

The power sharing is one of the key tasks to perform the energy management in a hybrid energy storage system (HESS). Regardless of the control scheme used, single level or multilevel, power sharing is necessary to optimally use both storage devices.

While it is true that the general concept of hybridization is based on the power and energy distribution, the way to achieve it usually differs depending on the application (Fig. 5.9). In photovoltaic applications is more common to control the system as a state machine, that is why rule based control is the prevailing trend. In the case of electric vehicle, due to the fast dynamics managed in this application the filtering technique is the most used one. Lastly, the use of virtual impedances is more common in microgrid applications where multiple devices with different dynamics are connected in parallel.

In the following subsections the most used power sharing techniques are presented and explained. Together with this, simulation results are presented for a better understanding of the different power sharing techniques.

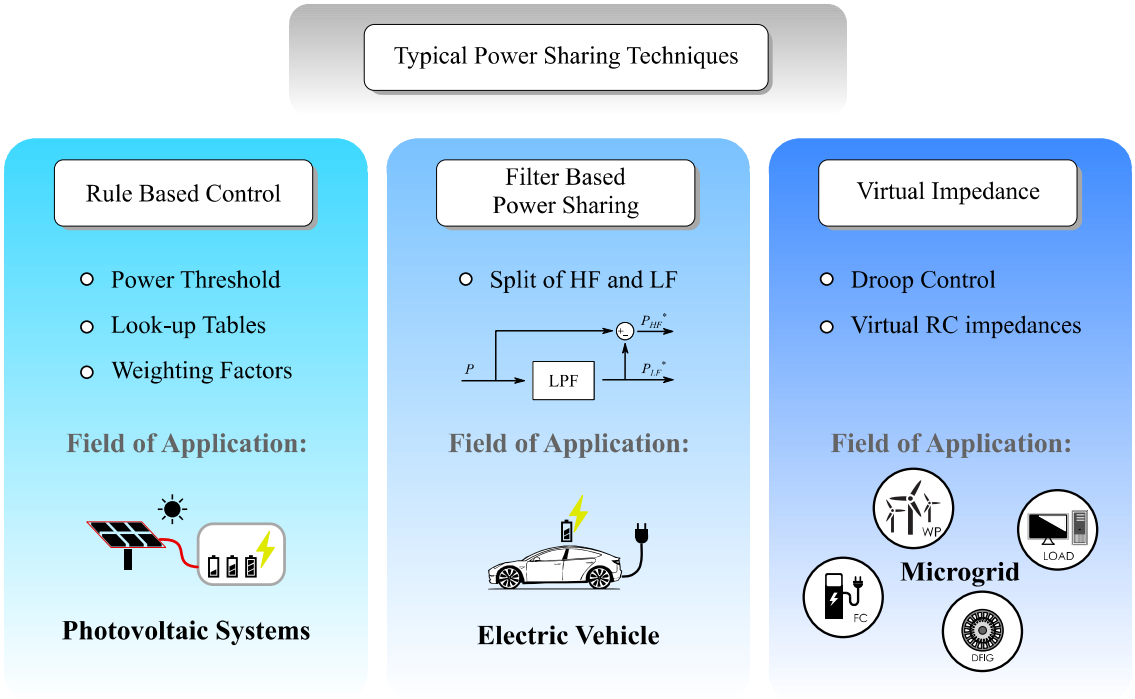

Fig. 5.9 Typical power sharing techniques and their field of application.

5.3.1 Rule based control

5.3.1.1 Power threshold

One of the simplest methods consists of applying a power level threshold to divide the power between the ESSs. In this sense, the high power density ESS would supply all the power demand exceeding the predefined threshold (eq.(5.15)).

$$P_{tot} = \begin{cases} P_{batt} + P_{UC}, & if\ P_{tot} > P_{batt\max} \\ P_{batt}, & Otherwise \end{cases} \tag{5.15}$$

In this case, the maximum power value is 300W, which corresponds to 25A in the ESS 12V side. The constant power consumption is set to 60W, what means 5A in the 12V side. Setting the Ibatt_max to ±6A, the following current distribution is obtained (Fig. 5.10).

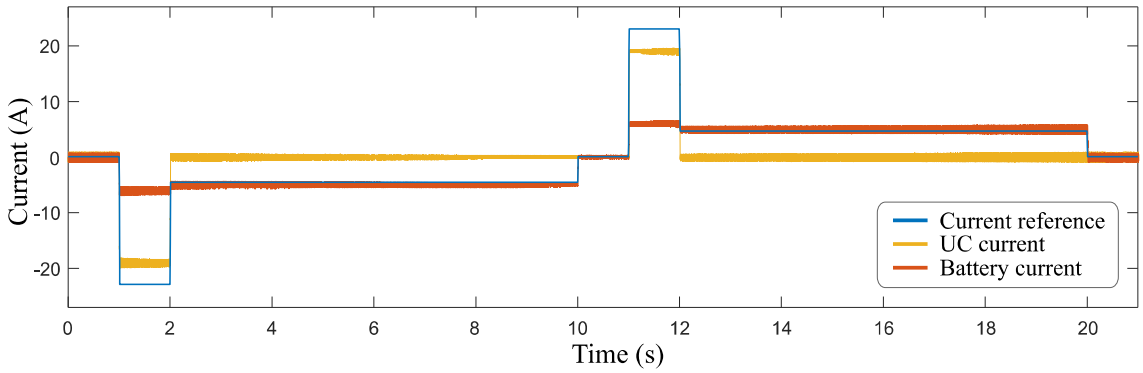

Fig. 5.10 Power distribution applying level threshold under pulsed load.

Now we have the same power sharing method considering the Ibatt_max to ±6A predefined threshold under an electric vehicle city power profile (Fig. 5.11). As it can be seen, the battery supplies all the required power when the power level is smaller than the threshold. The UCs would supply only the power levels greater than the threshold.

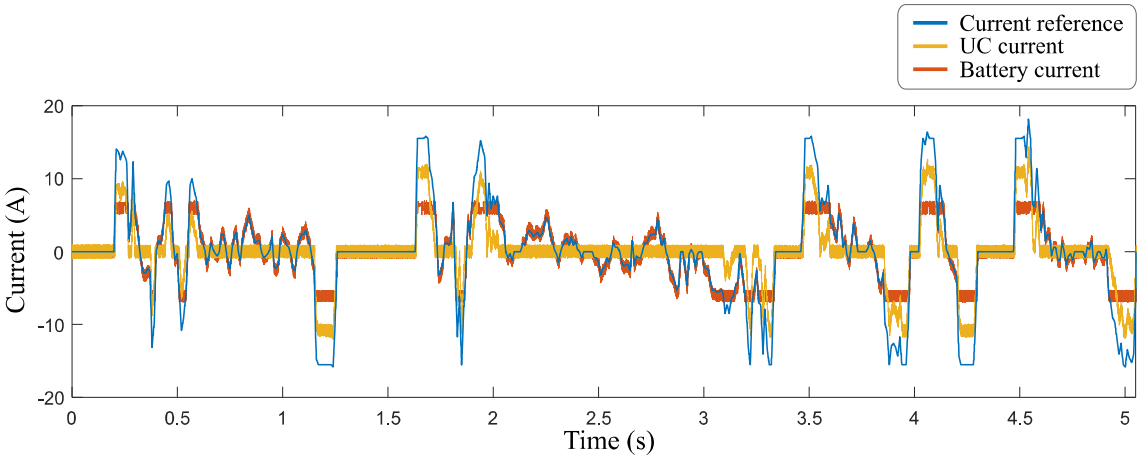

Fig. 5.11 Power distribution applying level threshold under EV city power profile.

5.3.1.2 Look-up tables

Some other methods are based on reference tables to perform the power distribution. Depending on the power level managed at each time, some predefined patterns are used to distribute it between the storage devices (Fig. 5.12).

These patterns can vary in order to obtain the most suitable solution depending on the needs of each application. In this sense, the definition of these tables or constraints is not fixed. Multiple tables can be designed and applied depending on different parameters such as the SoC of each storage device. This can be programed as a state machine where the SoC, power level, temperature and some other parameters are the inputs that define the look-up table used at each instant.

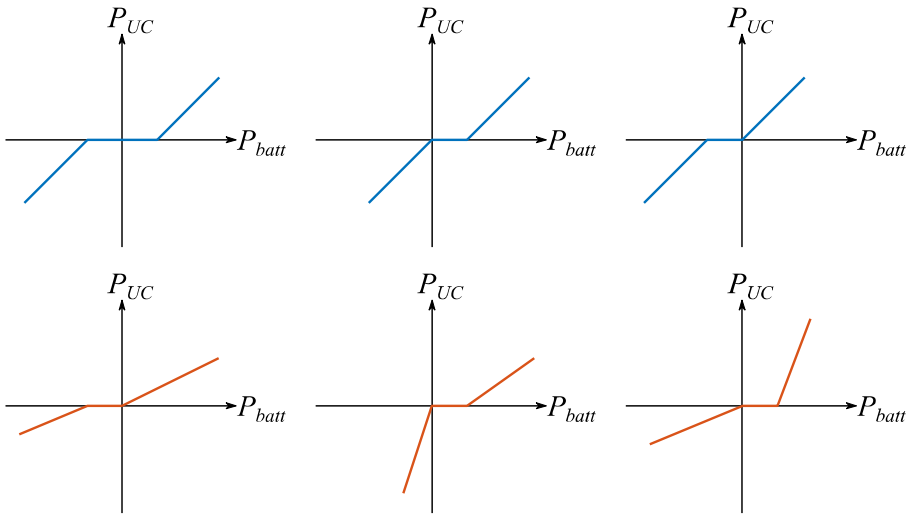

Fig. 5.12 Examples of look-up table power distribution patterns.

An example of this is presented below (Fig. 5.13 and Fig. 5.14).

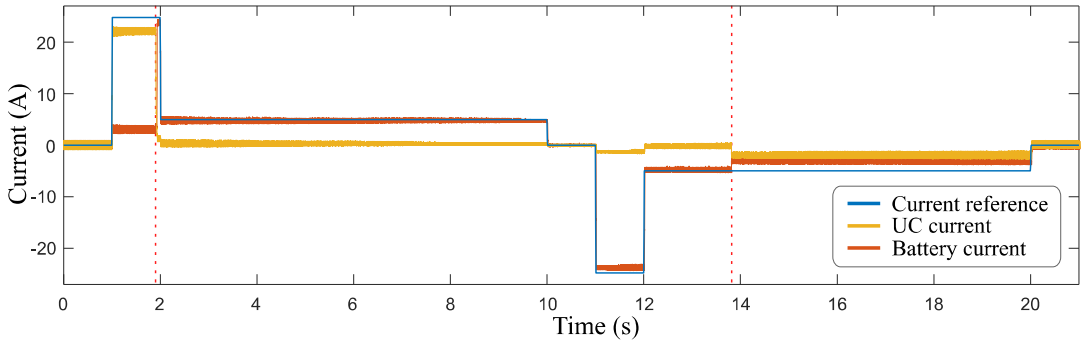

Fig. 5.13 Look-up table based power distribution.

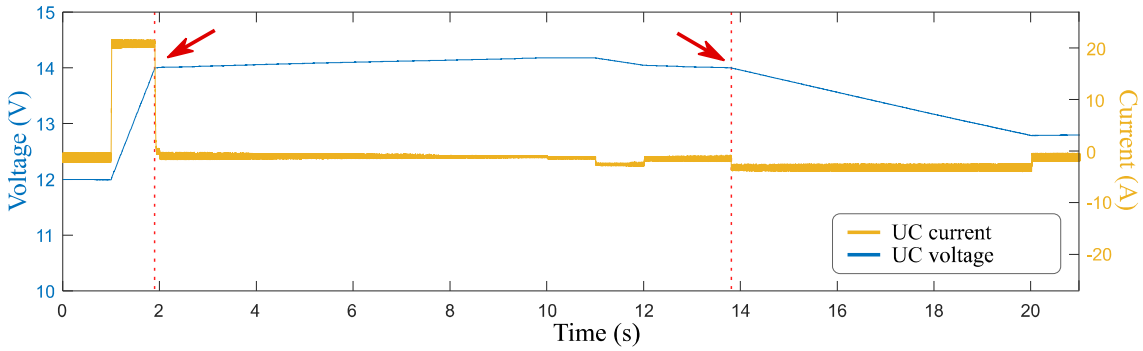

Fig. 5.14 Look-up table based power distribution. Voltage and current levels of the UCs.

In this example, even though the battery is able to provide higher current levels, it is limited to ±3A provided that the UCs maintain their voltage within the safety limits (between 6 and 14V). If any of these limits are exceeded, the system changes the look-up table to another one reducing the availability of UCs until their voltage returns again within its operating range. At this point, the battery would manage nearly all the required input or output power until the voltage level of the UCs is back within the limits. When that happens, the battery current will again be limited to ±3A. These two specific moments are marked with a red arrow in the Fig. 5.14.

This is just a simple example of how the control logic could be configured, but there exist multiple options. In this sense, the so-called barrier functions (Fig. 5.15) could also be used, which could reduce some lines of code. These barrier functions avoid the violation of the predefined constraints by growing to infinity when its arguments approach the operating limits [212]. This can provide a more gradual power distribution, in this way avoiding abrupt transitions. Barrier functions can be designed to be symmetric

for the whole operating range as it is shown in Fig. 5.15, or asymmetric to fit the desired working mode.

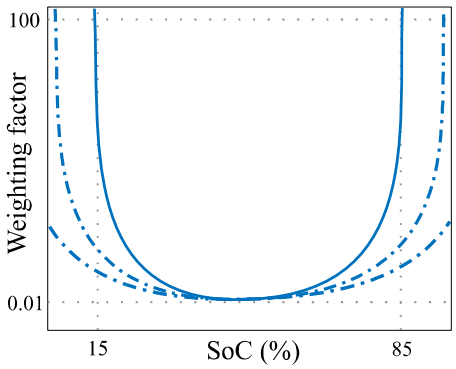

Fig. 5.15 Barrier function relating the SoC with a weighting factor.

5.3.1.3 Weighting factors

Other authors make use of weighting factors λ to determine the power proportion supplied by each storage device. Based on the difference in power to energy ratios of some storage technologies, a dynamically varying weighting factor can be also applied [204]. But not only that, as it has been mentioned before in the case of the look-up tables, this weighting factor can be modified according to different criteria behaving like a state machine. In that sense, it has many similarities with the look-up tables.

$$P_{tot} = \lambda \cdot P_{batt} + (1-\lambda) \cdot P_{UC} \tag{5.16}$$

An example of this is presented below. On the Fig. 5.16, the weighting factor is fixed to 0.3 for the UCs and 0.7 for the battery.

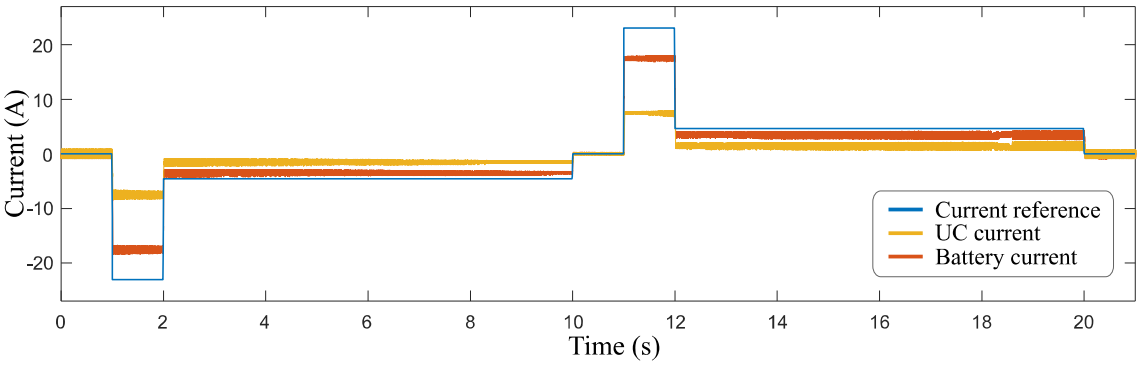

Fig. 5.16 Weighting factor based power distribution under pulsed load.

The effect of the weighting factor can be more clearly appreciated in the electric vehicle power profile. In the example outlined below, the proportion of the current supplied by each storage device have been reversed with respect to the previous example. In this case (Fig. 5.17), the weighting factor for the UCs is 0.3 and 0.7 for the battery.

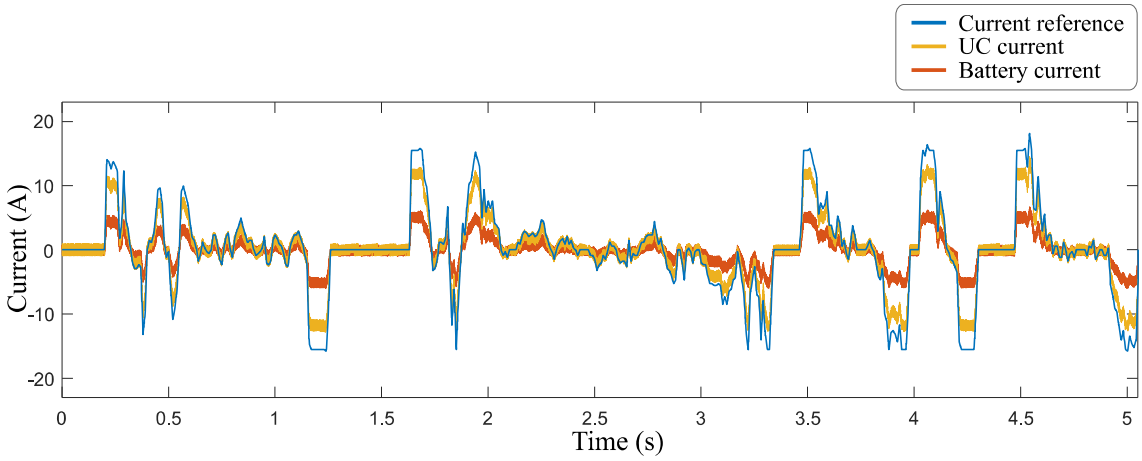

Fig. 5.17 Weighting factor based power distribution under EV city power profile.

5.3.2 Filters based power sharing

Other methods perform the power sharing by means of a high pass filter to separate the high frequency and low frequency components of the power signal [116], [169], [213]. The high pass filter consists of a low pass filter, whose output is subtracted from the original signal. This can be more clearly seen in Fig. 5.18. In this way, as the high energy density ESS (typically a battery) manages the low frequency component of the required power, lower and more constant discharge rates are applied to it.

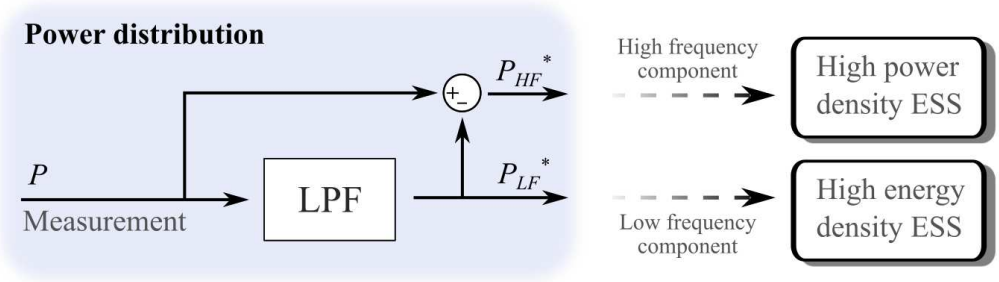

Fig. 5.18 Filter based high-level power distribution.

Considering the same consumption profiles from the previous cases, the following results are obtained with the filtering technique (Fig. 5.19). In the first instant, due to the fast power increase, the filter forces the UCs to supply nearly the total power. Thanks to this, the battery can start rising with a smaller slope until it reaches the reference power level. In this cases, if the power step lasts long enough, the battery will end up driving the total power required by the application because there is not power threshold limit.

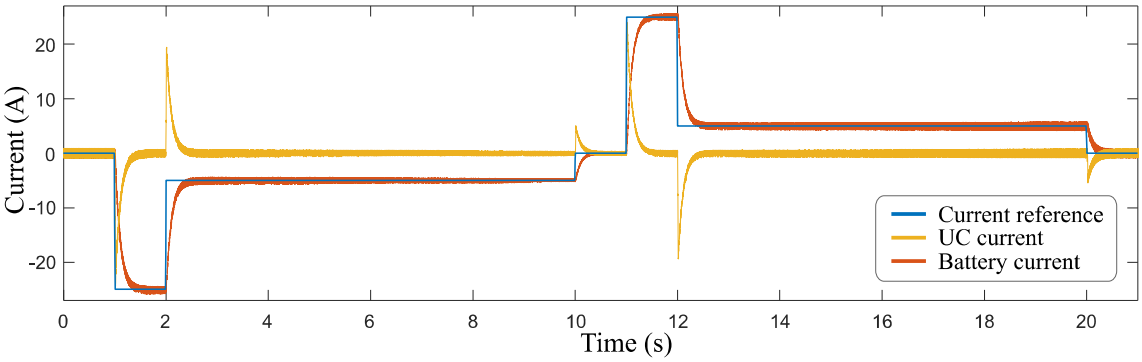

Fig. 5.19 Filter based power distribution under pulsed load.

In any case, the filter can be modified to adjust the behavior of the application. In this sense, if we consider the previously mentioned electric vehicle city power profile, we

can see that the battery never reaches the total power (Fig. 5.20). Due to the fast reference change and the unpredictability of the car consumption, the filtering technique makes more sense in these types of scenarios. In any case, power limitation should be considered as a hard constraint as a security measure.

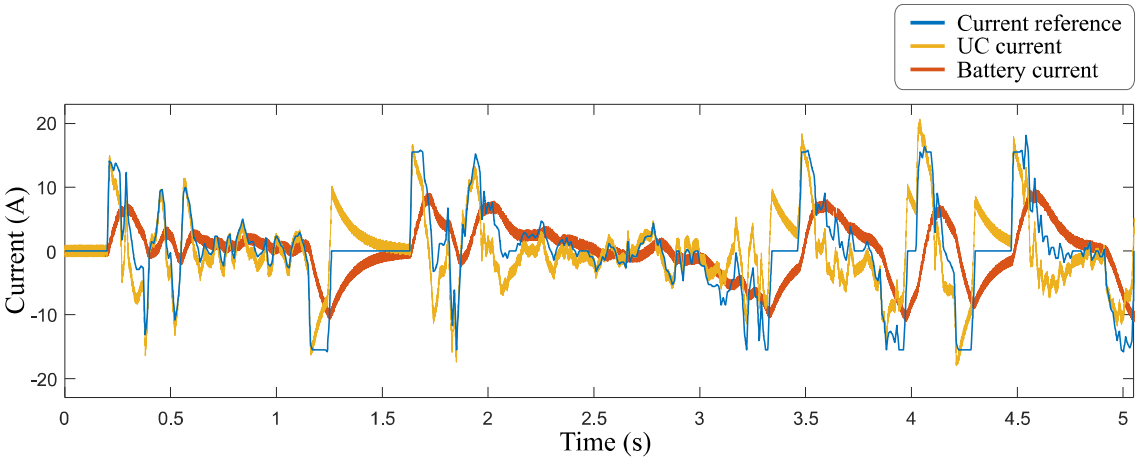

Fig. 5.20 Filter based power distribution under EV city power profile.

One the drawbacks of the filtering technique is its difficulty in stopping the supply of the current when the reference goes abruptly to zero. This can be seen in the time range from 1.25 to 1.7 seconds, where there is a current recirculation between the battery and the UCs so that the effective output current is set to zero.

5.3.3 Virtual impedance

In general terms, a virtual impedance is a passive element that is not physically in the circuit but is virtually added to the control algorithm so that it behaves as if it were there. Virtual impedances are used to change the output impedance of the converters connected to the same bus or grid. Therefore this contributes to the output impedance matching, what at the same time improves the current sharing between the parallel connected converters.

The droop represents a real value, what in practice can be interpreted as a virtual resistor. Its effect is the generation of a virtual voltage drop at the output of the converter, directly proportional to the current flowing through that output. This type of control has often been used for the parallel connection of different power supplies such as UPSs, achieving good power sharing [214].

In addition to the droop control, other impedance elements such as virtual inductors or capacitors can be added based on the same concept. In this sense, the output impedance can be considered as an additional control variable. Between both, virtual capacitors are more commonly used in combination with virtual resistors for inertia emulation in islanded DC microgrids. Nevertheless, this virtual impedance concept is equally valid for AC systems connected to the main grid.

5.3.3.1 Droop control

The droop control is a proportional (P) type of control, typically used in microgrid applications where a great amount of Power Electronic Converters (PECs) are connected in parallel. The main objective of droop control is to emulate the droop characteristic of grid connected generators due to the inertia. Inertia is an inherent physical characteristic of rotary generators. This type of control does not require communication between the different PECs so it can regulate the primary response in a stand-alone mode. For this reason, such physical behavior is emulated in the control of each converter separately. With this type of control, it is possible to react automatically against load consumption variations before the rest of controls start operating.

In AC grids, load changes directly affect the frequency and the voltage amplitude of the grid, whilst in DC grids only the voltage level is affected. Considering this, droop control in AC grids regulates the output frequency by controlling the active power of the converter while the output voltage is regulated by controlling the reactive power (Fig. 5.21).

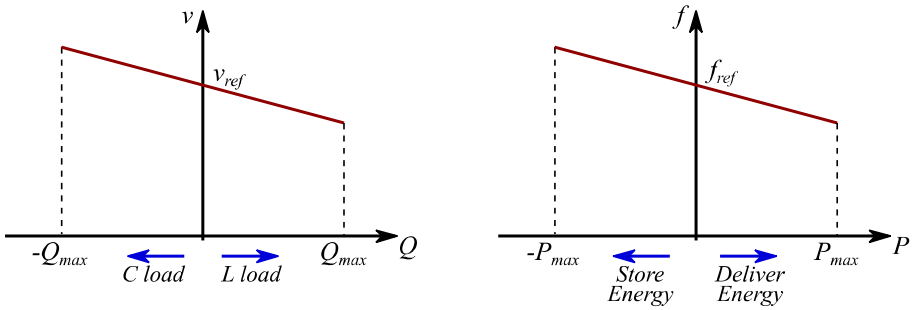

Fig. 5.21 Droop control characteristic for AC systems [215]**.**

In the case of DC grids, the droop control reacts proportionally to the difference between the grid voltage reference and the measured one. Thanks to this, each converter will behave like a voltage source with high inertia. In this case, active power is exchanged to regulate the grid voltage (Fig. 5.22).

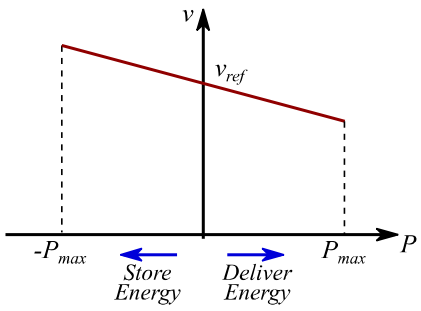

Fig. 5.22 Droop control characteristic for DC systems.

The possibility of applying different droop characteristics for each parallel connected PEC, enables the integration of devices like loads or storage elements with completely different operating dynamics. This makes it an appropriate candidate for its integration in the control of HESSs.

5.3.3.2 Virtual RC impedance

Including different electrical components directly into the circuit would modify the general behavior of the system, nevertheless this would imply more unnecessary power losses. In order to emulate the same behavior but avoiding the physical modification of the system the integration of virtual impedances within the control algorithm can be a suitable solution (Fig. 5.23).

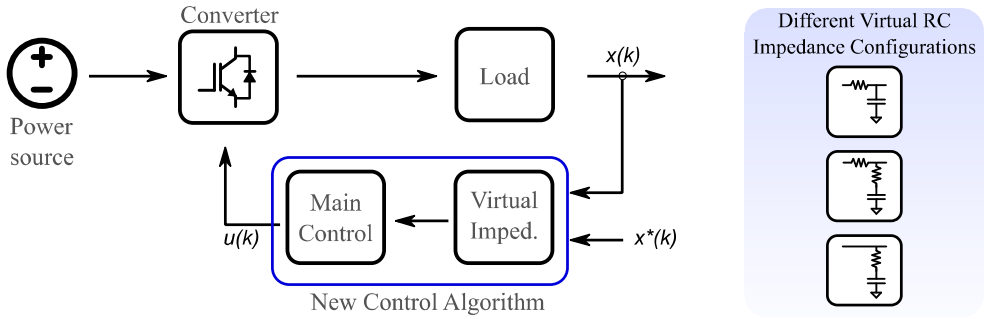

Fig. 5.23 Control scheme integrating the virtual impedance into the control algorithm.

Among the different virtual impedance component variants that can be implemented, the most interesting components to include in DC systems would be resistors and capacitors. With these components, the dynamic behavior of the converter can be modified emulating different inertial responses to abrupt load changes.

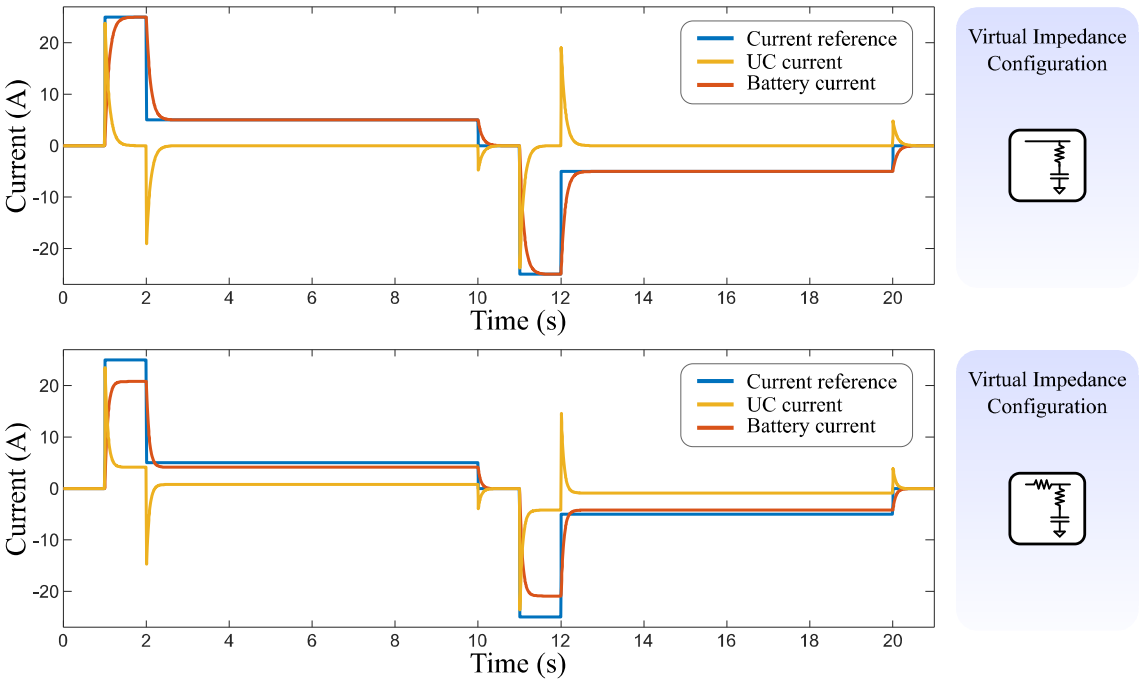

Fig. 5.24 System response under two different virtual impedance configurations.

In Fig. 5.24 the response of the system is analyzed for two different virtual impedance configurations. In the upper configuration the virtual impedance is composed of a RC branch emulated to be in parallel with the converter output. In this case the transient response of the converter is filtered but it has no effect in steady state operation.

On the other hand, the lower configuration is slightly different since it adds a virtual resistor in series with the output of the converter. In this case, the transient response is filtered as in the previous configuration by making use of the parallel RC branch. However, this configuration is able to modify the output steady state value thanks to the virtual series resistor. This resistor emulates a voltage droop that can be modified to converge to the desired value.

5.4 Conclusion

There are several methods for the control of power converters and drives. In this sense, the most common choice is the use of multilevel control structure composed of proportional-integral (PI) controllers. This configuration implies the tuning of several cascaded control loops.

Model predictive control is presented as an alternative to this multilevel structure. The use of this kind of control makes it possible to operate with a single control loop. In this sense, all the necessary parameters should be included within the cost function, together with the operating constraints.

According to the different power sharing techniques, several methods have been found on the literature. In most cases, the use of one method or the other will depend on the particular features of the application.

Classical rule based methods are robust and widely used in photovoltaic and industrial applications. Although they can provide a suitable power distribution in steady state, the transient response behavior is their weakest point. Nevertheless, this weak point can be partially solved making use of predefined barrier functions.

Just the opposite occurs in the case of the filtering method. This method works well for systems with abrupt and unpredictable operating changes such as electric cars. However, it does not provide a suitable solution for the steady state.

Novel control strategies such as virtual impedances are presented as an interesting solution for future high performance applications. The different virtual impedance configurations can be useful to modify separately the transient response and steady state of the system. In this sense, the virtual impedance can be configured to make the system behave like a filtered system while at the same time it imposes an operating threshold in steady state.

Chapter 6

CASE STUDY I: PI VS FCS-MPC AND CCS-MPC

In this Chapter, a system composed of a battery and a DC-DC converter has been evaluated under two different Model Predictive Control strategies and classical PI control. The two MPC strategies are the Finite Control Set MPC and the Continuous Control Set MPC.

In Finite Control Set MPC the switching states are directly selected and applied, while in Continuous Control Set MPC an additional modulation stage is needed to do that job. The particularities of each control structure have been studied and analyzed.

Simulation results are included to display the steady state and dynamic response, and also to show the main differences between the algorithms. Experimental results are included to validate the previously simulated comparative analysis.

6.1 Finite Control Set MPC vs Continuous Control Set MPC

There are two main categories comprising the MPC techniques applied to power electronics [216]: Continuous Control Set MPC (CCS-MPC) and Finite Control Set MPC (FCS-MPC).

The CCS-MPC (Fig. 6.1 (a)) uses an average model of the converter to perform an optimization that minimizes the error between the reference and the future state. In this case, the controller output is the duty cycle reference applied to the modulator, which then generates the proper switch positions. On this basis, due to the use of a modulator, the converter presents a fixed switching frequency. On the other hand, the FCS-MPC (Fig. 6.1 (b)) makes use of the discrete nature of power converters to select the optimal switch positions. This control method evaluates all the possible switching states and selects the one which minimizes the designed cost function. The optimization stage in this case is simpler than the one used in CCS-MPC since the amount of possible solutions is limited.

Once the main mathematical model is developed, constraints have to be defined to prevent the system from working outside of its safe operating limits. However, there are different types of constraints depending on the physical nature of the variable to be limited. When the variable can be slightly violated, as is the case of inductor current, it is defined as a soft constraint. On the other hand, the switch positions are defined as hard constraints to prevent the converter from working under forbidden states. Thus, in the CCS-MPC where a modulator is used, the duty cycle values will be constrained by:

$$d(k) \in \mathbb{U} \triangleq [0,1] \subset \mathbb{R},\ k \in \{0,1,2,...\} \tag{6.1}$$

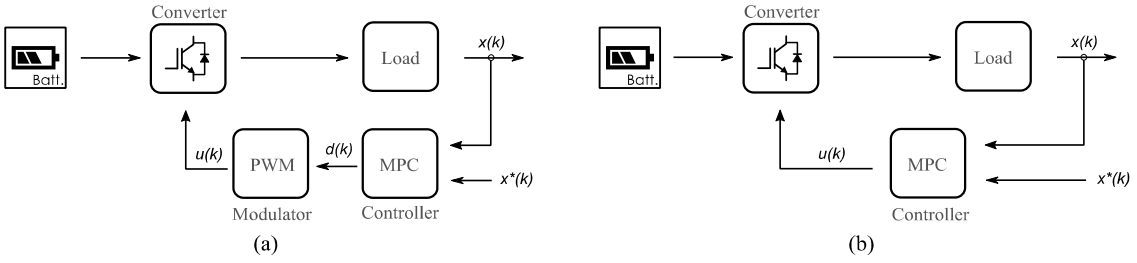

Fig. 6.1 (a) Continuous Control Set MPC (CCS-MPC). (b) Finite Control Set MPC (FCS-MPC).

While under the FCS-MPC strategy, the switch positions are constrained to belong to a finite set:

$$u(k) \in \mathbb{U} = \{0,1\} \subset \mathbb{R},\ k \in \{0,1,2,...\} \tag{6.2}$$

In addition to defining the corresponding constraints, a cost function should be added to the predictive control scheme. The cost function must contain the necessary terms to ensure the desired behavior of the system. In this sense, it will penalize the deviation of the controlled variables from their reference values.

Although the overall functioning of CCS-MPC and FCS-MPC is very similar, there are certain differences in the way its cost functions and optimization stages are approached. In the case of CCS-MPC, the control makes use of an averaged model of the system to calculate the optimal duty cycle. In this case, the cost function (eq.(6.3)) is depicted as a single-variable function which is minimized on a fixed interval (eq.(6.4). Once the optimal duty cycle is selected, a modulator is used to generate the proper switching commands.

$$J(d) = \left| i^* - i^p(d) \right| \tag{6.3}$$

$$J_{opt} = \min_d J(d), \quad \text{such that} \quad d \in [0,1] \subset \mathbb{R} \tag{6.4}$$

In the case of FCS-MPC, the control uses a switched model of the converter to predict the future behavior of the state variables for all possible switching states. The cost function value is calculated considering the predicted state variable values and the results are stored in a matrix. Finally, the resulting matrix is evaluated and the switch position that minimizes the cost function is selected and directly applied.

Equation (6.5) shows the cost function used for the FCS-MPC implementation. The main objective is to penalize the current tracking error. To achieve this, the difference between the predicted current and the reference has been computed in quadratic form. A second term has been added to penalize the switching effort and λ is a weighting factor that can be adjusted in order to modify its importance.

$$J = \left(i^{*}\left(k+1\right) - i^{p}\left(k+1\right)\right)^{2} + \lambda_{u}\left|\Delta u\left(k\right)\right| \tag{6.5}$$

Since the CCS-MPC presents a fixed switching frequency, the switching effort penalization makes no sense. Instead, the duty cycle change is sometimes penalized with the aim of limiting the transient response. As the switching effort penalization is not used in CCS-MPC in this case, its analysis has been done only for FCS-MPC as will be shown later.

The evaluation of these cost functions for long prediction horizons, can slow down calculations in both algorithms. In this sense, the use of a one-step prediction horizon reduces the computational cost of the MPC, and normally suffices for current tracking in power electronics applications. In addition to that, differing from the FCS-MPC strategy, the performance obtained by using CCS-MPC can be different depending on some particular aspects.

On the one hand, the output duty cycle constraints can vary the transient response speed of the system. If the duty cycle range is fixed between 0,1 and 0,9 instead of 0 and 1, for example, the transient response will be slower. In spite of this, it has the benefit of maintaining the switching frequency constant avoiding the over modulation. This can be interesting when designing output filters. On the other hand, the number of iterations inside the optimization stage influences the choice of the optimal duty cycle. The more times the algorithm is executed, and the greater the number of iterations, the greater the computational cost. However, if both are too low, the accuracy of the control drops and the current tracking control may end up failing. That is why it is convenient to seek a compromise between these aspects.

6.1.1 Simulation results

The main task is to achieve an accurate control of the battery current for both charge and discharge processes. For the simulation, the power electronic converter and the battery were built in Simulink while the MPC algorithm was implemented in a Matlab function. The system parameters are displayed in Annex C.

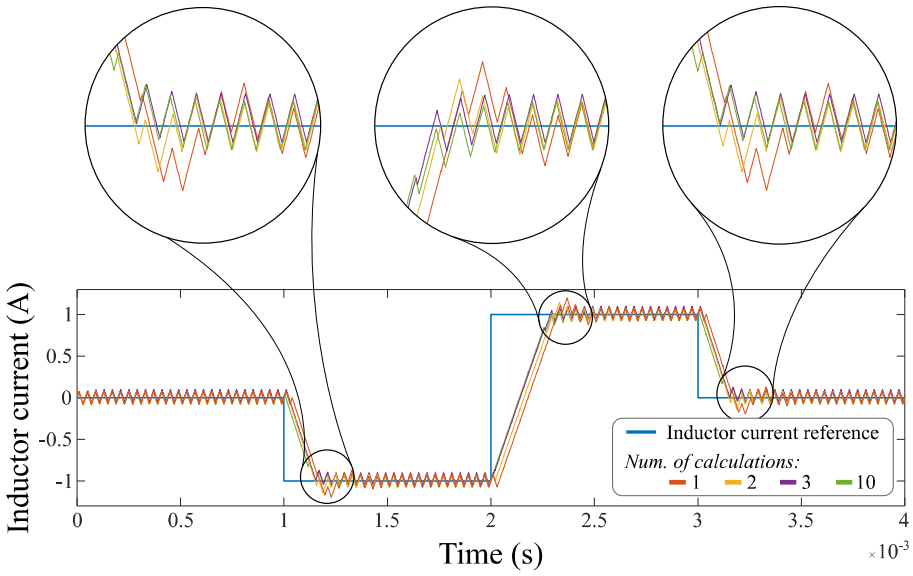

Fig. 6.2 Number of times the algorithm is executed (Number of calculations) per PWM period.

As it has been mentioned before, the amount of times the algorithm is executed and the number of iterations, directly affect the performance of the system. If the algorithm is executed a small number of times, the transient step response of the inductor current suffers a slight delay followed by an overshoot (Fig. 6.2). However, these problems occur when the algorithm is executed once or twice per each PWM period. If the algorithm is executed three or more times, these problems are drastically reduced.

The abovementioned simulation was carried out performing 10 iterations inside the optimization stage, which is a suitable number of iterations as shown in the subsequent analysis. To evaluate the effect of the number of iterations, first of all the number of calculations per each triangular carrier period was fixed to 6.

The number of iterations has direct influence on the response speed of the converter facing a fast change in the reference. The more iterations the greater the precision in the search for the optimal duty cycle. As the number of iterations increases, the response speed of the converter increases as well (Fig. 6.3). However, there is a threshold from which no substantial improvement is obtained. As it happens with the number of calculations, a great number of iterations provides good accuracy but slows down the speed of the algorithm. It is important to adjust these two parameters in order to obtain a proper relationship between the performance and the computational cost. In this sense,

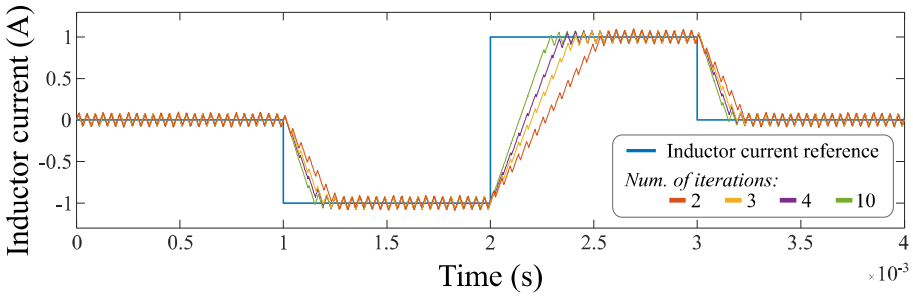

Fig. 6.3 Effect of the number of iterations over the transient response.

with an appropriate number of calculations and iterations the CCS-MPC can provide a transient response very similar to that of the FCS-MPC.

With respect to the FCS-MPC, the algorithm programmed in Matlab is shown in (Fig. 6.4). This algorithm should take into account the two switching states of the Synchronous Buck converter. Together with this, the state-space model of the system must be discretized in order to implement it in the microcontroller. Finally the control algorithm was implemented in Matlab, whereas the controlled plant was built in Simulink.

Since the switching frequency is not fixed in FCS-MPC, the weighting factor that penalizes the switching effort has a significant influence on it. As it can be seen in Fig. 6.5, the switching frequency and the current tracking error are directly dependent on the weighting factor value. As the weighting factor increases, so does the current error

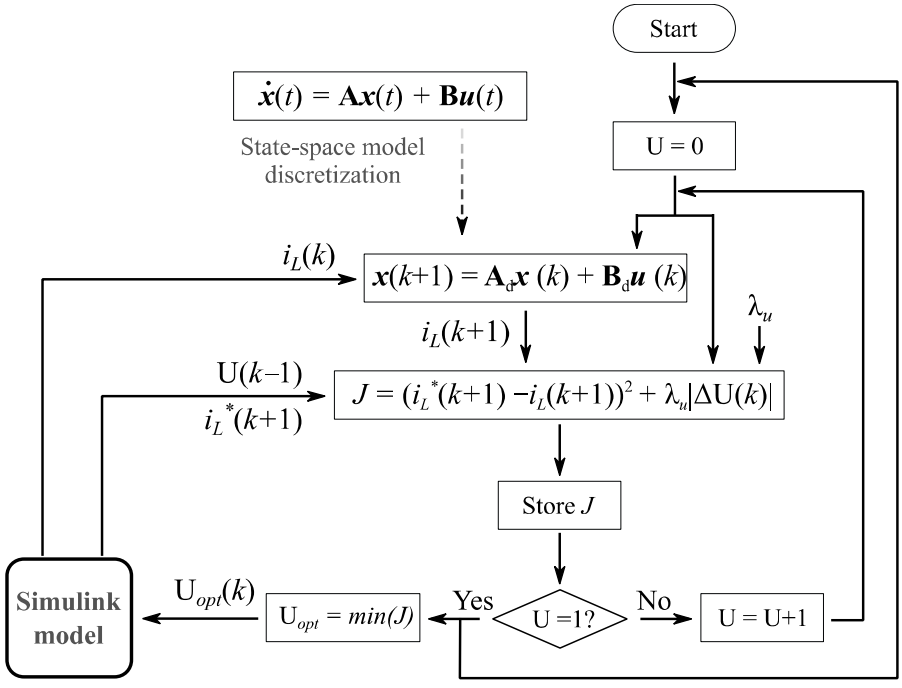

Fig. 6.4 Flow chart of the MPC algorithm for its implementation in Matlab-Simulink.

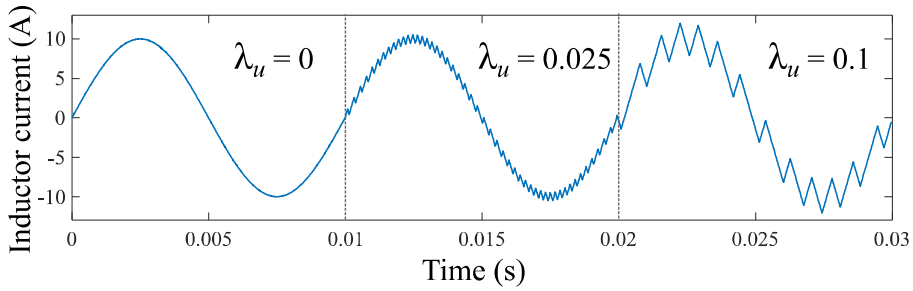

Fig. 6.5 Effect of the weighting factor on the switching frequency and current tracking error.

whereas the switching frequency decreases. It can be observed a linear relationship between the current tracking error and the weighting factor. On the other hand, the switching frequency and the weighting factor present an inverse relationship (Fig. 6.6).

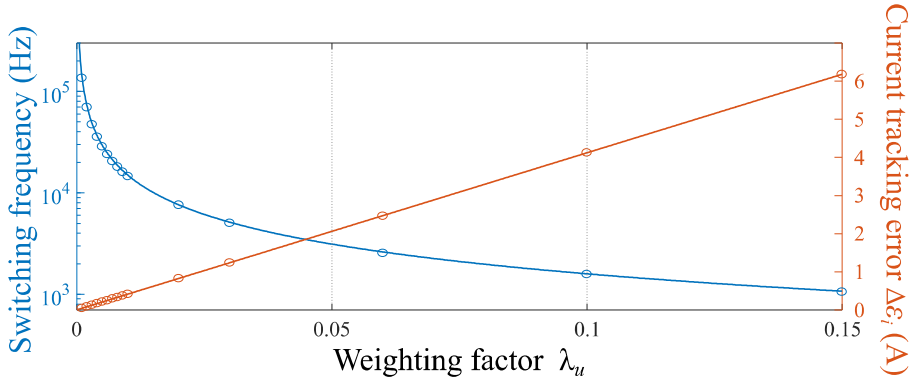

Fig. 6.6 Graph that relates the weighting factor with the switching frequency and the current tracking error.

With regard to its transient step response, it is faster than the CCS-MPC. The reason for this is that the FCS-MPC leaves the switches locked in what is supposed to be the optimal position until reaching the reference.

In order to compare the results of both algorithms, it was simulated under similar conditions in terms of switching frequency. In this sense, regarding to the CCS-MPC algorithm, the switching frequency of the PWM was set to 25 kHz. As for FCS-MPC, the algorithm execution period was set to $4 \cdot 10^{-5}$ seconds. In this case, if the system is working in steady state and the second term of the cost function (6.5) is neglected, this will correspond to a switching frequency of 25 kHz. In spite of this, the resulting switching frequency will vary during transients since the FCS-MPC choses the best switch position at each moment.

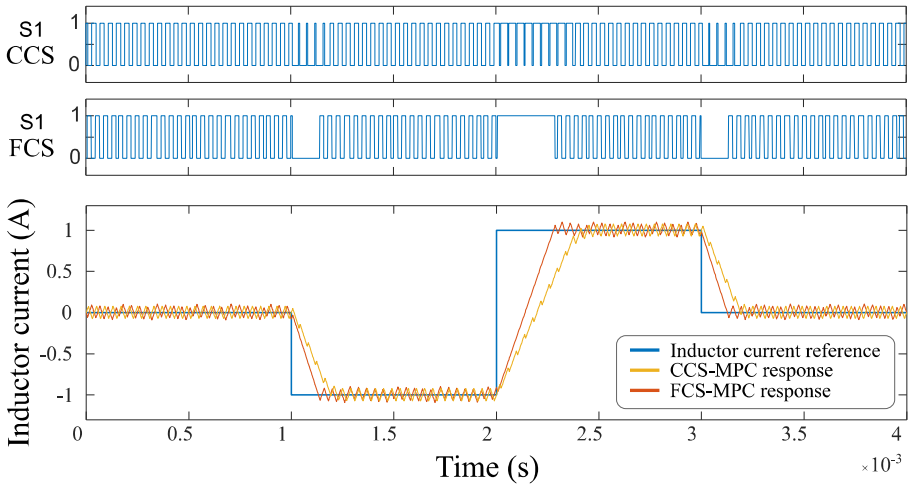

Fig. 6.7 Comparative analysis of CCS-MPC and FCS-MPC under step response.

As it has been mentioned before, CCS-MPC presents a constant switching frequency due to the use of a modulator. Because of this, during a step change in the reference, the converter continues switching. This makes it slightly slower than the FCS-MPC in response to reference changes (Fig. 6.7). It can be concluded that the Finite Control Set is more aggressive than the Continuous Control Set when facing a change in the reference. This behavior can produce more stress in the battery, but there is not a significant difference to conclude if this can cause a battery failure or not. Nevertheless, such precise control of the current and the fast transient behavior, can also be interesting for other energy storage devices with high power density like UCs.

6.1.2 Experimental results

Among the different hardware platforms used for the digital control of power converters, Microcontrollers (µCs), Digital Signal Processors (DSPs) and Field Programmable Gate Arrays (FPGAs) are the most common devices [217], [218]. For this study, a TI F28379D µC is used given the possibility of being able to program it directly form Simulink. This µC provides sufficient processing capacity required to evaluate the above mentioned model so that the optimal switching state is selected.

For the experimental validation of the previously simulated MPC current control, automatic code generation tools have been used. In this case, the algorithm implemented in Matlab was compiled and built into the TI F28379D µC [219] making use of Code

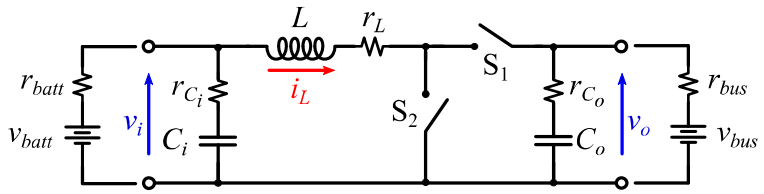

Fig. 6.8 Schematic of the synchronous buck converter used for testing.

Composer Studio v6. Note that the converter used for the test is the abovementioned synchronous buck converter shown in Fig. 6.8.

After implementing the MPC control on the microcontroller, the step response of the converter was tested for both MPC algorithms. In CCS-MPC the converter continues switching during the transient region only varying the duty cycle. In this sense, the modulator ensures a constant frequency (Fig. 6.9 (a)). On the other hand, the FCS-MPC presents a different transient behavior. As it can be seen in Fig. 6.9 (b), the switches are locked in the same position during the transient, until the new current value is reached. In this case, the inductance value is the factor that directly influences the transient response speed. For this reason, the FCS-MPC has a faster transient response than the CCS-MPC. Fig. 6.10 shows a comparison of both MPC control methods facing a step change in the inductor current reference. Taking this into account it can be said that the FCS-MPC takes advantage of the physical limits of the system.

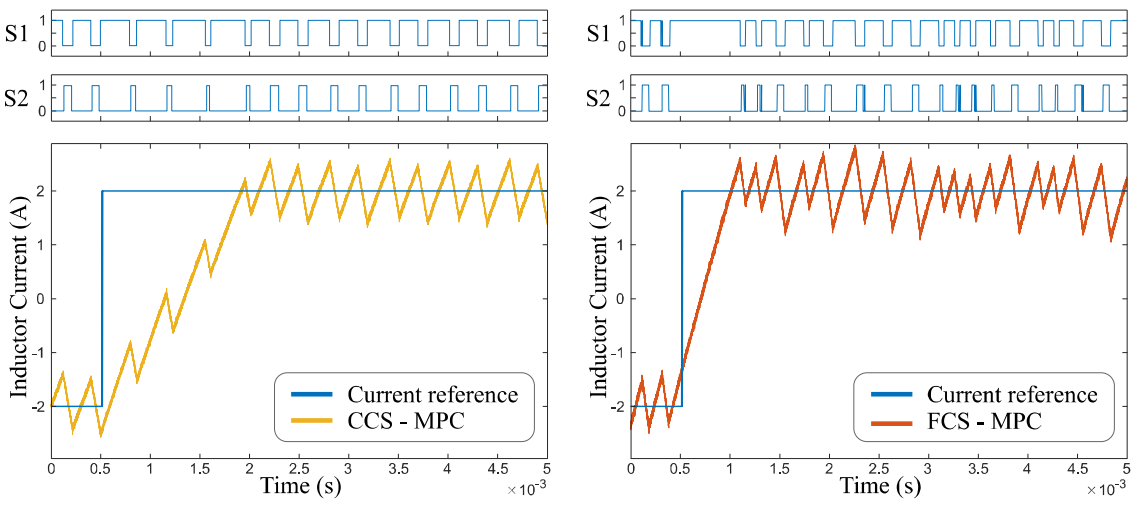

Fig. 6.9 Inductor current step response in experimental test: (a) CCS-MPC. (b) FCS-MPC.

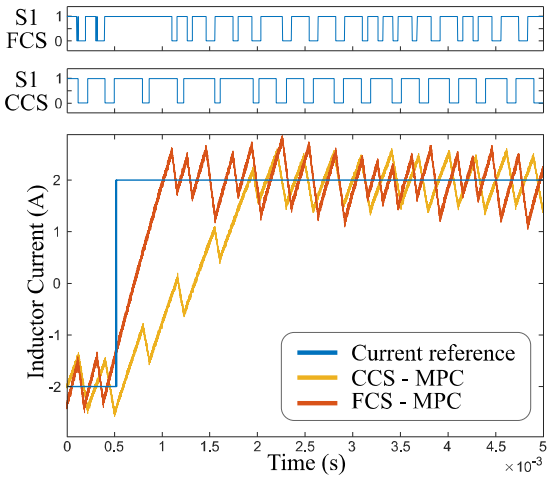

Fig. 6.10 Inductor current step response in experimental test. CCS-MPC and FCS-MPC transient performance comparison.

6.2 PI control vs FCS-MPC and CCS-MPC

Both MPC and PI control schemes require a model of the system. In the case of PI control, the knowledge of the model is used to adjust the proportional and integral gain parameters. In order to perform this adjustment, a linear model of the system is needed. The MPC control instead makes predictions using a discrete-time model, which does not need to be linear.

The difference between these two control methods is summarized in Table 4. As it is widely known, the PI controller consists of two parts. The first part compensates the current tracking error proportionally applying the K_p gain factor. The latter, integrates the current tracking error over time while it applies the K_i gain factor. On the other hand, the MPC based control, minimizes a cost function to achieve the optimal set-point value. As

Table 4:

Difference between PI and MPC based current control.

PI based current control	MPC based current control
$\boldsymbol{u}^* = K_p \cdot \varepsilon_i(t) + K_i \int_0^t \varepsilon_i(\tau) d\tau$	$\boldsymbol{u}^* = \arg \text{ minimize } J$
$\varepsilon_i = (i^* - i)$	$J = (i^* - i^p)^2 + \lambda_u \lvert \Delta u \rvert$

it was studied in the previous subchapter, the output parameter of the optimization stage can be the optimal duty cycle value (CCS-MPC) or the optimal switch position (FCS-MPC).

In order to control multiple variables within a PI controller based system, it is required one PI for each control variable. This makes it a complicated and time-consuming tuning process. The MPC, on the contrary, includes all the required variables within the cost function. In any case, in order to perform a suitable comparison between both control strategies, appropriate K_p and K_i values should be chosen for the PI controller.

Once that the model of the system is developed and the transfer functions are obtained, certain initial assumptions must be made to perform the controller design. In this regard, the step response of the system should be fast enough to reach the reference as fast as possible but at the same time avoiding excessive overshot and oscillations. A suitable way to meet all these specifications is by designing the controller so that the system displays a slightly underdamped behavior. This transient response of the system can be studied by analyzing the poles of the linearized model around its operating point. For the case of underdamped systems, the closed-loop poles are complex conjugates and lie in the left-half S-plane.

The variation of proportional and integral gain values will modify the pole location into the root locus. In order to define the best pole location, some transient-response characteristics should be defined. The most important characteristics in this case are the rise time, settling time and maximum overshoot. Since these variables are not independent of each other and will always depend on the particular characteristics of the system, the design must seek a compromise in order to reach an acceptable step response behavior.

In this case, if the rise time wants to be reduced by increasing the proportional gain value, the overshoot will increase. An experimental example of this behavior is shown in Fig. 6.11, where the system was tested under different K_p values. As it can be seen, increasing the proportional gain value the rising time experiments a decrease while the overshoot increases. Taking this into account, the maximum overshoot value was fixed to 25% as a key design parameter. Considering this as the maximum allowable overshoot

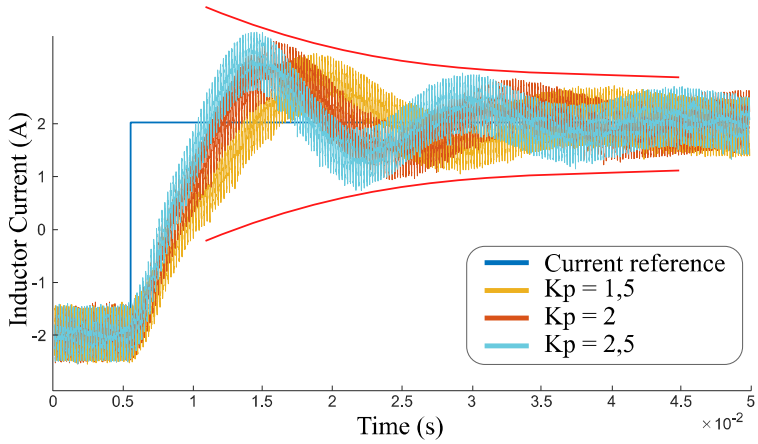

Fig. 6.11 Experimental example of the step response of the system under different proportional gain values.

and making use of the system model obtained in Subchapter 4.2.4 for the tuning process, the gain values resulted in $K_p = 2$ and $K_i = 0{,}15$. After implementing these gain values the system was tested and compared with the two MPC algorithms (Fig. 6.12).

Unlike FCS-MPC, PI control presents a fixed switching frequency what can be desirable in certain situations. In general it presents good steady state current tracking but it is slower than the MPC during transients.

The MPC presents a faster transient behavior. In the FCS-MPC, the switches are locked in the same position during transients, until the new current value is reached. In this case, the inductance value is the factor that directly influences the transient response speed. In CCS-MPC the transient is slightly slower than in FCS-MPC, but still has a faster transient response than the PI. Both MPC algorithms provide more accuracy than the PI since they can obtain small rising times without overshoot. In the same way, they always work within the current constraint limits.

The non-fixed switching frequency of the FCS-MPC may not be a desired feature, but it can be solved by introducing in the cost function a new term that penalizes the frequency deviation. Nevertheless, this feature is not present in the CCS-MPC since it makes use of a modulator stage to generate the switching commands. Unlike the PI, the parameter tuning process in MPC is simpler and more intuitive since all the parameters stated in the cost function can be weighted to meet the design specifications.

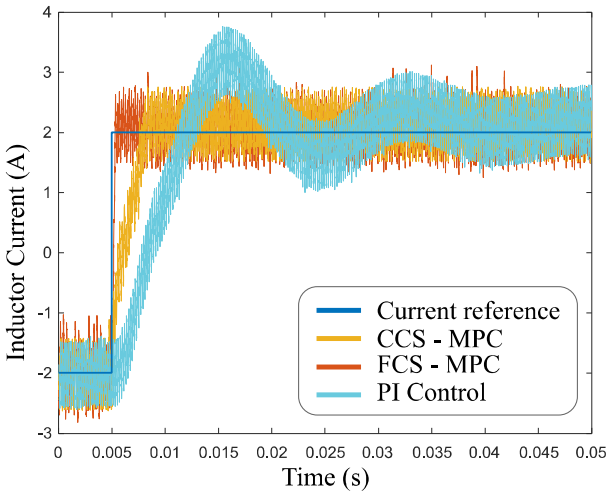

Fig. 6.12 Inductor current step response in experimental test. PI Control versus CCS-MPC and FCS-MPC transient performance comparison.

6.2.1 Conclusions

In CCS-MPC the transient is slightly slower than in FCS-MPC, but still has a faster transient response than the PI. The CCS-MPC and PI control present a fixed switching frequency which is an advantage in terms of filter design. On the other hand, the optimization stage CCS-MPC is more complex than the FCS-MPC since the algorithm needs to evaluate a bounded continuous set of values to select the optimal duty cycle.

In order to speed up the optimization stage, one of the options is to limit the number of iterations. This results in a certain loss of accuracy, but at the same time, the execution speed is improved. In this respect, it is necessary to seek a compromise between these two aspects so that the algorithm is able to work in real time without excessively compromising the calculation precision.

In the FCS-MPC, the switching frequency and the current tracking error are directly dependent on the weighting factor value. As the weighting factor increases, so does the current error whereas the switching frequency decreases. The non-fixed switching frequency may not be a desired feature, but it can be solved by introducing in the cost function a new term that penalizes the frequency deviation. Nevertheless, unlike the CCS-MPC, the optimization stage is simpler and more intuitive since the algorithm only evaluates a finite set of possible switching states.

With regard to the battery management, the FCS-MPC offers more accuracy when applying the operating constraints. This is because the outcome of each switch position is directly evaluated, in contrast to what happens when a modulator is used.

The transient response analysis shows that the FCS-MPC is faster than the CCS-MPC because it leaves the switches locked in the same position during the transient, until the new current value is reached.

Chapter 7

CASE STUDY II: OUTPUT VOLTAGE CONTROL

The Finite Control Set MPC strategy presents certain problems when trying to control the DC bus voltage of the Synchronous Buck converter. When working in boost mode, the response of the converter presents a non-minimum phase behavior with respect to the switching sequence.

In order to solve that problem, different alternatives have been studied. Finally, the solution of an external PI voltage control loop together with an inner FCS-MPC current control loop was selected.

This case study presents simulation results for the different alternatives under study and experimental results for the final solution.

7.1 The challenge of voltage control using FCS-MPC

The FCS-MPC strategy applied to the control of the output voltage has been widely developed for DC-AC converters [220], [221]. In this type of converters, the output voltage is directly imposed selecting the proper switch positions on each time instant. In this sense, the resulting current level and direction will depend on the applied output voltage and the load type. This is because these types of converters are normally configured as voltage source inverters.

In the case of DC-DC converters, the voltage is not directly imposed selecting a specific switch position. In these cases, the obtained voltage level is the result of applying a sequence of different switch positions. On the other hand, manipulating the position of the switches, the current can be directly controlled. This makes it easier to control the DC-DC converters as a current source.

In our case, considering the synchronous buck topology, the storage device is located in the lower voltage side of the converter (Fig. 7.1). The reason for this is the smoothing action of the inductor over the battery current, in this sense acting as a filter.

When trying to control the battery voltage, the FCS-MPC is able to control the battery voltage by selecting the correct switch position. It makes use of the model to predict the future values of inductor current and battery voltage. In this case the voltage is not directly controlled but there is a relationship between the position of the switches and the voltage level increase or decrease.

If the converter starts from a 12V and 0A steady state reference position and the battery voltage reference goes down, the control will react by closing the S2 switch. This will force the battery to discharge until it reaches its new value. The same happens in charging mode by closing the S1 switch (Fig. 7.2).

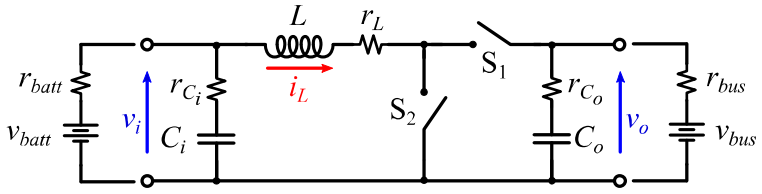

Fig. 7.1 Schematic of the synchronous buck converter used for testing.

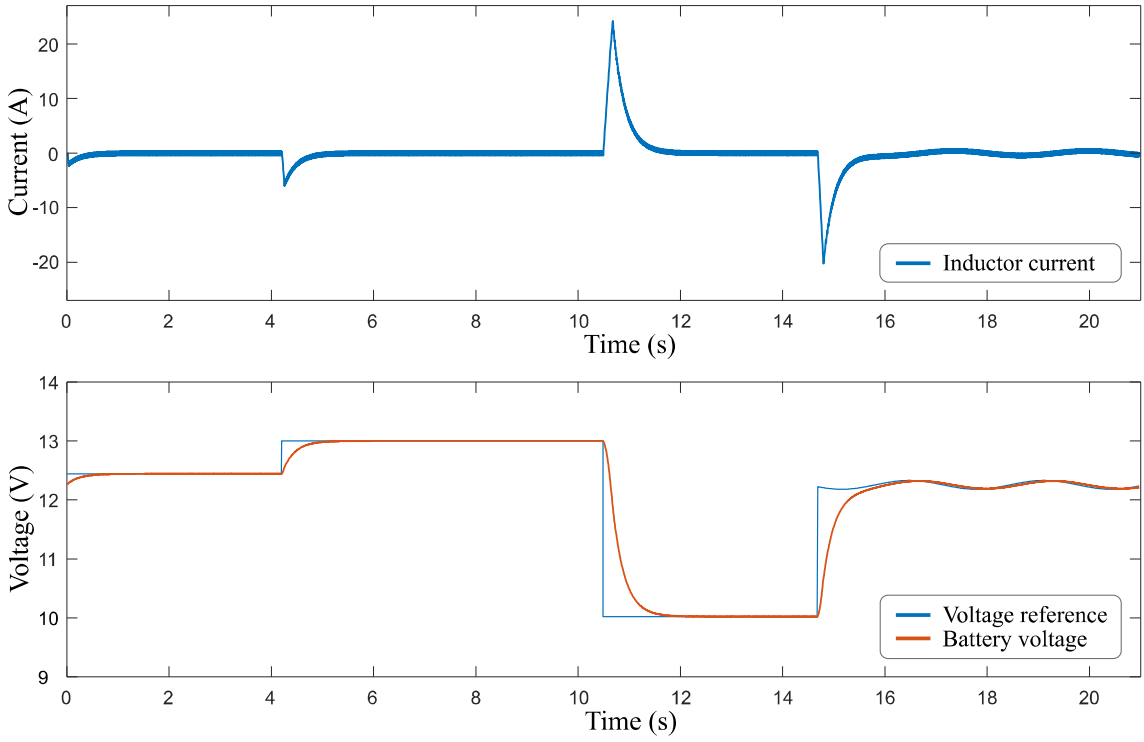

Fig. 7.2 Battery voltage control using FCS-MPC.

The problem comes when the variable that wants to be controlled is the output voltage, which in this case would be the DC bus voltage. When working in boost mode, the response of the converter presents a non-minimum phase behaviour with respect to the switching sequence. This feature produces an initial inverse dynamic that misleads the optimization stage selecting a wrong switching state [222]. This means that the response of the system to an input step, presents an undershoot in the output before approaching its new steady state value. Analysing the pole and zero location, this behaviour is due to the presence of a right half plane zero (RHPZ) in the S-plane.

Let us consider the following example. Assuming that the converter is working in steady state but for whatever reason it is necessary to increase the output voltage. To achieve that, the converter needs to keep the lower switch closed for a longer time in order to store more energy in the inductor. In this situation, the load is supplied only by the output capacitor. If the circuit is observed in detail during that interval, the output voltage will drop more than in the previous switching cycle as the output capacitor keeps discharging for longer. That is why when trying to increase the output voltage, what you

get is the opposite effect in the first steps until it starts increasing to approach the reference value.

By applying Finite Control Set Model Predictive Control (FCS-MPC), the inductor current can be directly controlled by manipulating the position of the power switches. Nevertheless, as mentioned above, when the control objective comprises the change in the bus voltage levels the control begins to present problems. In this sense, the control is not able to solve these problems by directly modifying the position of the switches.

Simulation example of the abovementioned control problem:

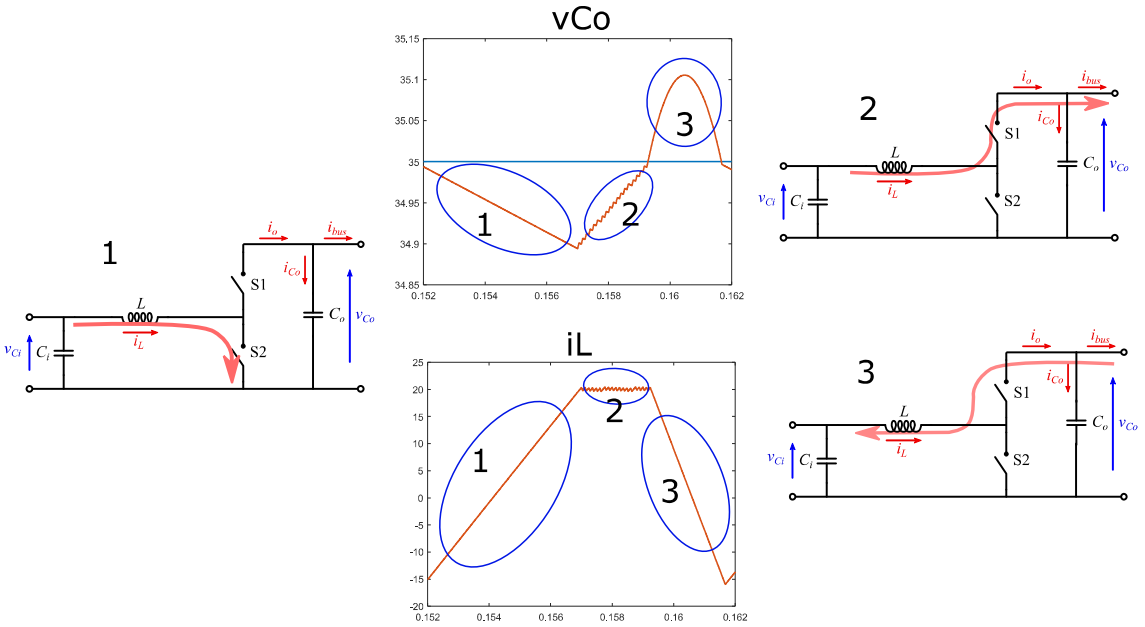

Fig. 7.3 DC bus voltage control problem of the FCS-MPC.

In boost mode, when the measured voltage is smaller than the reference voltage, the control generates a positive current reference for the inductor. During the following cycle the inductor is going to be charged by closing the lower switch (state 1). The problem comes here; in the next step the output voltage has dropped even more, what generates a greater current reference for the inductor. Because of that, if the current is not limited to a certain value, the inductor current will never reach its reference. This process continues charging the inductor until it reaches the maximum allowable current value, which in this case is set to 20A. In that specific moment, the switch position is changed in order to maintain the current within the limits (state 2). This second state starts transferring energy to the output in this way increasing the output voltage. When the voltage reference is

achieved, the converter tries to maintain the output voltage. However, the inductor current is positive and relatively high, so it needs to change the current flow to a negative value. To achieve that, the upper switch is maintained closed (state 3). Once the output voltage is lower than the reference, the process starts again.

7.2 Solutions for the voltage control

Some studies create compatible references starting from the error between the reference and the measurement of the variable under control. It is a kind of proportional control, based on the output capacitor voltage equations.

Other studies solve this issue by making use of a modulator based MPC, together with longer prediction horizons [223]. Since an extended prediction horizon exponentially increases the number of calculations required, the authors of [223] manipulate the sampling time in order to obtain fine accuracy in the first prediction steps and more coarse in the following ones. In any case, the computational cost minimization for MPC using long prediction horizons is beyond the scope of this work.

As another option, some others consider the use of an external PI control loop for the voltage and the MPC for the current.

7.2.1 Create compatible state variable references

Returning to the issue of the output voltage control, a possible solution can come through the design of compatible control references as proposed by D.Quevedo et al. [224]. To do this, it is necessary to develop the equations that relate all the state variables, while at the same time they ensure a power balance between the input and the output of the converter.

To solve this, the general equations that describe the system are taken into account. The inductor current reference (i_L^*) is derived from the output capacitor voltage error. By developing the equations, the resulting inductor current reference is as follows:

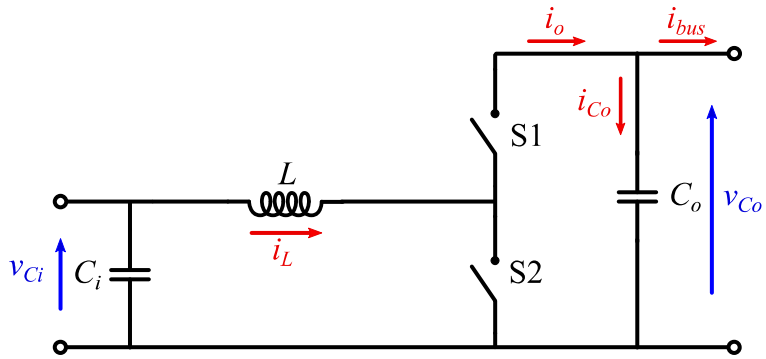

$$P_{in} = P_{out}$$

$$P_{in} = v_{Ci}(k) \cdot i_L^{*}(k+1) \qquad P_{out} = P_{Co}(k+1) + P_{bus}(k+1)$$

$$\text{From capacitor eq.} \rightarrow i_{Co}^{*}(k+1) = C_o \cdot \left(v_{Co}^{*}(k+1) - v_{Co}(k)\right) \cdot \frac{1}{\Delta t}$$

$$P_{Co}(k+1) = \frac{\left(v_{Co}^{*}(k+1) + v_{Co}(k+1)\right)}{2} \cdot i_{Co}^{*}(k+1)$$

$$P_{bus}(k+1) = \frac{\left(v_{Co}^{*}(k+1) + v_{Co}(k+1)\right)}{2} \cdot i_{bus}(k+1)$$

$$i_L^{*}(k+1) = \frac{P_{out}(k+1)}{v_{Ci}(k+1)}$$

$$\text{(Cost Function)} \longrightarrow J = \left(i_L^{*}(k+1) - i_L^{p}(k+1)\right)^2$$

It should be noticed that the current of the converter must be limited within safety values determined by the components. In this test the inductor current was limited to ±2A.

After performing simulations of different values of Δt, the following results have been obtained (Fig. 7.4).

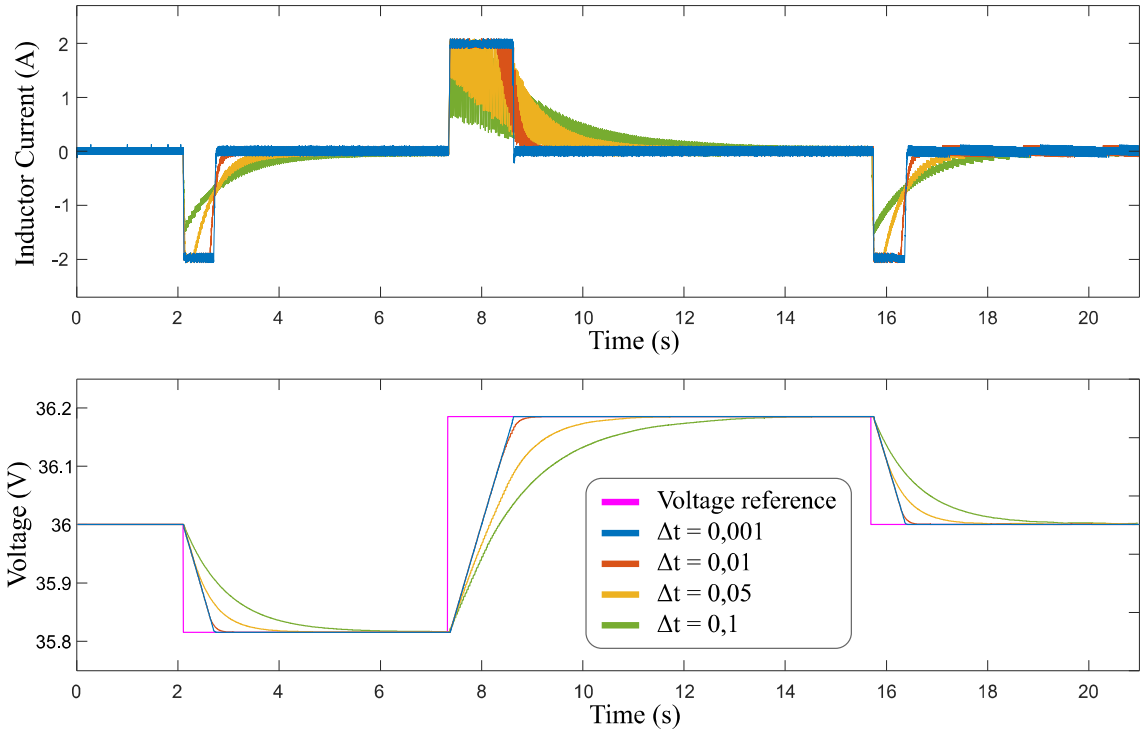

Fig. 7.4 DC bus voltage control using compatible references.

As it can be seen, the DC bus voltage control with compatible references achieves an acceptable behaviour of the converter. Nevertheless, the performance of the converter in boost mode is not that good since the current ripple appears to be notably high.

7.2.2 Continuous Control Set MPC

When a modulator is considered for the generation of the switching commands, it enables the linearization of the nonlinear converter. In this sense, the CCS-MPC is a proper candidate since it uses a model predictive strategy together with a modulator. This method prevents the converter from getting stuck in a wrong switching position.

With this control method a duty cycle reference is generated and then the modulator forces the converter to continue switching unlike what happens with the FCS-MPC. Since the most problematic working mode is the boost mode the converter was tested under a resistive load connected to the DC_{bus} (Fig. 7.5). Together with this consumption, the voltage reference was changed to test the algorithm performance.

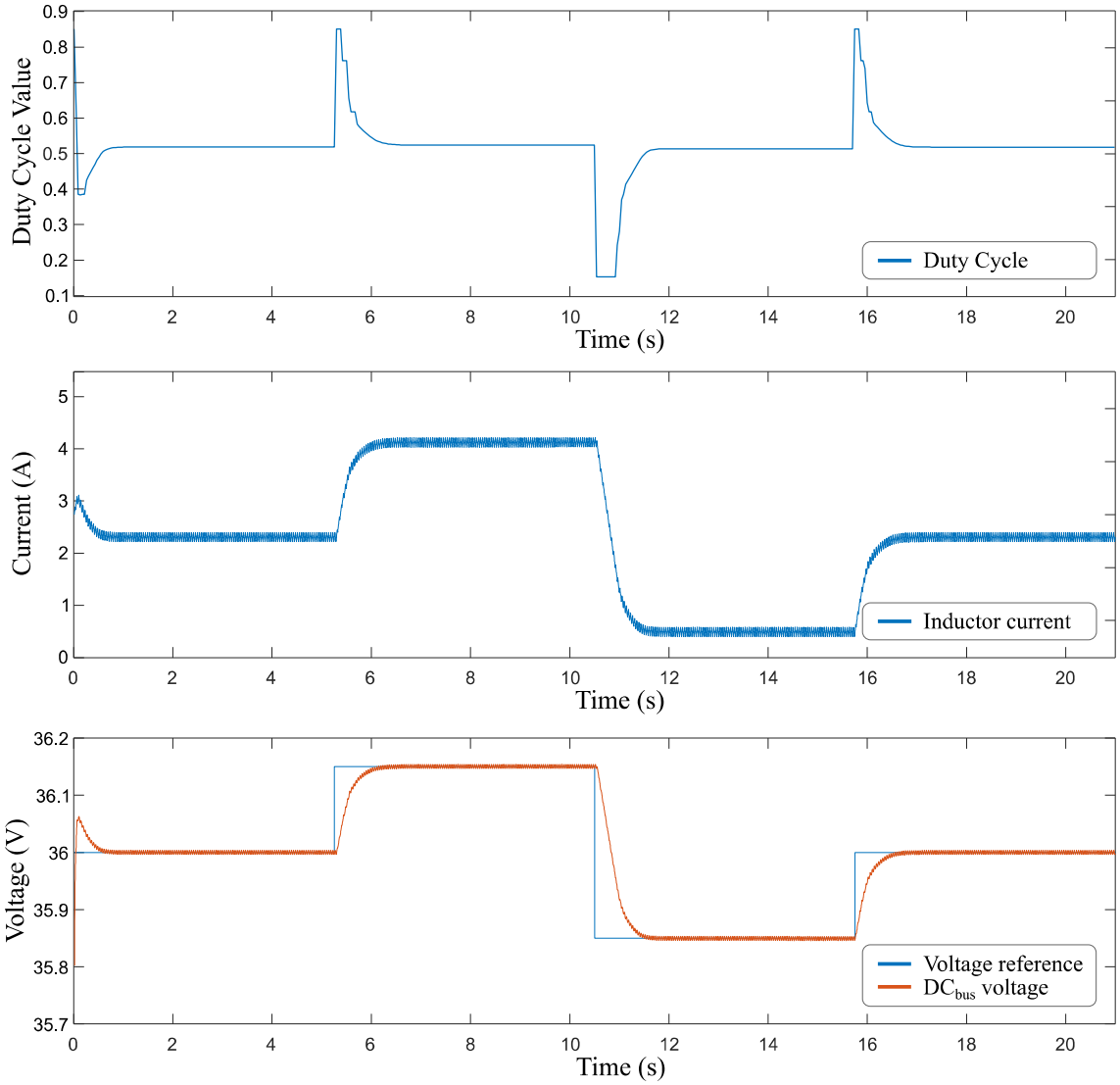

Fig. 7.5 DC bus voltage control using CCS-MPC under resistive load.

The use of the CCS-MPC for output voltage control presents a good performance in simulation, however in the experimental platform it presents certain instability. This aspect, together with the better dynamic performance provided by FCS-MPC for current control, leads us to the las option consisting in the use of an external PI voltage control loop.

7.2.3 External PI voltage control loop

This method consists in the combination of two different control strategies. On the one hand, there is an outer PI control loop for the DC bus voltage regulation. While on the other hand, the inner loop responsible for the inductor current control is based on

FCS-MPC strategy. In this case, the outer loop uses the error between the DC bus voltage reference and the measurement to generate the reference for the inductor current, while the inner loop uses the switched model of the system to predict the future states that better fit the current reference.

Many authors do not hesitate to raise this option as the solution to the voltage control problem. As an example of this, Rodriguez et al. follow this strategy to solve the DC bus voltage regulation problem of an Active Front-End (AFE) rectifier [225]. In this sense, they state that this method achieves good dynamic and static behavior; nevertheless, its performance will depend on the quality of the current control used.

While it is true that it would no longer be a purely predictive control, the current control would maintain all the advantages the MPC provides. Together with this, another advantage with respect to a full PI based system is the ease and speed of the tuning process. In this case, only one control loop needs to be tuned. The absence of cascaded PI controllers reduces the influence between both loops due to the tuning parameter values.

7.3 Experimental results

As mentioned above, using a FCS-MPC inner control loop together with a PI outer voltage control loop makes it easier the tuning process of the PI gain values. In this sense, making use of the system model obtained in Subchapter 4.2.4 for the tuning process, the approximated gain values resulted in $K_p = 1$ and $K_i = 100$ for the selected operating point. At all events, the system was tested under the calculated values together with certain values close to them (Fig. 7.6).

In this case, if the rise time wants to be reduced by increasing the proportional gain value, the overshoot will increase. Conversely, if the proportional gain value is reduced, the rise time will be reduced but the settling time is increased due to a reduction in the oscillations. In any case, since all aspects of the transient response cannot be improved, a compromise must be reached between the different parameters to obtain a suitable

solution. In the case of the integral gain value, no notable difference has been observed in values close to 100.

Note that some of the figures containing multiple graphics have been filtered for clarity in order to make a proper comparison between the results.

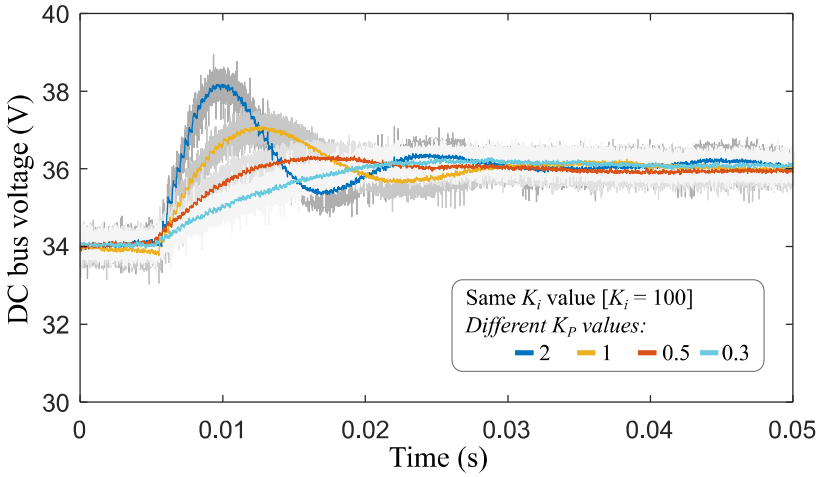

Fig. 7.6 V_{bus} voltage step change response for different K_p values using an inner MPC current loop together with an outer PI voltage control loop.

After implementing the previously calculated gain values the system was tested to observe the current and voltage response for a step change in the reference (Fig. 7.7). As it can be seen, the dynamic response of the current is fast enough so that the speed of the control will depend on the PI voltage control loop and the physical elements of the converter such as inductor and capacitor values.

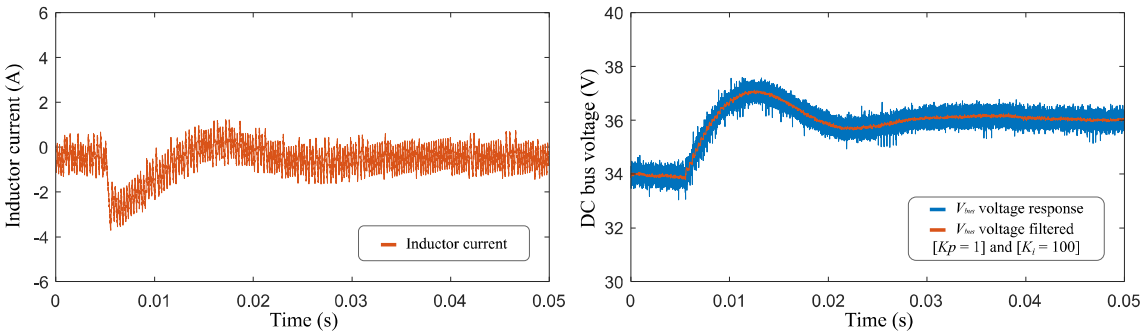

Fig. 7.7 Inductor current i_L (Left) and V_{bus} voltage (right) step change response using an inner MPC current loop together with an outer PI voltage control loop.

The system was also tested to check its stability under power injection or consumption from the energy bus (Fig. 7.8). In this case the system presents a 2V deviation from the reference in both cases for a 2A change in the consumption. In both cases, after establishing the new required current level, the system recovers the reference voltage.

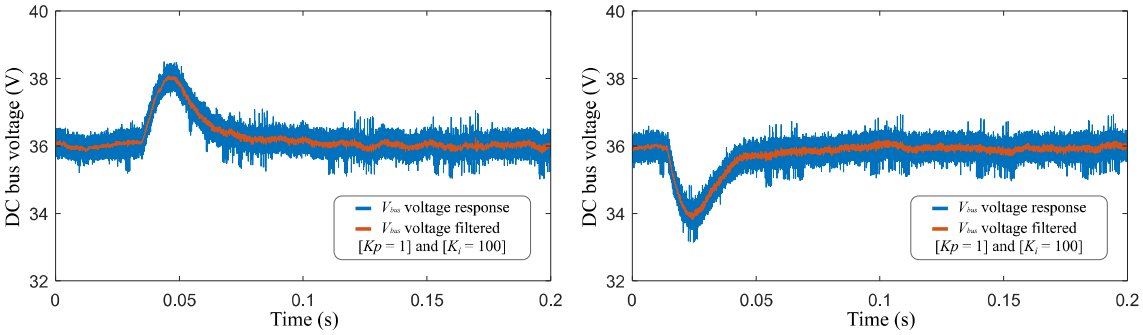

Fig. 7.8 V_{bus} voltage control under power injection to the energy bus (left) and power consumption from the energy bus (right) using an inner MPC current loop together with an outer PI voltage control loop.

7.4 Summary

FCS-MPC presents serious problems in the synchronous buck converter when the DC bus voltage needs to be controlled. An in-depth analysis has been done and different alternatives have been studied.

The creation of compatible references offers an acceptable behavior of the converter but together with this it presents a reduced performance when working in boost mode.

The application of CCS-MPC algorithms has been confirmed as a promising option. This algorithm provides the optimal duty cycle to the modulator by minimizing a cost function that computes the future DC bus voltage values. However, this option presents certain instability in the experimental platform.

As a last option, the integration of an external PI loop was considered. In this sense, after reviewing the literature it was concluded that this solution was used by other researchers to solve this particular problem. Finally, this option was tested experimentally with satisfactory results.

Chapter 8

CASE STUDY III: DC-DC HYBRID SYSTEM

In this Chapter, the hybridization is implemented making use of batteries and UCs. Among the different HESS topologies, the Fully Decoupled Parallel connection mode was selected since it is the most flexible one for our analysis.

In this case, the parallel connected converters are modeled as a single unit assuming that there exist 4 possible switching states.

After analyzing the different power sharing methods, it was concluded that the best option is the virtual impedance power sharing. One of the main reasons for selecting this method is the flexibility it offers.

This case study presents simulation results for the selected power sharing technique together with experimental results for the final solution.

8.1 Background

As it has been mentioned in the previous chapters, the difference between peak power and average consumption limits the performance of applications where a single energy storage technology is used. The reason for this is that the vast majority of storage technologies are not able to meet both parameters. In this regard, the hybridization of different storage technologies is emerging as a suitable solution to solve this problem. Several studies can be found on the literature with the purpose of identifying topologies and control strategies capable of meeting these needs [48], [53], [55], [60], [61].

Regarding the different energy storage devices, there are multiple options in terms of technology, power versus energy ratio and scale of the application [87], [126]–[132]. After analyzing the literature, it can be said that the most common technologies used for developing the storage hybridization concept are electrostatic (Ultracapacitors) and electrochemical (batteries).

With regard to the MPC strategy required for the control of the whole system, Finite Control Set MPC (FCS-MPC) [226] has been selected since it can directly work with the switched model of the converter. MPC may be intuitive but its use in Hybrid Energy Storage Systems (HESSs) is highly nontrivial. In this case, the cost function must include the converter parameters to be controlled together with a set of constraints to perform the power sharing while ensuring the security of the storage devices. The challenges include:

- Accurate converter current control.
- State of charge estimation of each storage device for all possible switching states.
- The choice of suitable constraints to perform the power sharing.
- Maximize the performance of the application in terms of power and energy ratio, while maintaining the storage devices within safe operating limits.

8.2 System description

The Fully Decoupled Parallel connection mode (Fig. 8.1) is the most flexible HESS topology for the analysis. It provides modularity and high scalability, which are important attributes to develop different configurations in terms of power scale.

This configuration basically consists of two DC-DC converters connected in parallel to the same energy bus. In order to develop a unified MPC based control strategy for the whole system, the parallel connected converters must be modeled as a single unit. Assuming that the converter works in continuous conduction mode, it has been modeled considering 4 possible switching states.

In the same vein, it is necessary to obtain an equivalent model of the energy storage devices in order to predict their State of Charge (SoC) and other important parameters. The information obtained from these models will be useful for the development of a suitable energy management strategy and to perform the power sharing.

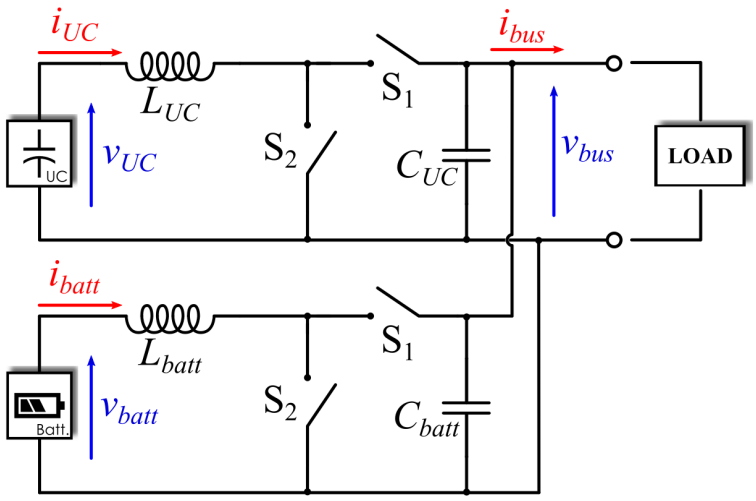

Fig. 8.1 Fully Decoupled Parallel connection mode composed of two different storage devices.

For further information about the system model or converter parameters, the reader is referred to Annex B and Annex C.

8.3 Energy storage devices

8.3.1 Battery

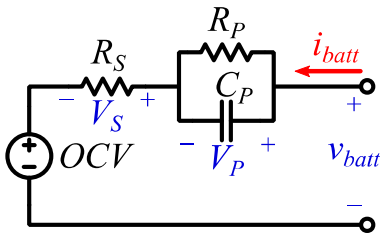

Fig. 8.2 One Time Constant battery model.

Considering the OTC model from Fig. 8.2, the differential equation that defines the voltage across the RC tank can be described as follows:

$$\frac{dV_P}{dt} = \frac{1}{C_P} \cdot i_{C_P} = \frac{1}{C_P}\left(i_{batt} - \frac{V_P}{R_P}\right) \tag{8.1}$$

When the battery is getting charged in CC mode, the charger sets i_{batt} current in this way turning v_{batt} into an output of the system.

$$v_{batt} = OCV + i_{batt} \cdot R_S + V_P \tag{8.2}$$

Once the battery is close to be fully charged and v_{batt} reaches the float voltage level, the charger changes to CV mode and sets v_{batt}. In this case, the v_{batt} voltage will become an input and hence i_{batt} will be an output of the system.

$$i_{batt} = \frac{V_S}{R_S} = \frac{v_{batt} - V_P - OCV}{R_S} \tag{8.3}$$

8.3.2 Ultracapacitor

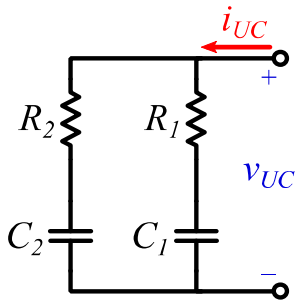

Fig. 8.3 Two Time Constant UC model.

The general equation describing the UC output voltage is developed in (eq(3.17)):

$$v_{UC}(t) = i_{C_1}(t) \cdot R_1 + v_{C_1}(t) = i_{C_2}(t) \cdot R_2 + v_{C_2}(t) \tag{8.4}$$

With respect to the total i_{UC} current, it will be the sum of the currents flowing through the parallel branches. In this sense, the individual currents are derived from the general capacitor differential equation:

$$i_{C_1}(t) = C_1 \frac{dv_{C_1}}{dt}, \qquad i_{C_2}(t) = C_2 \frac{dv_{C_2}}{dt} \tag{8.5}$$

8.4 Control and Power Sharing

With regard to the power sharing, there exist several ways to carry it out based on the specific features of each application [227].

- Power threshold
  It consists of applying a power level threshold to divide the power between the ESSs. In this sense, the high power density ESS would supply all the power demand exceeding the predefined threshold [201].

- Look-up tables
  This method is based on reference tables to perform the power distribution [202]. Depending on the power level managed at each time, some predefined reference patterns are used to distribute it between the storage devices.

- Weighting factors
  Weighting factors can be used to determine the power proportion supplied by each storage device at each time instant. Based on the difference in power to energy ratios of some storage technologies, a dynamically varying weighting factor can be also applied [204].

- Filters
  This method performs the power sharing by means of a high pass filter to separate the high frequency and low frequency components of the power signal [203]. In this method, the high energy density ESS (battery) manages the low frequency component of the required power, while the high power density ESS (UCs) would do so with the high frequency part. This method can be applied by including the cutoff frequency of the filter into the cost function in order to adjust the power sharing.

- Droop Control and Virtual Impedance
  The droop control is typically used in microgrid applications where a great amount of electric sources and loads with different dynamics are connected in parallel [228]. Its integration into the cost function would involve to set a predefined droop value for each storage device and introduce variations around that value considering the predictions of the ESS models.
  Including different electrical components directly into the circuit would modify the general behavior of the system, nevertheless this would imply more unnecessary power losses. In order to emulate the same behavior but avoiding the physical modification of the system the integration of virtual impedances within the control algorithm can be a suitable solution.

Summarizing the points above; all the constraints, references and threshold values used to perform the power sharing, can be modified based on the information provided by the mathematical models. By doing this, the system is able to dynamically modify the power sharing to adjust it depending on the SoC of the storage devices.

8.5 Simulation results

After analyzing the different power sharing methods, it was concluded that the best option is the virtual impedance power sharing (Fig. 8.4). One of the main reasons for selecting this method is the flexibility it offers. In this sense, the different virtual impedance configurations can be useful to modify separately the transient response and steady state of the system. These can be configured to make the system behave like a filtered system while at the same time it imposes an operating threshold in steady state.

The simplest virtual impedance form is composed of a RC branch emulated to be in parallel with the converter output. In this case the transient response of the converter is filtered but it has no effect in steady state operation.

On the other hand, the lower configuration in Fig. 8.4 is slightly different since it adds a virtual resistor in series with the output of the converter. In this case, the transient response is filtered as in the previous configuration by making use of the parallel RC branch. However, this configuration is able to modify the output steady state value thanks to the virtual series resistor.

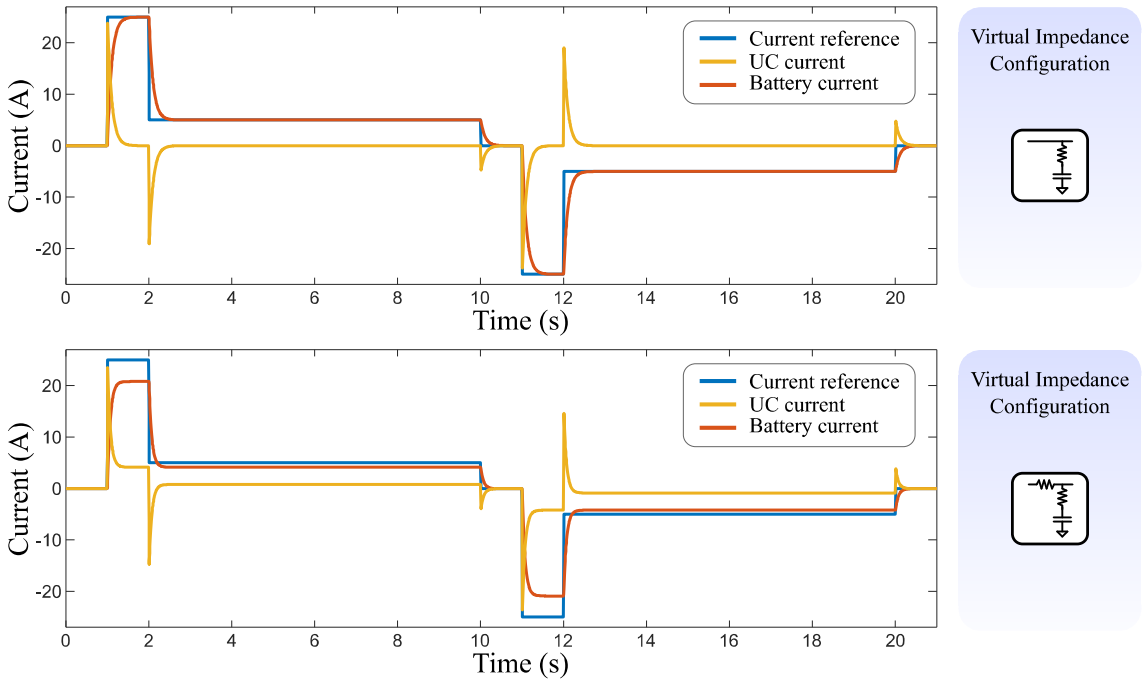

Fig. 8.4 HESS performance under two different virtual impedance configurations.

By means of simulations, the influence each component has on the response of the system has been observed. In the case of a single RC branch, when the value of the resistor or the capacitor increases the response speed of the system decreases. After observing that the variation of one or the other does not affect the system differently, it has been decided to fix the resistance value for the following tests and only modify the capacitor value. Thanks to this, we have a single variable to modify the dynamic of the system.

As for the second configuration consisting of the previously described RC branch together with an additional series resistor, it is possible to modify the transient response and the steady state value independently. If the series resistor value increases the steady state value of the controlled variable decreases. In this particular case, since the steady state value is lower due to the series resistance increase, the capacitor value should be also increased to obtain the same dynamic response and settling time.

In addition to the power sharing, some other constraints were included to operate the storage devices within safety limits. Together with this, the cost function also includes the terms responsible for the current tracking and the penalization of the switching effort in order to limit the power losses.

8.6 Experimental results

For the experimental validation of the previously simulated control algorithm, automatic code generation tools have been used. In this case, the algorithm implemented in Matlab was compiled and built into the TI F28379D μC.

In the following test, the virtual impedance form composed of a parallel RC branch is analyzed. As it has been mentioned above, the value of the components that make up the virtual impedance has a direct influence on the performance of the system. In this case, the system was tested for two different capacitor values obtaining the results shown in Fig. 8.5. As it can be seen, the converter responds faster when the capacitor value is reduced. In any case, regardless of the capacitor value, the steady state response will not be modified.

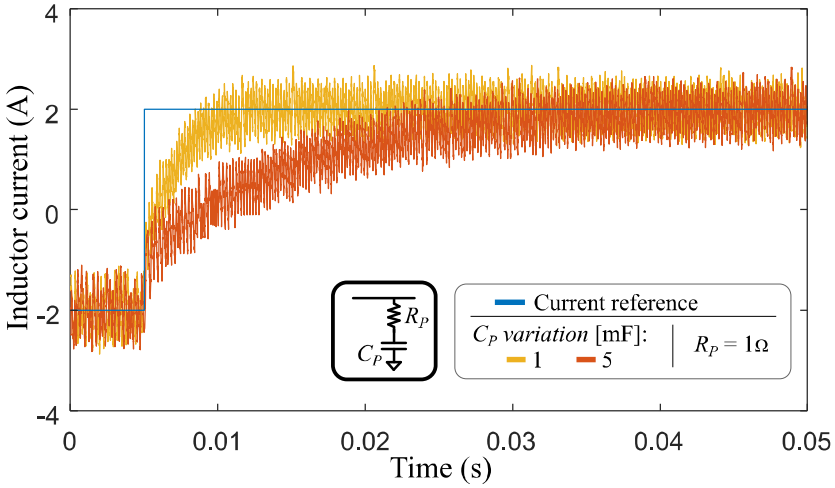

Fig. 8.5 Step response of the converter with different virtual capacitor values.

In Fig. 8.6 the response of the whole HESS is shown. As it can be seen, the two storage devices respond in complementary fashion to a step change in the reference signal. In this case, as the battery current always converges to the reference value, the UCs will only come into play during transients. Due to this, the amount of energy provided by the UCs will always depend on the selected capacitor value.

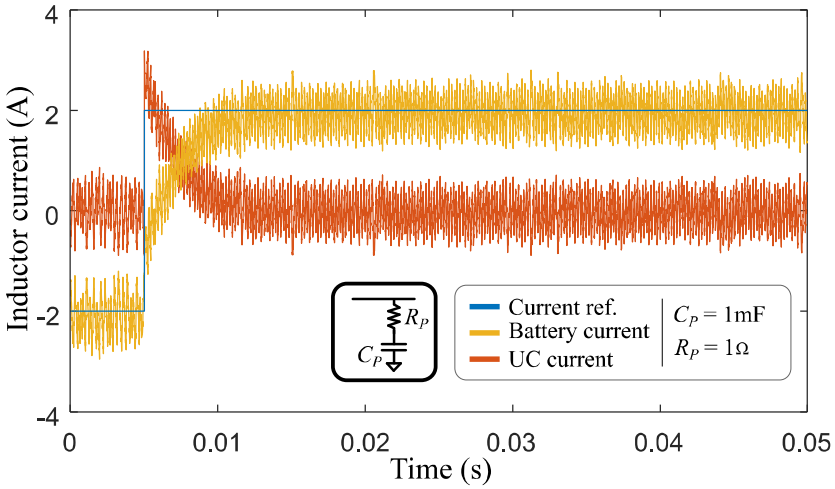

Fig. 8.6 Battery and UC currents under step response with virtual parallel capacitor.

In the following tests, the configuration consisting of the RC branch together with an additional series resistor is used. In this case, both the transient response and the steady state values are modified. Fig. 8.7 shows the step response of the system for different capacitor values but including the series resistor. As it can be seen, in this case the signals do not converge to the reference resulting in a constant offset during steady state.

Note that the capacitor values used in this test are higher than the values from the previous test where the virtual impedance was composed of a single RC branch.

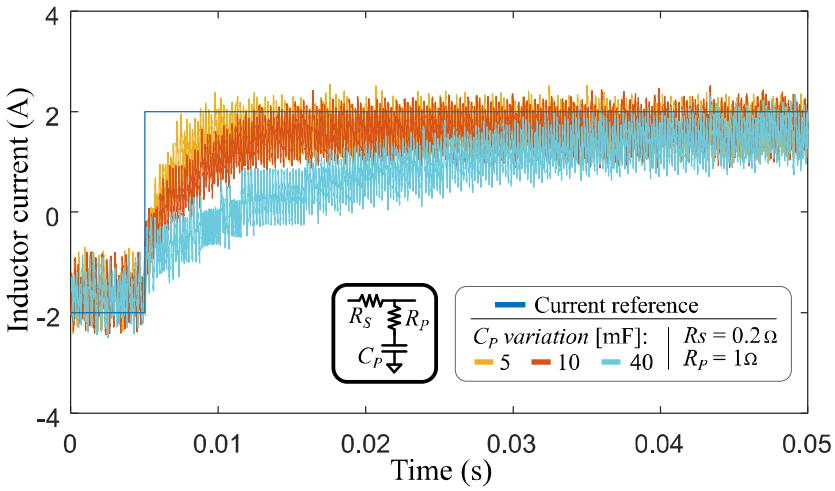

Fig. 8.7 Step response of the converter with virtual series resistor and different virtual parallel capacitor values.

In order to have a more detailed view on the effect that series resistance has on the steady state operation, the comparison shown in Fig. 8.8 has been made. Leaving the RC branch values fixed, the system response was tested for two different series resistance values. As it can be clearly seen, a greater series resistance makes the signal converge to a smaller value. In such a case, the battery do not supply the full power in steady state what forces the UCs to provide the remaining part. Accordingly, the UCs should be sized considering the energy supplied during the transient and during the steady state as well.

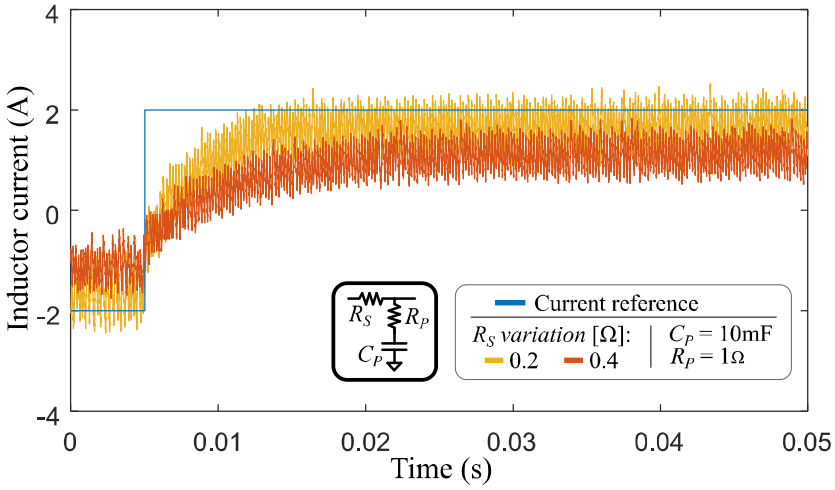

Fig. 8.8 Step response of the converter with virtual parallel capacitor and different virtual series resistor values.

This effect can be more clearly seen in the following figures. In Fig. 8.9 the system was tested considering a 0.2Ω series resistor, while on Fig. 8.10 the resistance value was fixed to 0.4Ω. On the first one (Fig. 8.9), the resulting battery current is close to the reference value, which means that the UCs have to provide a relatively low amount of energy during the steady state. In the second case (Fig. 8.10) the final battery current is lower, hence the UCs have to provide the remaining part that will be greater than in the previous case.

Note that the change in the series resistance value has a small but noticeable influence on the settling time of the system.

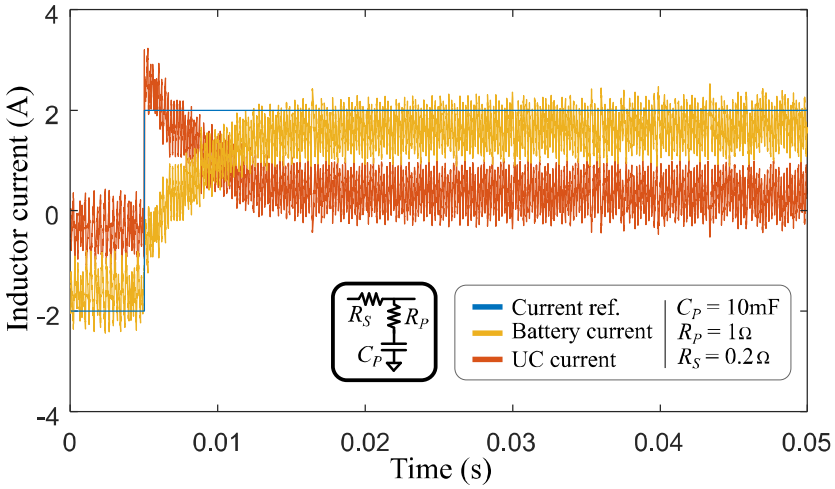

Fig. 8.9 Battery and UC currents under step response with virtual parallel capacitor and 5 ohm virtual series resistor.

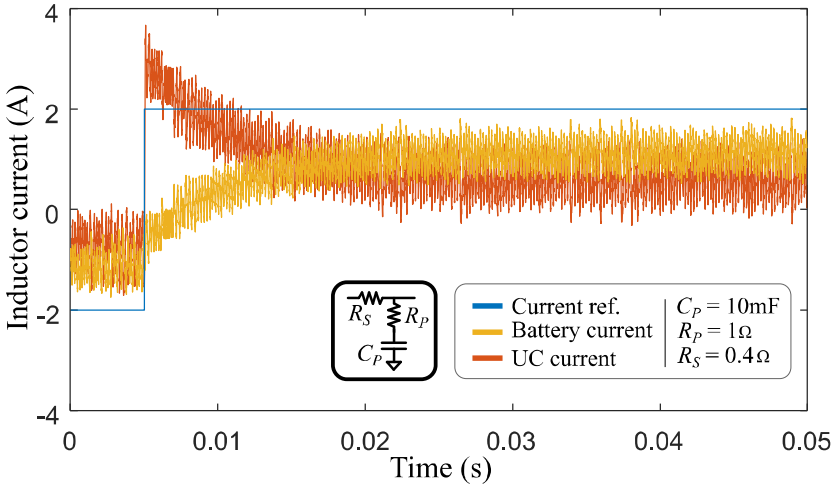

Fig. 8.10 Battery and UC currents under step response with virtual parallel capacitor and 10 ohm virtual series resistor.

Chapter 9

CONCLUSIONS AND OUTLOOK

In this final chapter the main conclusions of this research work are presented. In this sense, the following steps of the research project will be based on the conclusions presented below.

9.1 Conclusions

The difference between peak power and average consumption, limits the performance of multiple applications. The hybridization of different storage technologies is emerging as a suitable solution to solve this problem. In this regard, several studies have been carried out with the purpose of identifying topologies and control strategies capable of meeting these needs.

With regard to the HESS topologies found on the literature, it is concluded that the Fully Decoupled Parallel connection mode is the most flexible one for the analysis. It also provides modularity and high scalability, which are important attributes to develop different configurations in terms of power scale.

Regarding the different energy storage devices, there are multiple options in terms of technology, power versus energy ratio and scale of the application. An analysis of the literature was made to observe the trends with regard to the number of studies or real installations using each storage technology. Taking this into account it can be said that the most common technologies used for developing the storage hybridization concept are batteries and ultracapacitors.

In order to perform a correct battery and ultracapacitor sizing, it is necessary to take into account the effect of variables such as temperature or charge/discharge current, over the rest. In this sense, it is convenient to perform several iterations to achieve a more optimized value. After all, the previous sizing examples only provide an approximate capacity value. Another key aspect is the Energy Management Strategy (EMS) followed by the application control algorithm. This EMS may include some operating constraints that must be considered in the design process to ensure that the HESS can deliver the performance demanded.

There are several methods for the control of power converters and drives. In this sense, the most common choice is the use of multilevel control structure composed of proportional-integral (PI) controllers. This configuration implies the tuning of several cascaded control loops. In this context, Model Predictive Control (MPC) is presented as an alternative to this multilevel structure. The use of this kind of control makes it possible

to operate with a single control loop. In this sense, all the necessary parameters should be included within the cost function, together with the operating constraints.

According to the different power sharing techniques, several methods have been found on the literature. Among those, we have to highlight the rule based control, filter based power sharing and virtual impedances.

Rule based methods are robust, but the transient response behavior is their weakest point. Just the opposite occurs in the case of the filtering method. This method works relatively well for systems with abrupt and unpredictable operating changes, but it does not provide a suitable solution for the steady state. In this context, virtual impedances are presented as an interesting solution for future high performance applications. The different virtual impedance configurations can be useful to modify separately the transient response and steady state of the system. This power sharing method has been tested with satisfactory results.

In the converter control level, the FCS-MPC presents good features for the current control mode. This control method allows to improve the performance of the system making the transient response notably faster than using classical PI controllers. In addition, the increase in the transient response speed does not imply a larger overshot or oscillations, as is the case for PI controllers when trying to reduce the rising time.

Nevertheless, Finite Control Set MPC has problems when performing the output voltage control of the DC-DC converter in boost mode. Different alternatives have been tested to solve this problem selecting the outer PI voltage control loop as the most suitable option. While it is true that it would no longer be a purely predictive control, the current control would maintain all the advantages the MPC provides.

9.2 Future Research Lines

According to the use of more complex battery models, the integration of the State of Health (SoH) estimation is considered as an important improvement to carry out in future works.

Other research line would be the use of different topologies apart from the Fully Decoupled Parallel one. Depending on the application and the storage technology under use, other topologies with a single converter can be an interesting option to improve the system efficiency.

Regarding the power electronic converter, after seeing the good performance of MPC for the control of the inductor current in the synchronous buck converter, it would be interesting to test the MPC algorithm for different DC-DC converter topologies. Most of the literature is focused on the implementation of MPC algorithms in AC converters and drives but there is still a lot of research work left for DC-DC converters.

Finally, another interesting research line would be to find other ways to perform the power sharing to better suit the application requirements. In this sense, the use of past experience of the application to improve the decision making would be an interesting way to improve to hybridization performance in terms of better energy management.

-

Annex A

TERMINOLOGY USED IN BATTERIES

The following summary is a small gathering of the principal parameters and the terminology used in batteries.

C_{inst} **Instantaneous Capacity** $[Ah]$: It is the supplied current summation in a defined time interval. In this case, the current is assumed to be positive when the battery is charging and negative when it is discharging.

$$C_{inst} = \int_0^t I(t)dt \tag{9.1}$$

C_{rated} **Rated Capacity** $[Ah]$: It is the capacity specified by the battery manufacturer, for a given discharge current rate.

C **Current rate**: It is the relation between the current applied to the battery and the required current level for charging or discharging the battery in one hour.

V_{rated} **Rated Voltage** $[V]$: This is the reference voltage of a battery, since most discharge curves are neither linear nor flat. It differs depending on the battery chemistry but is typically measured at 50% of state of charge (SOC).

V_{batt} **Terminal Voltage** $[V]$: It is the voltage measured directly at battery terminals while it is connected to the load. This voltage varies depending on State of Charge (SOC) and charge / discharge current.

OCV **Open Circuit Voltage** $[V]$: It is the voltage measured directly at battery terminals with no load condition. The battery needs to be under relaxed conditions to perform a reliable measurement. It also depends on the battery State of Charge (SOC).

E **Stored Energy** $[Wh]$: It is determined by the stored capacity $[Ah]$ multiplied by the battery voltage at each time instant.	$E = C(t) \cdot V(t)$ (9.2)
$P_{batt}(t)$ **Instantaneous power** $[W]$: The power that a battery can deliver is the product of the instantaneous current and instantaneous voltage.	$P(t) = V(t) \cdot I(t)$ (9.3)
SOC **State of Charge** $[\%]$: This parameter indicates the charge level of a battery as a percentage. It is calculated taking into account the initial SOC_0 and the rated capacity of the battery.	$SOC = SOC_0 + \frac{1}{C_{rated}} \int_0^t I(t)dt \ (\times 100)$ (9.4)
DOD **Depth of Discharge** $[\%]$: It is the complement of SOC presented as a percentage. While one increases, the other decreases proportionally.	$DOD = (1 - SOC) \cdot 100$ (9.5)
SOH **State of Health** $[\%]$: This is the ratio between the aged rated capacity and initial rated capacity.	$SOH = 100 \cdot \frac{C_{aged\_rated}}{C_{rated}}$ (9.6)

-

Annex B

STATE SPACE MODEL OF THE PARALLEL DC-DC CONVERTER

Below the state-space model **A** and **B** matrices of the parallel converter are shown:

$$[\mathbf{A}]=\begin{bmatrix} -\frac{1}{C_{i1}(r_{batt}+r_{C_{i1}})} & 0 & 0 \\ 0 & -\frac{1}{C_{i2}(r_{UC}+r_{C_{i2}})} & 0 \\ 0 & 0 & -\frac{1}{C_o(r_{bus}+r_{C_o})} \\ \frac{1}{L_1}\frac{r_{batt}}{r_{batt}+r_{C_{i1}}} & 0 & -(M1+M2)\frac{1}{L_1}\frac{r_{bus}}{r_{bus}+r_{C_o}} \\ 0 & \frac{1}{L_2}\frac{r_{UC}}{r_{UC}+r_{C_{i2}}} & -(M1+M3)\frac{1}{L_2}\frac{r_{bus}}{r_{bus}+r_{C_o}} \end{bmatrix}$$

$$\begin{bmatrix} -\frac{r_{batt}}{C_{i1}(r_{batt}+r_{C_{i1}})} & 0 \\ 0 & -\frac{r_{UC}}{C_{i2}(r_{UC}+r_{C_{i2}})} \\ (M1+M2)\frac{r_{bus}}{C_o(r_{bus}+r_{C_o})} & (M1+M3)\frac{r_{bus}}{C_o(r_{bus}+r_{C_o})} \\ -\frac{1}{L_1}\left(\frac{r_{batt}\cdot r_{C_{i1}}}{r_{batt}+r_{C_{i1}}}+r_{L_1}+(M1+M2)\left(\frac{r_{bus}\cdot r_{C_o}}{r_{bus}+r_{C_o}}+r_{DS_{on}1}\right)+(M3+M4)r'_{DS_{on}1}\right) & -\frac{1}{L_1}\left(\frac{r_{batt}\cdot r_{C_{i1}}}{r_{batt}+r_{C_{i1}}}+M1\frac{r_{bus}\cdot r_{C_o}}{r_{bus}+r_{C_o}}\right) \\ -\frac{1}{L_2}\left(\frac{r_{UC}\cdot r_{C_{i2}}}{r_{UC}+r_{C_{i2}}}+M1\frac{r_{bus}\cdot r_{C_o}}{r_{bus}+r_{C_o}}\right) & -\frac{1}{L_2}\left(\frac{r_{UC}\cdot r_{C_{i2}}}{r_{UC}+r_{C_{i2}}}+r_{L_2}+(M1+M3)\left(\frac{r_{bus}\cdot r_{C_o}}{r_{bus}+r_{C_o}}+r_{DS_{on}2}\right)+(M2+M4)r'_{DS_{on}2}\right) \end{bmatrix}$$

$$[\mathbf{B}]=\begin{bmatrix} \frac{1}{C_{i1}(r_{batt}+r_{C_i})} & 0 & 0 \\ 0 & \frac{1}{C_{i2}(r_{UC}+r_{C_i})} & 0 \\ 0 & 0 & \frac{1}{C_o(r_{bus}+r_{C_o})} \\ \frac{1}{L_1}\frac{r_{C_i}}{r_{batt}+r_{C_i}} & 0 & -(M1+M2)\frac{1}{L_1}\frac{r_{C_o}}{r_{bus}+r_{C_o}} \\ 0 & \frac{1}{L_2}\frac{r_{C_i}}{r_{UC}+r_{C_i}} & -(M1+M3)\frac{1}{L_2}\frac{r_{C_o}}{r_{bus}+r_{C_o}} \end{bmatrix}$$

Below the state and input vectors are shown:

$$x=\begin{bmatrix} v_{Ci1} & v_{Ci2} & v_{Co} & i_{L1} & i_{L2} \end{bmatrix}$$

$$u=\begin{bmatrix} v_{batt} & v_{UC} & v_{bus} \end{bmatrix}$$

-

Annex C

POWER ELECTRONIC CONVERTER PARAMETERS

-

TABLE V
Power Electronic Converter parameters for single ESS simulations.

Parameter	Symbol	Value
Sampling time	T_S	40μs
Input capacitance	C_i	100μF
Input capacitor resistance (ESR)	r_{Ci}	10mΩ
Output capacitance	C_o	200μF
Output capacitor resistance (ESR)	r_{Co}	20mΩ
Inductance	L	1,6mH
Inductor resistance	r_L	40μΩ
Drain-source on state resistance	r_{DSon}	4,3mΩ
Battery series resistor	r_S	47mΩ
Battery parallel resistor	r_P	18mΩ
Battery parallel capacitor	C_P	11mF
Battery nominal voltage	$V_{batt,nom}$	12V
DC bus resistance	r_{bus}	10mΩ
DC bus nominal voltage	$V_{bus,nom}$	36V

TABLE VI
Power Electronic Converter parameters for HESS simulations and experimental tests.

Parameter	Symbol	Value
Sampling time	T_S	40μs
Input capacitance	C_i	100μF
Input capacitor resistance (ESR)	r_{Ci}	10mΩ
Output capacitance	C_o	200μF
Output capacitor resistance (ESR)	r_{Co}	20mΩ
Inductance (on each parallel converter)	L	0,8mH
Inductor resistance	r_L	10μΩ
Drain-source on state resistance	r_{DSon}	4,3mΩ
Battery series resistor	r_S	47mΩ
Battery parallel resistor	r_P	18mΩ
Battery parallel capacitor	C_P	11mF
Battery nominal voltage	$V_{batt,nom}$	12V
UC module nominal voltage	$V_{UC,nom}$	24V
DC bus resistance	r_{bus}	10mΩ
DC bus nominal voltage	$V_{bus,nom}$	36V

REFERENCES

[1] C. Uhlmann, J. Illig, M. Ender, and R. Schuster, "In situ detection of lithium metal plating on graphite in experimental cells," vol. 279, pp. 428–438, 2015.

[2] European Comission, *Horizon 2020 Challenge 10. Secure, Clean and Efficient Energy: Work Programme 2016 - 2017*, vol. 2017, no. 7. 2016.

[3] A. Ulbig, T. S. Borsche, and G. Andersson, *Impact of low rotational inertia on power system stability and operation*, vol. 19, no. 3. IFAC, 2014.

[4] P. Tielens and D. Van Hertem, "The relevance of inertia in power systems," *Renew. Sustain. Energy Rev.*, vol. 55, pp. 999–1009, 2016.

[5] A. Ulbig, T. S. Borsche, and G. Andersson, "Analyzing Rotational Inertia, Grid Topology and their Role for Power System Stability," *IFAC-PapersOnLine*, vol. 48, no. 30, pp. 541–547, 2015.

[6] J. I. Pérez-Díaz and J. Jiménez, "Contribution of a pumped-storage hydropower plant to reduce the scheduling costs of an isolated power system with high wind power penetration," *Energy*, vol. 109, pp. 92–104, 2016.

[7] Red Eléctrica de España, "Proyecto Volante de inercia," 2014. [Online]. Available: http://www.ree.es/es/red21/idi/proyectos-idi/proyecto-volante-inercia.

[8] Red Eléctrica de España, "Proyecto Almacena," 2013. [Online]. Available: http://www.ree.es/es/red21/idi/proyectos-idi/proyecto-almacena.

[9] C. E. Technologies, S. Lin, W. Song, Y. Chen, L. Luo, and Z. Feng, "Study on the Model of Elevator Regeneration Energy and its Energy Storage Control Method," pp. 125–128, 2015.

[10] L. Martín-martín, J. Gastelurrutia, N. Nieto, J. Carlos, A. Rivas, and I. Gil, "Modeling based on design of thermal management systems for vertical elevation applications powered by lithium-ion batteries," *Appl. Therm. Eng.*, vol. 102, pp. 1081–1094, 2016.

[11] N. Jabbour, C. Mademlis, and I. Kioskeridis, "Improved Performance in a Supercapacitor-Based Energy Storage Control System with Bidirectional DC-DC Converter for Elevator Motor Drives," pp. 1–6.

[12] C. A. V Nardi and F. P. G. Tomasso, "High Performances Supercapacitor Recovery System Including Power Factor Correction (PFC) For Elevators Keywords."

[13] G. Nobile *et al.*, "Energy Harvesting in Roped Elevators," pp. 533–540, 2014.

[14] S. Tominaga, I. Suga, H. Araki, and H. Ikejima, "Development of Energy-Saving Elevator Using Regenerated Power Storage System," pp. 890–895, 2002.

[15] D. Zhang, L. Wang, L. Jin, X. Hong, L. Jin, and Z. Lu, "A new method for dynamic energy management of energy-saving elevators based on super capacitors," pp. 1403–1407, 2012.

[16] A. Xu, S. Xie, Y. Yao, X. Liu, H. Xiao, and J. Feng, “An Ultra-capacitor Based Regenerating Energy Storage System for Urban Rail Transit,” pp. 1626–1631, 2009.
[17] M. Iwase, T., Kawamura, J., Tokai, K., & Kageyama, “Development of battery system for railway vehicle.,” *IEEE*, no. Conference on Electrical Systems for Aircraft, Railway, Ship Propulsion and Road Vehicles (ESARS), pp. 1–6, 2015.
[18] A. Frilli, E. Meli, D. Nocciolini, L. Pugi, and A. Rindi, “Energetic optimization of regenerative braking for high speed railway systems,” *Energy Convers. Manag.*, vol. 129, pp. 200–215, 2016.
[19] M. Conte, F. Vellucci, and M. Pasquali, “Design Procedures of Lithium-ion Battery Systems : the Application to a Cable Railway .,” pp. 257–264, 2011.
[20] K. Ogura *et al.*, “Test Results of a High Capacity Wayside Energy Storage System Using Ni-MH Batteries for DC Electric Railway at New York City Transit,” pp. 6–11, 2011.
[21] M. Ogasa and Y. Taguchi, “Development of Contact-wire / battery Hybrid LRV Hybrid Technology with Lithium Ion Rechargeable Battery for LRV.”
[22] T. Furuya, K. Ogawa, and T. Yamamoto, “Drive Control for Fuel Cells and Lithium ion Battery Hybrid Railway Vehicle,” 2009.
[23] TheEconomist, “Evolution of Li-Ion battery energy density and cost,” 2017. [Online]. Available: https://www.economist.com/graphic-detail/2017/08/14/the-growth-of-lithium-ion-battery-power.
[24] F. Kalhammer, “Status and prospects for Zero Emissions Vehicle Technlogy,” in *Report of the ARB Independent expert Panel*, 2007.
[25] P. Poizot and F. Dolhem, “Clean energy new deal for a sustainable world: from non-CO2 generating energy sources to greener electrochemical storage devices,” *Energy Environ. Sci.*, vol. 4, no. 6, pp. 2003–2019, 2011.
[26] B. Dunn, H. Kamath, and J.-M. Tarascon, “Electrical Energy Storage for the Grid: A Battery of Choices,” *Science (80-.).*, vol. 334, no. 6058, pp. 928–935, Nov. 2011.
[27] R. Padbury and X. Zhang, “Lithium–oxygen batteries—Limiting factors that affect performance,” *J. Power Sources*, vol. 196, no. 10, pp. 4436–4444, May 2011.
[28] Y. Zhang, X. Tang, Z. Qi, and Z. Liu, “The Ragone plots guided sizing of hybrid storage system for taming the wind power,” *Int. J. Electr. Power Energy Syst.*, vol. 65, pp. 246–253, 2015.
[29] P. Adelmann *et al.*, “Topology and control strategy for hybrid storage systems. Pub. No .: US 2015/0270731 A1,” 2015.
[30] G. Merei, C. Berger, and D. Uwe, “Optimization of an off-grid hybrid PV – Wind – Diesel system with different battery technologies using genetic algorithm,” *Sol. ENERGY*, vol. 97, pp. 460–473, 2013.
[31] A. Saez-de-ibarra, “Second Life Battery Energy Storage System for Residential Demand Response Service,” pp. 2941–2948, 2015.
[32] D. Stroe, M. Swierczynski, A. Warnecke, J. M. Timmermans, S. Goutam, and P. Rodriguez, “Evaluation of Lithium-ion Battery Second Life Performance and Degradation,” 2016.
[33] W. Lih, J. Yen, F. Shieh, and Y. Liao, “Second Use of Retired Lithium-ion Battery Packs from Electric Vehicles : Technological Challenges , Cost Analysis and Optimal Business Model,” 2012.
[34] M. Abdel-monem, O. Hegazy, N. Omar, K. Trad, P. Van Den, and J. Van Mierlo,

"Lithium-ion Batteries : Comprehensive Technical Analysis of Second-Life Batteries for Smart Grid Applications Vito , Unit of Energy Technology Acknowledgments Keywords," pp. 1–16.
[35] M. Dubarry *et al.*, "Identifying battery aging mechanisms in large format Li ion cells," *J. Power Sources*, vol. 196, no. 7, pp. 3420–3425, 2011.
[36] M. M. Kabir and D. E. Demirocak, "Degradation mechanisms in Li-ion batteries : a state-of- the-art review," no. April, pp. 1963–1986, 2017.
[37] K. Young and S. Yasuoka, "Capacity Degradation Mechanisms in Nickel / Metal Hydride Batteries," pp. 1–28, 2016.
[38] P. Ruetschi, "Aging mechanisms and service life of lead – acid batteries," vol. 127, pp. 33–44, 2004.
[39] C. R. Birkl, M. R. Roberts, E. Mcturk, P. G. Bruce, and D. A. Howey, "Degradation diagnostics for lithium ion cells," *J. Power Sources*, vol. 341, pp. 373–386, 2017.
[40] B. Xu, S. Member, A. Oudalov, A. Ulbig, G. Andersson, and D. S. Kirschen, "Modeling of Lithium-Ion Battery Degradation for Cell Life Assessment," vol. 9, no. 2, pp. 1131–1140, 2018.
[41] J. Vetter, P. Nov, M. R. Wagner, and C. Veit, "Ageing mechanisms in lithium-ion batteries ☪," vol. 147, pp. 269–281, 2005.
[42] M. Safari, M. Morcrette, A. Teyssot, and C. Delacourt, "Life-Prediction Methods for Lithium-Ion Batteries Derived from a Fatigue Approach," pp. 713–720, 2010.
[43] M. Safari, M. Morcrette, A. Teyssot, and C. Delacourt, "Life Prediction Methods for Lithium-Ion Batteries Derived from a Fatigue Approach II . Capacity-Loss Prediction of Batteries Subjected to Complex Current," pp. 892–898, 2010.
[44] K. Amine *et al.*, "Factors responsible for impedance rise in high power lithium ion batteries," vol. 98, pp. 684–687, 2001.
[45] B. V Ratnakumar and M. C. Smart, "Lithium Plating Behavior in Lithium-ion Cells," vol. 25, no. 36, pp. 241–252, 2010.
[46] H. Borhan, A. Vahidi, A. M. Phillips, M. L. Kuang, I. V. Kolmanovsky, and S. Di Cairano, "MPC-based energy management of a power-split hybrid electric vehicle," *IEEE Trans. Control Syst. Technol.*, vol. 20, no. 3, pp. 593–603, 2012.
[47] S. Zhang, R. Xiong, and F. Sun, "Model predictive control for power management in a plug-in hybrid electric vehicle with a hybrid energy storage system," *Appl. Energy*, 2015.
[48] A. Ostadi, M. Kazerani, and S. K. Chen, "Hybrid Energy Storage System (HESS) in vehicular applications: A review on interfacing battery and ultra-capacitor units," *IEEE Transp. Electrif. Conf. Expo*, 2013.
[49] A. Khaligh and Z. Li, "Battery, ultracapacitor, fuel cell, and hybrid energy storage systems for electric, hybrid electric, fuel cell, and plug-in hybrid electric vehicles: State of the art," *IEEE Trans. Veh. Technol.*, vol. 59, no. 6, pp. 2806–2814, 2010.
[50] J. Cao and A. Emadi, "A New Battery/UltraCapacitor Hybrid Energy Storage System for Electric, Hybrid, and Plug-In Hybrid Electric Vehicles," *IEEE Trans. Power Electron.*, vol. 27, no. 1, pp. 122–132, 2012.
[51] L. Wai, Y. W. Wong, R. K. Rajkumar, R. K. Rajkumar, and D. Isa, "Hybrid energy storage systems and control strategies for stand-alone renewable energy power systems," *Renew. Sustain. Energy Rev.*, vol. 66, pp. 174–189, 2016.
[52] T. Bocklisch, "Hybrid energy storage approach for renewable energy applications," *Energy Procedia*, vol. 73, no. 2015, pp. 103–111, 2015.
[53] A. Kuperman and I. Aharon, "Battery–ultracapacitor hybrids for pulsed current

loads: A review," *Renew. Sustain. Energy Rev.*, vol. 15, no. 2, pp. 981–992, 2011.
[54] I. Aharon and A. Kuperman, "Topological overview of powertrains for battery-powered vehicles with range extenders," *IEEE Trans. Power Electron.*, vol. 26, no. 3, pp. 868–876, 2011.
[55] A. Etxeberria, I. Vechiu, H. Camblong, J. M. Vinassa, and H. Camblong, "Hybrid Energy Storage Systems for renewable Energy Sources Integration in microgrids: A review," *2010 Conf. Proc. IPEC*, pp. 532–537, 2010.
[56] O. A. Ahmed and J. A. M. Bleijs, "An overview of DC-DC converter topologies for fuel cell-ultracapacitor hybrid distribution system," *Renew. Sustain. Energy Rev.*, vol. 42, pp. 609–626, 2015.
[57] C. Xiang, Y. Wang, S. Hu, and W. Wang, "A new topology and control strategy for a hybrid battery-ultracapacitor energy storage system," *Energies*, vol. 7, no. 5, pp. 2874–2896, 2014.
[58] O. Onar and A. Khaligh, "Dynamic modeling and control of a cascaded active battery/ultra-capacitor based vehicular power system," *2008 IEEE Veh. Power Propuls. Conf. VPPC 2008*, pp. 4–7, 2008.
[59] S. M. Lukic, S. G. Wirasingha, F. Rodriguez, J. Cao, and A. Emadi, "Power management of an ultracapacitor/battery hybrid energy storage system in an HEV," *2006 IEEE Veh. Power Propuls. Conf. VPPC 2006*, p. 6, 2006.
[60] O. Laldin, M. Moshirvaziri, and O. Trescases, "Predictive algorithm for optimizing power flow in hybrid ultracapacitor/battery storage systems for light electric vehicles," *IEEE Trans. Power Electron.*, vol. 28, no. 8, pp. 3882–3895, 2013.
[61] W. S. H. Jing, W., Lai, C. H., Dennis Wong, M. L., & Wong, "Smart Hybrid Energy Storage for Stand-alone PV Microgrid: Optimization of Battery Lifespan through Dynamic Power Allocation," 2015, vol. 3, pp. 3–7.
[62] J. M. Blanes, R. Gutiérrez, A. Garrigós, J. L. Lizán, and J. M. Cuadrado, "Electric vehicle battery life extension using ultracapacitors and an FPGA controlled interleaved buck-boost converter," *IEEE Trans. Power Electron.*, vol. 28, no. 12, pp. 5940–5948, 2013.
[63] S. K. Kollimalla, M. K. Mishra, A. Ukil, and H. B. Gooi, "DC Grid Voltage Regulation Using New HESS Control Strategy," *IEEE Trans. Sustain. Energy*, vol. 3029, no. c, pp. 1–1, 2016.
[64] E. Unamuno and J. A. Barrena, "Hybrid ac/dc microgrids—Part I: Review and classification of topologies," *Renew. Sustain. Energy Rev.*, vol. 52, pp. 1251–1259, 2015.
[65] K. Ma and X. Wang, "HyStore : Hybrid Energy Storage for Cost-efficient Server Power Shaving in Data Centers," 2015.
[66] D. Cericola, P. W. Ruch, R. Kötz, P. Novák, and A. Wokaun, "Simulation of a supercapacitor/Li-ion battery hybrid for pulsed applications," *J. Power Sources*, vol. 195, no. 9, pp. 2731–2736, 2010.
[67] R. Mars, B. Bouzidi, and A. Yangui, "On the Comparison of Two Hybrid Energy Storage Systems: Parallel Connection of Battery-RC Ultracapacitor/- Multibranch Ultracapacitor Circuits," no. i, 2016.
[68] P. Bentley and D. a. Stone, "The parallel combination of a valve regulated lead acid cell and supercapacitor for use as a hybrid vehicle peak power buffer," *2005 Eur. Conf. Power Electron. Appl.*, vol. 9, pp. 1–10, 2005.
[69] E. Manla, M. Sabbah, and A. Nasiri, "Hybrid Energy Storage System for Conventional Vehicle Start-Stop Application," pp. 6199–6205, 2015.

[70] D. Kim, H. Cha, Daesik Kim, and Hanju Cha, "Comparison of capacity design of lead-acid battery bank and hybrid energy storage bank for nuclear power plant," *2013 IEEE Conf. Clean Energy Technol.*, pp. 427–431, 2013.
[71] A. W. Stienecker, T. Stuart, and C. Ashtiani, "A combined ultracapacitor - Lead acid battery energy storage system for mild hybrid electric vehicles," *2005 IEEE Veh. Power Propuls. Conf. VPPC*, vol. 2005, pp. 350–355, 2005.
[72] H. Dai and X. Chang, "A study on lead acid battery and ultra-capacitor hybrid energy storage system for hybrid city bus," *Proc. - 2010 Int. Conf. Optoelectron. Image Process. ICOIP 2010*, vol. 1, pp. 154–159, 2010.
[73] S. Chung *et al.*, "Hybrid Lead-Acid / Lithium-Ion Energy Storage System with Power-Mix Control for Light Electric Vehicles Keywords Energy Storage System Modeling and IHBM Architecture."
[74] M. Asensio, G. Magall, and C. De Angelo, "Experimental evaluation of different semi-active configurations for battery-ultracapacitor hybrid energy storage system (HESS)."
[75] X. Tang and Z. Qi, "Economic Analysis of EDLC / Battery Hybrid Energy Storage," *Electr. Mach. Syst. 2008. ICEMS*, pp. 2729–2733, 2008.
[76] M. R. Rade and P. S. S. Dhamal, "Battery-Ultracapacitor Combination used as Energy Storage System in Electric Vehicle," 2015.
[77] S. Dusmez, "Loss analysis of non-isolated bidirectional DC/DC converters for hybrid energy storage system in EVs," *Isie 2014*, pp. 543–549, 2014.
[78] M. Ortúzar, J. Moreno, and J. Dixon, "Ultracapacitor-based auxiliary energy system for an electric vehicle: Implementation and evaluation.," vol. 54, no. 4, pp. 2147–2156, 2007.
[79] R. Dhaouadi, Y. Hori, and H. Xiaoliang, "Robust control of an ultracapacitor-based hybrid energy storage system for electric vehicles," *2014 IEEE 13th Int. Work. Adv. Motion Control*, pp. 161–166, 2014.
[80] J. Shen and A. Khaligh, "A Supervisory Energy Management Control Strategy for a Battery/ Ultracapacitor Hybrid Energy Storage System," *IEEE Trans. Transp. Electrif.*, vol. 7782, no. 1, pp. 1–1, 2015.
[81] Z. Song, H. Hofmann, J. Li, J. Hou, X. Zhang, and M. Ouyang, "The optimization of a hybrid energy storage system at subzero temperatures: Energy management strategy design and battery heating requirement analysis," *Appl. Energy*, vol. 159, pp. 576–588, 2015.
[82] Z. Song, H. Hofmann, J. Li, X. Han, and M. Ouyang, "Optimization for a hybrid energy storage system in electric vehicles using dynamic programing approach," *Appl. Energy*, vol. 139, no. Dc, pp. 151–162, 2015.
[83] A. Gee, "Design and analysis of a sliding-mode power electronic controlled battery / supercapacitor hybrid energy storage system for remote wind power applications .," no. September, 2011.
[84] J. Bauman, M. Kazerani, and S. Member, "An Analytical Optimization Method for Improved Fuel Cell – Battery – Ultracapacitor Powertrain," *Topology*, vol. 58, no. 7, pp. 3186–3197, 2009.
[85] J. Bauman and M. Kazerani, "A comparative study of fuel-cell-battery, fuel-cell-ultracapacitor, and fuel-cell-battery-ultracapacitor vehicles," *IEEE Trans. Veh. Technol.*, vol. 57, no. 2, pp. 760–769, 2008.
[86] J. Bauman and M. Kazerani, "An improved powertrain topology for fuel cell-battery-ultracapacitor vehicles," *IEEE Int. Symp. Ind. Electron.*, vol. 1, no. c, pp.

1483–1488, 2008.
[87] G. Ren, G. Ma, and N. Cong, “Review of electrical energy storage system for vehicular applications,” *Renew. Sustain. Energy Rev.*, vol. 41, pp. 225–236, 2015.
[88] M. Y. Ayad, A. Aboubou, A. Henni, and M. Becherif, “Sliding Mode Control of Fuel Cell , Supercapacitors and Batteries Hybrid Sources for Vehicle Applications,” pp. 478–483, 2010.
[89] M. Y. Ayad, M. Becherif, and A. Henni, “Vehicle hybridization with fuel cell, supercapacitors and batteries by sliding mode control,” *Renew. Energy*, vol. 36, no. 10, pp. 2627–2634, 2011.
[90] S. Colton, “A Simple Series Battery/Ultracapacitor Drive System for Light Vehicles and Educational Demonstration,” *EVER Conf.*, 2009.
[91] A. Burke, M. Miller, H. Zhao, M. Radenbaugh, and Z. Liu, “Ultracapacitors in micro-and mild hybrids with lead-acid batteries: Simulations and laboratory and in-vehicle testing,” *2013 World Electr. Veh. Symp. Exhib. EVS 2014*, pp. 1–14, 2014.
[92] B. Wang, J. Xu, B. Cao, and X. Zhou, “A novel multimode hybrid energy storage system and its energy management strategy for electric vehicles,” *J. Power Sources*, vol. 281, pp. 432–443, 2015.
[93] B. Vural, O. Erdinc, and M. Uzunoglu, “Parallel combination of FC and UC for vehicular power systems using a multi-input converter-based power interface,” *Energy Convers. Manag.*, vol. 51, no. 12, pp. 2613–2622, 2010.
[94] D. Liu and H. Li, “A ZVS bi-directional DC-DC converter for multiple energy storage elements,” *IEEE Trans. Power Electron.*, vol. 21, no. 5, pp. 1513–1517, 2006.
[95] Y. Tang, S. Member, A. Khaligh, and S. Member, “Bidirectional Hybrid Battery / Ultracapacitor Energy Storage Systems for Next Generation MVDC Shipboard Power Systems,” pp. 1–6, 2011.
[96] Z. Li, O. Onar, A. Khaligh, and E. Schaltz, “Design and Control of a Multiple Input DC/DC Converter for Battery/Ultra-capacitor Based Electric Vehicle Power System,” *2009 Twenty-Fourth Annu. IEEE Appl. Power Electron. Conf. Expo.*, pp. 591–596, 2009.
[97] B. G. Dobbs and P. L. Chapman, “A multiple-input DC-DC converter topology,” *IEEE Power Electron. Lett.*, vol. 99, no. 1, pp. 862–868, 2003.
[98] B. Vural, “FC/UC hybridization for dynamic loads with a novel double input DC-DC converter topology,” *Int. J. Hydrogen Energy*, vol. 38, no. 2, pp. 1103–1110, 2013.
[99] Z. Ding, C. Yang, Z. Zhang, C. Wang, and S. Xie, “A novel soft-switching multiport bidirectional dc-dc converter for hybrid energy storage system,” *IEEE Trans. Power Electron.*, vol. 29, no. 4, pp. 1595–1609, 2014.
[100] A. Etxeberria, I. Vechiu, H. Camblong, and J. M. Vinassa, “Comparison of three topologies and controls of a hybrid energy storage system for microgrids,” *Energy Convers. Manag.*, vol. 54, no. 1, pp. 113–121, 2012.
[101] I. Vechiu, A. Etxeberria, H. Camblong, S. Baudoin, and S. Kreckelbergh, “Hybrid energy storage system with unique power electronic interface for microgrids,” *2013 4th IEEE/PES Innov. Smart Grid Technol. Eur. ISGT Eur. 2013*, no. November 2015, pp. 1–5, 2013.
[102] Z. Liang, S. Hu, Y. Liu, W. Li, X. He, and F. Ieee, “Application of Bi-directional Z-Source in UltraCapacitor-Battery Hybrid Energy Storage System for EV,” vol.

1, pp. 3124–3127, 2015.
[103] S. Hu, Z. Liang, and X. He, “Ultracapacitor-Battery Hybrid Energy Storage System Based on the Asymmetric Bi-Directional Z-Source Topology for EV,” *IEEE Trans. Power Electron.*, vol. PP, no. 99, pp. 1–1, 2015.
[104] J. Cai, Q. Zhong, S. Member, and D. Stone, “A Γ Z -source Based Hybrid Power Converter for Battery-Fuel Cell Hybrid Electric Vehicle,” no. July, pp. 419–424, 2014.
[105] D. B. W. Abeywardana, B. Hredzak, and V. G. Agelidis, “An integration scheme for a direct AC line battery-supercapacitor hybrid energy storage system,” *2013 Australas. Univ. Power Eng. Conf. AUPEC 2013*, no. October, pp. 1–6, 2013.
[106] D. B. W. Abeywardana, B. Hredzak, and V. G. Agelidis, “Single-Phase Grid-Connected LiFePO Battery-Supercapacitor Hybrid Energy Storage System With Interleaved Boost Inverter,” *IEEE Trans. Power Electron.*, vol. 30, no. 10, pp. 5591–5604, 2015.
[107] L. K. Gan, D. E. Macpherson, and J. K. H. Shek, “Synchronisation control and operation of microgrids for rural/island applications,” *Proc. Univ. Power Eng. Conf.*, 2013.
[108] A. M. Van Voorden, L. M. Ramirez Elizondo, G. C. Paap, J. Verboomen, and L. Van Der Sluis, “The application of super capacitors to relieve battery-storage systems in autonomous renewable energy systems,” *2007 IEEE Lausanne POWERTECH, Proc.*, pp. 479–484, 2007.
[109] M. Momayyezan, B. Hredzak, and V. G. Agelidis, “A New Multiple Converter Topology for Battery / Ultracapacitor Hybrid Energy System,” pp. 464–468, 2015.
[110] A. Melero-Pérez, W. Gao, and J. J. Fernández-Lozano, “Fuzzy logic energy management strategy for fuel cell/ultracapacitor/battery hybrid vehicle with multiple-input DC/DC converter,” *5th IEEE Veh. Power Propuls. Conf. VPPC ’09*, pp. 199–206, 2009.
[111] Y. Kim, J. Koh, Q. Xie, Y. Wang, N. Chang, and M. Pedram, “A scalable and flexible hybrid energy storage system design and implementation,” *J. Power Sources*, vol. 255, pp. 410–422, 2014.
[112] A. Di Napoli, F. Crescimbini, F. G. Capponi, and L. Solero, “Control strategy for multiple input DC-DC power converters devoted to hybrid vehicle propulsion systems,” *Ind. Electron. 2002. ISIE 2002. Proc. 2002 IEEE Int. Symp.*, vol. 3, pp. 1036–1041, 2002.
[113] A. Di Napoli, F. Crescimbini, S. Rodo, and L. Solero, “Multiple input DC-DC power converter for fuel-cell powered hybrid vehicles,” *2002 IEEE 33rd Annu. IEEE Power Electron. Spec. Conf. Proc. (Cat. No.02CH37289)*, vol. 4, pp. 1685–1690, 2002.
[114] O. C. Onar and a. Khaligh, “A novel integrated magnetic structure based DC/DC converter for hybrid battery/ultracapacitor energy storage systems,” *IEEE Trans. Smart Grid*, vol. 3, no. 1, pp. 296–307, 2012.
[115] X. Liu, P. Wang, P. C. Loh, F. Gao, and F. H. Choo, “Control of hybrid battery/ultra-capacitor energy storage for stand-alone photovoltaic system,” *2010 IEEE Energy Convers. Congr. Expo. ECCE 2010 - Proc.*, pp. 336–341, 2010.
[116] A. Jaafar, C. Turpin, X. Roboam, E. Bru, and O. Rallieres, “Energy management of a hybrid system based on a fuel cell and a Lithium Ion battery: Experimental tests and integrated optimal design,” *Math. Comput. Simul.*, pp. 1–17, 2016.
[117] P. Zhao, Y. Dai, and J. Wang, “Design and thermodynamic analysis of a hybrid

energy storage system based on A-CAES (adiabatic compressed air energy storage) and FESS (flywheel energy storage system) for wind power application," *Energy*, vol. 70, pp. 674–684, 2014.
[118] T.-T. Nguyen, H.-J. Yoo, and H.-M. Kim, "A Flywheel Energy Storage System Based on a Doubly Fed Induction Machine and Battery for Microgrid Control," *Energies*, vol. 8, no. 6, pp. 5074–5089, 2015.
[119] S. Bae, S. U. Jeon, and J. W. Park, "A Study on Optimal Sizing and Control for Hybrid Energy Storage System with SMES and Battery," *IFAC-PapersOnLine*, vol. 48, no. 30, pp. 507–511, 2015.
[120] F. Li, K. Xie, and J. Yang, "Optimization and Analysis of a Hybrid Energy Storage System in a Small-Scale Standalone Microgrid for Remote Area Power Supply (RAPS)," *Energies*, vol. 8, pp. 4802–4826, 2015.
[121] N. Mendis, K. M. Muttaqi, and S. Perera, "Active power management of a super capacitor-battery hybrid energy storage system for standalone operation of DFIG based wind turbines," *2012 IEEE Ind. Appl. Soc. Annu. Meet.*, pp. 1–8, 2012.
[122] N. Mendis, K. Muttaqi, and S. Perera, "Management of Low and High Frequency Power Components in Demand-Generation Fluctuations of a DFIG based Wind Dominated RAPS System Using Hybrid Energy Storage," *IEEE Trans. Ind. Appl.*, vol. 50, no. c, pp. 1–1, 2013.
[123] N. Mendis, K. M. Muttaqi, S. Sayeef, and S. Perera, "Application of a hybrid energy storage in a remote area power supply system," *Energy Conf. Exhib. (EnergyCon), 2010 IEEE Int.*, pp. 576–581, 2010.
[124] J. W. Shim, Y. Cho, S. J. Kim, S. W. Min, and K. Hur, "Synergistic control of SMES and battery energy storage for enabling dispatchability of renewable energy sources," *IEEE Trans. Appl. Supercond.*, vol. 23, no. 3, 2013.
[125] Y. K. Zeng, T. S. Zhao, L. An, X. L. Zhou, and L. Wei, "A comparative study of all-vanadium and iron-chromium redox flow batteries for large-scale energy storage," *J. Power Sources*, vol. 300, pp. 438–443, 2015.
[126] K. C. Divya and J. Østergaard, "Battery energy storage technology for power systems—An overview," *Electr. Power Syst. Res.*, vol. 79, no. 4, pp. 511–520, 2009.
[127] J. G. Kim *et al.*, "A review of lithium and non-lithium based solid state batteries," *J. Power Sources*, vol. 282, pp. 299–322, 2015.
[128] S. Sabihuddin, A. Kiprakis, and M. Mueller, "A Numerical and Graphical Review of Energy Storage Technologies," *Energies*, vol. 8, no. 1, pp. 172–216, 2014.
[129] X. Luo, J. Wang, M. Dooner, and J. Clarke, "Overview of current development in electrical energy storage technologies and the application potential in power system operation," *Appl. Energy*, vol. 137, pp. 511–536, 2015.
[130] M. Budt, D. Wolf, R. Span, and J. Yan, "A review on compressed air energy storage: Basic principles, past milestones and recent developments," *Appl. Energy*, vol. 170, pp. 250–268, 2016.
[131] E. Barbour, I. A. G. Wilson, J. Radcliffe, Y. Ding, and Y. Li, "A review of pumped hydro energy storage development in significant international electricity markets," *Renew. Sustain. Energy Rev.*, vol. 61, pp. 421–432, 2016.
[132] M. Aneke and M. Wang, "Energy storage technologies and real life applications - A state of the art review," *Appl. Energy*, vol. 179, pp. 350–377, 2016.
[133] S. M. G. Mousavi, F. Faraji, A. Majazi, and K. Al-haddad, "A comprehensive review of Flywheel Energy Storage System technology," *Renew. Sustain. Energy*

Rev., vol. 67, pp. 477–490, 2017.
[134] A. A. K. Arani, H. Karami, G. B. Gharehpetian, and M. S. A. Hejazi, "Review of Flywheel Energy Storage Systems structures and applications in power systems and microgrids," *Renew. Sustain. Energy Rev.*, vol. 69, no. September 2015, pp. 9–18, 2017.
[135] I. Hamzaoui, F. Bouchafaa, and A. Talha, "Advanced control for wind energy conversion systems with flywheel storage dedicated to improving the quality of energy," *Int. J. Hydrogen Energy*, vol. 41, no. 45, pp. 20832–20846, 2016.
[136] D. Lefebvre and F. H. Tezel, "A review of energy storage technologies with a focus on adsorption thermal energy storage processes for heating applications," *Renew. Sustain. Energy Rev.*, vol. 67, pp. 116–125, 2017.
[137] A. Killer, A. Armstorfer, A. E. Díez, and H. Biechl, "Ultracapacitor Assisted Regenerative Braking in Metropolitan Railway Systems," 2012.
[138] L. Battistelli, F. Ciccarelli, D. Lauria, and D. Proto, "Optimal Design of DC Electrified Railway Stationary Storage System," pp. 739–745, 2009.
[139] C. Ashtiani, R. Wright, and G. Hunt, "Ultracapacitors for automotive applications," vol. 154, pp. 561–566, 2006.
[140] S. Werkstetter, "Existing and Future Ultracapacitor-Applications in the Renewable Energy Market," *PCIM Eur.*, no. May, pp. 20–22, 2014.
[141] A. Schneuwly, "WHITE PAPER ULTRACAPACITORS IMPROVE RELIABILITY FOR WIND TURBINE," *Technol. Maxwell*.
[142] S. Werkstetter, "WHITE PAPER Ultracapacitor Usage in Wind Turbine Pitch Control Systems," *Technol. Maxwell*, 2015.
[143] S. Succar and R. Williams, "Princeton Environmental Institute PRINCETON UNIVERSITY Energy Systems Analysis Group Compressed Air Energy Storage : Theory , Resources , And Applications For Wind Power Acknowledgments," *Princet. Environ. Inst. Rep.*, vol. 8, no. April, p. 81, 2008.
[144] S. Rehman, L. M. Al-Hadhrami, and M. M. Alam, "Pumped hydro energy storage system: A technological review," *Renew. Sustain. Energy Rev.*, vol. 44, pp. 586–598, 2015.
[145] J. P. Deane, B. P. Ó Gallachóir, and E. J. McKeogh, "Techno-economic review of existing and new pumped hydro energy storage plant," *Renew. Sustain. Energy Rev.*, vol. 14, no. 4, pp. 1293–1302, 2010.
[146] J. Lizana, R. Chacartegui, Á. Barrios-Padura, and J. M. Valverde, "Characterization of thermal energy storage materials for building applications," no. 1, pp. 606–620.
[147] F. Agyenim, N. Hewitt, P. Eames, and M. Smyth, "A review of materials, heat transfer and phase change problem formulation for latent heat thermal energy storage systems (LHTESS)," *Renew. Sustain. Energy Rev.*, vol. 14, no. 2, pp. 615–628, 2010.
[148] R. T. Carlin, H. C. De Long, J. Fuller, and P. C. Trulove, "ELECTROCHEMICAL SOCIETY LETTERS Dual Intercalating Molten Electrolyte Batteries," vol. 141, no. 7, pp. 7–10, 1994.
[149] E. Chemali, M. Preindl, P. Malysz, and A. Emadi, "Electrochemical and Electrostatic Energy Storage and Management Systems for Electric Drive Vehicles: State-of-the-Art Review and Future Trends," *IEEE J. Emerg. Sel. Top. Power Electron.*, vol. 4, no. 3, pp. 1117–1134, 2016.
[150] C. Nygaard, D. Version, and H. Larsen, *Electromagnetic and electrostatic storage*

DTU International Energy Report. 2013.
[151] T. Watanabe and A. Ishiyama, "Superconducting magnetic energy storage system (SMES)," *J. Inst. Electr. Eng. Japan*, vol. 134, no. 8, pp. 546–548, 2014.
[152] M. Daowd, M. Antoine, N. Omar, P. Lataire, P. Van Den Bossche, and J. Van Mierlo, "Battery management system-balancing modularization based on a single switched capacitor and bi-directional DC/DC converter with the auxiliary battery," *Energies*, vol. 7, no. 5, pp. 2897–2937, 2014.
[153] M. Daowd, M. Antoine, N. Omar, P. van den Bossche, and J. van Mierlo, "Single switched capacitor battery balancing system enhancements," *Energies*, vol. 6, no. 4, pp. 2149–2179, 2013.
[154] J. Cao, N. Schofield, and A. Emadi, "Battery balancing methods: A comprehensive review," *2008 IEEE Veh. Power Propuls. Conf. VPPC 2008*, pp. 3–8, 2008.
[155] W. X. Shen, "Optimally sizing of solar array and battery in a standalone photovoltaic system in Malaysia," *Renew. Energy*, vol. 34, no. 1, pp. 348–352, 2009.
[156] T. Khatib, I. A. Ibrahim, and A. Mohamed, "A review on sizing methodologies of photovoltaic array and storage battery in a standalone photovoltaic system," *Energy Convers. Manag.*, vol. 120, pp. 430–448, 2016.
[157] Trojan_Battery_Company, "Battery sizing guidelines." pp. 0–1.
[158] Saft Batteries, "Sunica Ni-Cd battery Technical manual." .
[159] Exide Technologies, "Handbook for Stationary Vented Lead-Acid Batteries Part 2: Installation, Commissioning and Operation," vol. 2, pp. 1–68, 2012.
[160] M. E. Glavin and W. G. Hurley, "Optimisation of a photovoltaic battery ultracapacitor hybrid energy storage system," *Sol. Energy*, vol. 86, no. 10, pp. 3009–3020, 2012.
[161] H. Douglas and P. Pillay, "Sizing ultracapacitors for hybrid electric vehicles," *IECON Proc. (Industrial Electron. Conf.*, vol. 2005, pp. 1599–1604, 2005.
[162] L. Zhang, X. Hu, Z. Wang, F. Sun, J. Deng, and D. G. Dorrell, "Multiobjective Optimal Sizing of Hybrid Energy Storage System for Electric Vehicles," *IEEE Trans. Veh. Technol.*, vol. 67, no. 2, pp. 1027–1035, 2018.
[163] a. M. Gee and R. W. Dunn, "Novel battery / supercapacitor hybrid energy storage control strategy for battery life extension in isolated wind energy conversion systems," *Univ. Power Eng. Conf. (UPEC), 2010 45th Int.*, 2010.
[164] I. Sanz-Gorrachategui *et al.*, "Partial state-of-charge mitigation in standalone photovoltaic hybrid storage systems," *Energies*, vol. 12, no. 22, pp. 1–20, 2019.
[165] J. D. Maclay, J. Brouwer, and G. S. Samuelsen, "Dynamic modeling of hybrid energy storage systems coupled to photovoltaic generation in residential applications," *J. Power Sources*, vol. 163, no. 2, pp. 916–925, 2007.
[166] C. H. Li, X. J. Zhu, G. Y. Cao, S. Sui, and M. R. Hu, "Dynamic modeling and sizing optimization of stand-alone photovoltaic power systems using hybrid energy storage technology," *Renew. Energy*, vol. 34, no. 3, pp. 815–826, 2009.
[167] R. Jallouli and L. Krichen, "Sizing, techno-economic and generation management analysis of a stand alone photovoltaic power unit including storage devices," *Energy*, vol. 40, no. 1, pp. 196–209, 2012.
[168] R. de Castro and C. Pinto, "Optimal sizing and energy management of hybrid storage systems," *Veh. Power …*, pp. 321–326, 2012.
[169] I. San Martín, A. Ursúa, and P. Sanchis, "Integration of fuel cells and supercapacitors in electrical microgrids: Analysis, modelling and experimental

validation," *Int. J. Hydrogen Energy*, vol. 38, no. 27, pp. 11655–11671, 2013.
[170] M. Masih-Tehrani, M. R. Ha'iri-Yazdi, V. Esfahanian, and A. Safaei, "Optimum sizing and optimum energy management of a hybrid energy storage system for lithium battery life improvement," *J. Power Sources*, vol. 244, pp. 2–10, 2013.
[171] A. Ostadi and M. Kazerani, "A Comparative Analysis of Optimal Sizing of Battery-only, Ultracapacitor-only, and Battery-Ultracapacitor Hybrid Energy Storage Systems for a City Bus," *IEEE Trans. Veh. Technol.*, vol. 9545, no. c, pp. 1–1, 2014.
[172] T. Zhou and W. Sun, "Optimization of battery-supercapacitor hybrid energy storage station in Wind/solar generation system," *IEEE Trans. Sustain. Energy*, vol. 5, no. 2, pp. 408–415, 2014.
[173] N. Meng, P. Wang, H. Wu, W. Wang, and W. Xu, "Optimal sizing of distributed generations in a connected DC micro-grid with hybrid energy storage system," *2015 IEEE Energy Convers. Congr. Expo. ECCE 2015*, pp. 3179–3183, 2015.
[174] Y. Liu, W. Du, L. Xiao, H. Wang, S. Bu, and J. Cao, "Sizing a Hybrid Energy Storage System for Maintaining Power Balance of an Isolated System With High Penetration of Wind Generation," pp. 1–9, 2015.
[175] T. Mesbahi, F. Khenfri, N. Rizoug, P. Bartholomeüs, and P. Le Moigne, "Combined Optimal Sizing and Control of Li-Ion Battery/Supercapacitor Embedded Power Supply Using Hybrid Particle Swarm-Nelder-Mead (PSO-NM) Algorithm," *IEEE Trans. Sustain. Energy J.*, vol. 3029, no. c, 2016.
[176] J. Li, Q. Yang, F. Robinson, F. Liang, M. Zhang, and W. Yuan, "Design and test of a new droop control algorithm for a SMES/battery hybrid energy storage system," *Energy*, vol. 118, pp. 1110–1122, 2017.
[177] N. Destro, A. Benato, A. Stoppato, and A. Mirandola, "Components design and daily operation optimization of a hybrid system with energy storages," *Energy*, vol. 117, pp. 569–577, 2016.
[178] I. Janghorban Esfahani, P. Ifaei, J. Kim, and C. Yoo, "Design of Hybrid Renewable Energy Systems with Battery/Hydrogen storage considering practical power losses: A MEPoPA (Modified Extended-Power Pinch Analysis)," *Energy*, vol. 100, pp. 40–50, 2016.
[179] B. Li, R. Roche, D. Paire, and A. Miraoui, "Sizing of a stand-alone microgrid considering electric power, cooling/heating, hydrogen loads and hydrogen storage degradation," *Appl. Energy*, vol. 205, no. August, pp. 1244–1259, 2017.
[180] A. S. Jacob, R. Banerjee, and P. C. Ghosh, "Sizing of hybrid energy storage system for a PV based microgrid through design space approach," *Appl. Energy*, vol. 212, no. December 2017, pp. 640–653, 2018.
[181] A. Rahmoun, "Mathematical Modeling andAnalysis of a Battery Energy Storage System for Microgrids," TALLINN UNIVERSITY OF TECHNOLOGY, 2017.
[182] L. Shi and M. L. Crow, "Comparison of ultracapacitor electric circuit models," *IEEE Power Energy Soc. 2008 Gen. Meet. Convers. Deliv. Electr. Energy 21st Century, PES*, pp. 1–6, 2008.
[183] R. L. Spyker and R. M. Nelms, "Classical equivalent circuit parameters for a double-layer capacitor," *IEEE Trans. Aerosp. Electron. Syst.*, vol. 36, no. 3 PART 1, pp. 829–836, 2000.
[184] L. Zubieta and R. Bonert, "Characterization of Double-Layer Capacitors for Power Electronics Applications," vol. 36, no. 1, pp. 199–205, 2000.
[185] S. Buller, E. Karden, D. Kok, and R. W. De Doncker, "Modeling the dynamic

behavior of supercapacitors using impedance spectroscopy," *IEEE Trans. Ind. Appl.*, vol. 38, no. 6, pp. 1622–1626, 2002.
[186] F. Belhachemi, S. Rael, and B. Davat, "Physical based model of power electric double-layer supercapacitors," *Conf. Rec. - IAS Annu. Meet. (IEEE Ind. Appl. Soc.*, vol. 5, no. Upresa 7037, pp. 3069–3076, 2000.
[187] J.-N. Marie-Francoise, H. Gualous, and B. A., "Supercapacitor thermal- and electrical-behaviour modelling using ANN," vol. 150, no. 20030259, pp. 255–262, 2003.
[188] R. M. Schupbach and J. C. Balda, "Comparing DC-DC converters for power management in hybrid electric vehicles," *IEEE Int. Electr. Mach. Drives Conf. 2003. IEMDC'03.*, vol. 3, no. C, pp. 1369–1374, 2003.
[189] S. Inoue and H. Akagi, "A Bidirectional DC – DC Converter for an Energy Storage System With Galvanic Isolation," *IEEE Trans. Power Electron.*, vol. 22, no. 6, pp. 2299–2306, 2007.
[190] N. M. L. Tan, T. Abe, and H. Akagi, "Design and performance of a bidirectional isolated DC-DC converter for a battery energy storage system," *IEEE Trans. Power Electron.*, vol. 27, no. 3, pp. 1237–1248, 2012.
[191] Y. Miura, M. Kaga, Y. Horita, and T. Ise, "Bidirectional Isolated dual full-bridge dc-dc converter with active clamp for EDLC," *2010 IEEE Energy Convers. Congr. Expo. ECCE 2010 - Proc.*, pp. 1136–1143, 2010.
[192] K. Yamamoto, E. Hiraki, T. Tanaka, M. Nakaoka, and T. Mishima, "Bidirectional DC-DC converter with full-bridge / push-pull circuit for automobile electric power systems," *PESC Rec. - IEEE Annu. Power Electron. Spec. Conf.*, pp. 2–6, 2006.
[193] C. Huang and P. K. T. Mok, "A 100 MHz 82.4% efficiency package-bondwire based four-phase fully-integrated buck converter with flying capacitor for area reduction," *IEEE J. Solid-State Circuits*, vol. 48, no. 12, pp. 2977–2988, 2013.
[194] B. D. Baba, "Benefits of a multiphase buck converter," *Analog Appl. J.*, no. 1, pp. 8–13, 2012.
[195] R. Taylor, "Power Tips: When to choose multiphase," *Texas Instruments web page*, 2013. [Online]. Available: https://e2e.ti.com/blogs_/b/powerhouse/archive/2013/10/31/powerlab-notes-when-to-choose-multiphase.
[196] MathWorks, "Trust-Region-Dogleg Implementation." [Online]. Available: https://es.mathworks.com/help/optim/ug/equation-solving-algorithms.html?lang=en.
[197] M. J. Powell, "A fortran subroutine for solving systems of non-linear algebraic equations," Harwell (England), 1968.
[198] L. Lu, X. Han, J. Li, J. Hua, and M. Ouyang, "A review on the key issues for lithium-ion battery management in electric vehicles," *J. Power Sources*, vol. 226, pp. 272–288, 2013.
[199] mpoweruk, "Lithium Battery Failures." [Online]. Available: http://www.mpoweruk.com/lithium_failures.htm.
[200] Maxwell, "K2 Series Ultracapacitors Datasheet." pp. 1–5, 2014.
[201] X. Zhang, Z. Dong, and C. Crawford, "Hybrid energy storage system for hybrid and electric vehicles: review and a new control strategy.," *Int. Mech. Eng. Congr. Expo. IMECE2011*, pp. 1–11, 2011.
[202] Y. Z. Y. Zhang, Z. J. Z. Jiang, and X. Y. X. Yu, "Control Strategies for Battery/Supercapacitor Hybrid Energy Storage Systems," *2008 IEEE Energy 2030*

Conf., pp. 5–10, 2008.
[203] F. S. Garcia, a. a. Ferreira, and J. a. Pomilio, "Control Strategy for Battery-Ultracapacitor Hybrid Energy Storage System," *2009 Twenty-Fourth Annu. IEEE Appl. Power Electron. Conf. Expo.*, pp. 826–832, 2009.
[204] L. Rosario and P. C. K. Luk, "Applying management methodology to electric vehicles with multiple energy storage systems," *Proc. Sixth Int. Conf. Mach. Learn. Cybern. ICMLC 2007*, vol. 7, no. August, pp. 4223–4230, 2007.
[205] E. Serri, "Comparative Study of Short Prediction MPC-KF with PI Controller for DC-DC Buck Converter," no. October, pp. 219–224, 2016.
[206] C. Bordons and C. Montero, "Basic Principles of MPC for Power Converters: Bridging the Gap between Theory and Practice," *IEEE Ind. Electron. Mag.*, vol. 9, no. 3, pp. 31–43, 2015.
[207] P. Karamanakos, T. Geyer, N. Oikonomou, F. D. Kieferndorf, and S. Manias, "Direct model predictive control: A review of strategies that achieve long prediction intervals for power electronics," *IEEE Ind. Electron. Mag.*, vol. 8, no. 1, pp. 32–43, 2014.
[208] P. Cortés, M. P. Kazmierkowski, R. M. Kennel, D. E. Quevedo, and J. Rodriguez, "Predictive Control in Power Electronics and Drives," *IEEE Trans. Ind. Electron.*, vol. 55, no. 12, pp. 4312–4324, 2008.
[209] B. Hredzak, V. G. Agelidis, and G. Demetriades, "Application of explicit model predictive control to a hybrid battery-ultracapacitor power source," *J. Power Sources*, vol. 277, pp. 84–94, 2015.
[210] J. Rodriguez and P. Cortes, "Model predictive control," *Predict. Control Power Convert. Electr. Drives*, vol. 19, no. 5, p. 2005, 2007.
[211] D. E. Quevedo, R. P. Aguilera, and T. Geyer, *predictive control in power electronics and drives basic concepts theory and methods*. 2014.
[212] K. P. Tee, S. S. Ge, and E. H. Tay, "Barrier Lyapunov Functions for the control of output-constrained nonlinear systems," *Automatica*, vol. 45, no. 4, pp. 918–927, 2009.
[213] W. Jing, C. Hung, D. K. X. Ling, W. S. H. Wong, and M. L. D. Wong, "Battery lifetime enhancement via smart hybrid energy storage plug-in module in standalone photovoltaic power system," *J. Energy Storage*, vol. 21, no. November 2018, pp. 586–598, 2019.
[214] J. M. Guerrero, S. Member, J. C. Vasquez, J. Matas, L. G. De Vicuña, and M. Castilla, "Hierarchical Control of Droop-Controlled AC and DC Microgrids — A General Approach Toward Standardization," vol. 58, no. 1, pp. 158–172, 2011.
[215] O. Palizban and K. Kauhaniemi, "Hierarchical control structure in microgrids with distributed generation: Island and grid-connected mode," *Renew. Sustain. Energy Rev.*, vol. 44, pp. 797–813, 2015.
[216] J. Rodriguez *et al.*, "State of the art of finite control set model predictive control in power electronics," *IEEE Trans. Ind. Informatics*, vol. 9, no. 2, pp. 1003–1016, 2013.
[217] C. Buccella, C. Cecati, and H. Latafat, "Digital control of power converters - A survey," *IEEE Trans. Ind. Informatics*, vol. 8, no. 3, pp. 437–447, 2012.
[218] Y. F. Liu, E. Meyer, and X. Liu, "Recent developments in digital control strategies for DC/DC switching power converters," *IEEE Trans. Power Electron.*, vol. 24, no. 11, pp. 2567–2577, 2009.
[219] Texas Instruments, "TMS320F2837xD Dual-Core Delfino ™ Microcontrollers,"

Prod. Datasheet, 2018.
[220] J. Rodriguez and P. Cortes, *Predictive Control of Power Converters and Electrical Drives*. 2012.
[221] T. Geyer, N. Oikonomou, and F. D. Kieferndorf, *Model Predictive Control of High Power Converters and Industrial Drives*. 2013.
[222] R. L. Fuentes and S. Mar, "Predictive Control of DC-link Voltage in an Active-Front-End Rectifier," pp. 1811–1816, 2011.
[223] P. Karamanakos, T. Geyer, and S. Manias, "Direct voltage control of DC-DC boost converters using model predictive control based on enumeration," *Power Electron. Motion Control Conf. (EPE/PEMC), 2012 15th Int.*, pp. 1–8, 2012.
[224] D. E. Quevedo, R. P. Aguilera, and A. P. Marcelo, "Model Predictive Control of an AFE Rectifier With Dynamic References," vol. 27, no. 7, pp. 3128–3136, 2012.
[225] J. Rodriguez and P. Cortes, *Control of an Active Front-End Rectifier*. 2012.
[226] T. Geyer and D. E. Quevedo, "Multistep finite control set model predictive control for power electronics," *IEEE Trans. Power Electron.*, vol. 29, no. 12, pp. 6836–6846, 2014.
[227] A. Santucci, A. Sorniotti, and C. Lekakou, "Power split strategies for hybrid energy storage systems for vehicular applications," *J. Power Sources*, vol. 258, pp. 395–407, 2014.
[228] N. R. Chaudhuri and B. Chaudhuri, "Adaptive droop control for effective power sharing in multi-terminal DC (MTDC) grids," *IEEE Trans. Power Syst.*, vol. 28, no. 1, pp. 21–29, 2013.